Wellbore Instability Detection in Real Time Using Ultrasonic Measurements

PhD Thesis

Behzad Elahifar

Chair of Drilling and Completion Engineering

Department of Mineral Resource and Petroleum Engineering

Supervisor: Univ.-Prof. Dipl.-Ing. Dr.mont. Gerhard Thonhauser

March 2013

Affidavit

I declare in lieu of oath, that I wrote this thesis and performed the associated research myself, using only literature cited in this volume.

………………………………………………

Behzad Elahifar, March 2013

Acknowledgements

Abstract

Drilling programs continue to push into new and more complex environments. As a result, accurate measurements of drilling data in real time are becoming more critical by means of minimizing the risks as well as the costs. A rotating ultrasonic caliper sensor is a key measurement for determining the borehole geometry in MWD (measurement while drilling) and LWD (logging while drilling) tools. The measurement of actual wellbore shape in real-time can be considered as one of the key components to detect problems such as borehole instability. Abnormal wellbore shape will allow drawing conclusions on the stress field. By knowing abnormal wellbore shapes the response of other sensors, as part of LWD and MWD, could be better interpreted.

The measurements are transmitted to the surface and used to compensate other logs of MWD and LWD measurements. Furthermore, with early and accurate real-time caliper measurements, borehole instability can be detected. For example, an elliptical wellbore can indicate the maximum and minimum stress directions. Borehole enlargement or washout can indicate that the mud is too heavy or too reactive with the formation. An under-gauge borehole might indicate bit wear.

The scope of this work is to (1) develop an ultrasonic caliper tool for borehole geometrical measurement and (2) developing an extra ultrasonic sensor to record the speed of sound in the drilling fluid at the desired depth. Using this package will allow gas kick detection in real time drilling operation.

In the beginning, this work discusses wellbore instability and causes of instabilities in detail. Methodology for solving the instability problems, introduction of the ultrasonic caliper and using it to monitor the wellbore profile in real time is illustrated.

Next, the development of new ultrasonic sensors and the physical properties of sound and echo are described in detailed. The measurement principle of an ultrasonic sensor and the method by which an echo is created by the sensor and sent towards an object and reflected back for distance measurement is explained.

Another chapter discusses the experiments related to the accuracy of the ultrasonic sensor measurements for estimation of the wellbore geometry. Numerical simulation of the ultrasonic measurements and comparison of the simulated results to the recorded data gives estimation how accurate the data are, depending on the position of the tool in the borehole.

Measurements are performed in artificial wellbores with geometrical anomalies like washouts and squeezing formations. It is shown that such anomalies can be detected with an appropriate accuracy if circle fitting methods like the Kasa method in combination with robust error models are applied. By developing a reference ultrasonic sensor, sound velocity in different drilling fluid was recorded and with this method a gas kick could be detected.

Kurzbeschreibung

Die Tiefbohrtechnik entwickelt sich zunehmend in Bereiche welche komplexer Lösungen bedürfen. Dadurch gewinnt zum Beispiel die genaue Bestimmung von Bohrparametern in Echtzeit an Bedeutung um Risiken und Kosten zu minimieren. Ein rotierender Ultraschall Kaliber Sensor ist ein vielversprechender Weg um genaue Daten über die Bohrlochsgeometrie während MWD (measurement while drilling) und LWD (logging while drilling) zu erhalten. Die Echtzeitmessung der Bohrlochgeometrie ist ein Schlüssel zum Erfolg um Probleme wie Bohrlochinstabilität rechtzeitig erkennen zu können. Abnormale Bohrlochgeometrien könne Rückschlüsse auf das Gebirgsspannungsfeld liefern. Ebenso kann durch Kenntnis von abnormalen Bohrlochgeometrien Messungen anderer LWD und MWD Sensoren besser interpretiert werden.

Die Daten werden zur Oberfläche geleitet und können dazu verwendet werden bestimmte Logs bei MWD und LWD Messungen zu ersetzen. Zusätzlich können mit genauen Kaliber Echtzeitmessungen Bohrlochinstabilitäten entdeckt werden. Zum Beispiel kann ein elliptisch geformtes Bohrloch Aufschlüsse zu minimaler und maximaler Gebirgsspannungsrichtung geben. Bohrlocherweiterungen oder Auswaschungen könne auf eine zu schwere Spülung hinweisen oder auch auf eine Reaktionen zwischen Formation und Spülung. Bohrlochverengungen weisen auch auf abgenützte Meißel hin.

Das Ziel dieser Arbeit ist es (1) ein Ultraschall Caliper Tool zur genauen Bestimmung der Bohrlochgeometrie sowie (2) einen Referenz Ultraschall Sensor zur Messung der Schallgeschwindigkeit in Bohrspülung zu entwickeln. Das Paket kann damit auch zur Echtzeitbestimmung von Gaszuflüssen in das Bohrloch verwendet werden.

Die Arbeit beschreibt zunächst Bohrlochinstabilitäten sowie deren Gründe im Detail. Die Methodik zur Lösung des Stabilitätsproblems sowie eine Einführung in Verwendung von Ultraschall Kaliber zur Darstellung der Bohrlochgeometrie wird beleuchtet.

Danach folgt eine detaillierte Beschreibung der neuen Ultraschall Sensor Entwicklung sowie die physikalischen Eigenschaften von Schall und Echo. Messprinzipien, das Prinzip der Schallerzeugung und Schallreflexionen entlang von Objekten, sowie die Bestimmung von Entfernungen werden erläutert.

Ein weiteres Kapitel diskutiert die Genauigkeit der experimentellen Daten zur Bestimmung der Bohrlochsgeometrie über Ultraschallmessungen. Eine numerische Simulation der Ultraschallmessungen und ein Vergleich der simulierten Resultate mit aufgenommen Werten lässt Rückschlüsse auf die Genauigkeit zu, abhängig von der Position des Instruments im Bohrloch.

Die Messungen wurden in künstlichen Bohrlöchern mit geometrischen Anomalien wie Auswaschungen und Verengungen durchgeführt. Es kann gezeigt werden, dass solche Anomalien mit genügender Genauigkeit bestimmt werden können, wenn

Kreisapproximationsmethoden, wie die Kasa Methode, in Kombination mit einem robusten Fehlermodell verwendet werden. Mit der Entwicklung eines Referenz Ultraschall Sensors konnte die Schallgeschwindigkeit in verschiedenen Bohrspülungen bestimmt werden. Mit dieser Methode lassen sich Zuflüsse von Gas in das Bohrloch bestimmen.

Table of Contents

List of Figures

Figure 7-42. Sensor rotates in salt water, 8.65ppg, with 100 RPM in 40 cm diameter wellbore (decentralized position) 98

Figure 7-43. Sensor rotates in salt water, 8.65ppg, with 60 RPM in 40 cm diameter wellbore (squeezed formation) 99

Figure 7-44. Sensor rotates in salt water, 8.65ppg, with 100 RPM in 40 cm diameter wellbore (squeezed formation) 99

Figure 7-45. Sensor rotates in salt water, 9 ppg, with 45 RPM in 40 cm diameter wellbore (centralized position) 100

Figure 7-46. Sensor rotates in salt water, 9 ppg, with 60 RPM in 40 cm diameter wellbore (centralized position) 100

Figure 7-47. Sensor rotates in salt water, 9 ppg, with 100 RPM in 40 cm diameter wellbore (centralized position) 101

Figure 7-48. Sensor rotates in salt water, 9 ppg, with 45 RPM in 40 cm diameter wellbore (decentralized position) 101

Figure 7-49. Sensor rotates in salt water, 9 ppg, with 60 RPM in 40 cm diameter wellbore (decentralized position) 102

Figure 7-50. Sensor rotates in salt water, 9 ppg, with 100 RPM in 40 cm diameter wellbore (decentralized position) 102

Figure 7-51. Sensor rotates in salt water, 9 ppg, with 45 RPM in 40 cm diameter wellbore (squeezed formation) 103

Figure 7-52. Sensor rotates in salt water, 9 ppg, with 60 RPM in 40 cm diameter wellbore (squeezed formation) 103

Figure 7-53. Sensor rotates in salt water, 9 ppg, with 100 RPM in 40 cm diameter wellbore (squeezed formation) 104

Figure 7-54. Sensor rotates in salt water, 10 ppg, with 45 RPM in 40 cm diameter wellbore (centralized position) 104

Figure 7-55. Sensor rotates in salt water, 10 ppg, with 60 RPM in 40 cm diameter wellbore (centralized position) 105

Figure 7-56. Sensor rotates in salt water, 10 ppg, with 100 RPM in 40 cm diameter wellbore (centralized position) 105

Figure 7-57. Sensor rotates in salt water, 10 ppg, with 45 RPM in 40 cm diameter wellbore (decentralized position) 106

Figure 7-58. Sensor rotates in salt water, 10 ppg, with 60 RPM in 40 cm diameter wellbore (decentralized position) 106

Figure 7-59. Sensor rotates in salt water, 10 ppg, with 100 RPM in 40 cm diameter wellbore (decentralized position) 107

Figure 7-60. Sensor rotates in salt water, 10 ppg, with 45 RPM in 40 cm diameter wellbore (squeezed formation) 107

Figure 7-61. Sensor rotates in salt water, 10 ppg, with 60 RPM in 40 cm diameter wellbore (squeezed formation) 108

List of Tables

1- Introduction

Wellbore instability is a major problem that drilling engineers faced with during drilling. This problem, costing the industry between 0.6 and 1 billion dollars per year, leads to major difficulties in some areas as the North Sea, Argentina, Nigeria and the Tarim basin. [1]

The causes of wellbore instability are often classified into either mechanical (for example, failure of the rock around the hole because of high stresses, low rock strength, or inappropriate drilling practice) or chemical effects which arise from damaging interaction between the rock, generally shale, and the drilling fluid. Often, field instances of instability are a result of a combination of both chemical and mechanical. This problem might cause serious complications in the well and in some case can lead to expensive operational problems. As result, a major concern of the drilling engineers is keeping the borehole wall from falling in or breaking down. Detailed attention is paid to drilling fluid programs, casing programs, and operating procedures in drilling a well to minimize these costly problems. Also the increasing demand for wellbore stability analyses during the planning stage of a field arises from economic considerations and the increasing use of deviated, extended reach and horizontal wells. [2], [3]

The ultrasonic caliper is a tool that can measure borehole diameter and create a 3D image of the wellbore while drilling is in progress. The measurement of actual wellbore shape in real-time can be considered as one of the key components to detect problems such as borehole instability. Abnormal wellbore shape will allow drawing conclusions on the stress field and the impact on other sensors' responses as part of LWD and MWD measurements.

A key use of borehole size information is for environmental correction of the measurements made by MWD or LWD tools. These might include the gamma ray, resistivity, neutron, and other logging sensors. Determining the presence of and accounting for the effects of washouts on these sensors' responses is an important aspect of log analysis which can be improved by the ultrasonic caliper results. [4], [40]

Recognition of variations in borehole shape in real time drilling allows the drilling engineer to actuate appropriate counteractions to avoid costly failures, or to implement alterations in the drilling practices to optimize the shape of the borehole and thus improve the drilling efficiency. The received data helps the driller to make proper decisions such as reaming a critical zone, changing the flow rate to reduce erosion or modifying the string rotation speed to reduce vibrations. [5]

Real time application of ultrasonic caliper tools also provides a method for calculating borehole volumes. On a final bit run for instance, the sensor may collect the caliper data during trip-out for the estimation of cement volumes. [4]

Wellbore stability and borehole shape and diameter have a direct relation with each other regarding to the instability problem in wellbore. Deviation of wellbore diameter from the bit size, even it is shorter or larger, is a sign of instability in the wellbore. Changing the shape of wellbore like key seat, oval shape and etc. is also a sign of instability in the wellbore while drilling.

Time based monitoring of the wellbore diameter and shape in real time drilling application will help to detect instabilities instantly. Ultrasonic caliper is a tool which is going to be used while drilling to monitor and record wellbore shape and diameter.

3D profile of the wellbore could be monitored while drilling is in progress. This image could help drilling engineer and also the driller to see the changes in wellbore shape (wash out, squeezed formation and etc.) so that the correct and proper decision could be made.

Time also has a great impact on the wellbore stability so by increasing the number of calipers along the drillstring 4D imaging of the wellbore could be done. By using multiple caliper tools along drillstring any changes in borehole shape could be detected as time passes. Any changes in wellbore profile that is a result of mechanical and chemical failure could be detected by time based monitoring of wellbore in 4D format.

The reason that ultrasonic caliper is selected in this project is the simplicity of the system, regarding to the other sensors like gamma ray or FMI tool, and also it is environmental friendly sensor and if the tool is lost in the wellbore it does not have any harmful effect to the environment. There are some tools like gamma ray, neutron density that care should be taking into account so that the tool retrieves safely. Finally, from economical point of view, an ultrasonic caliper promise to be a cheaper sensor to construct and use in comparison to the other sensors.

This thesis is divided into five different chapters. In the second chapter a review on wellbore instability is performed. Definition of instabilities, causes of instabilities in the borehole and the tools that are used to detect and monitor wellbore profile and finally preparing a methodology in real time drilling application to detect instabilities and finding a solution to cure the problems were explained.

In the third chapter a review on ultrasonic sensing is done and all physical and measurement principle is described. In this chapter the measurement principle of an ultrasonic sensor and the method by which an echo is created by the sensor and send towards an object and reflected back for distance measurement is explained. Different types of ultrasonic sensors that are used in different drilling fluids are discussed. Environmental effects on reflected echoes is described and explained in detail.

In the fourth chapter experiments and tests for developing an ultrasonic caliper were described. Tools and instruments were constructed to simulate the wellbore and the drillstring to perform laboratory ultrasonic tests and experiments. Different ultrasonic calipers designed are used to measure borehole diameter in different drilling fluids. Weak points and problems were identified during tests and upgrading was performed to improve the caliper so that reasonable results could be determined. New ideas were used during tool development and results were described and explained in details in this chapter.

Finally, in the last chapter the conclusion was done based on all tests and experiments and a method for determining 4D imaging of wellbore was developed.

2- Wellbore Instability

2.1 Wellbore instability

The maintenance of wellbore stability is one of the most critical considerations in any drilling operation. An unstable wellbore will reduce drilling performance; result in drilling and tripping difficulties and in the worst case could result in the loss of the hole through borehole collapse. In this chapter, causes of the instability in the borehole will be discussed and explained. Methodology for solving and detecting this problem is mentioned. Ultrasonic caliper is introduced and comparison with the wireline caliper will be explained. Finally, using ultrasonic caliper in real time will be discussed.

Wellbore instability can occur as a result of (Figure 2-1):
- Mechanical effects,
- Chemical effects,
- Combination of both.

Mechanical effects are usually related to:
- Inadequate mud weight (too high or too low)
- Inappropriate drilling practices (rate of penetration, vibration effects, torque and drag, poor practices, frequency of trips and etc)

Chemical effects which are related to the mud type and interactions to formation being drilled may result due to:
- Inappropriate mud type

- Inadequate inhibition.
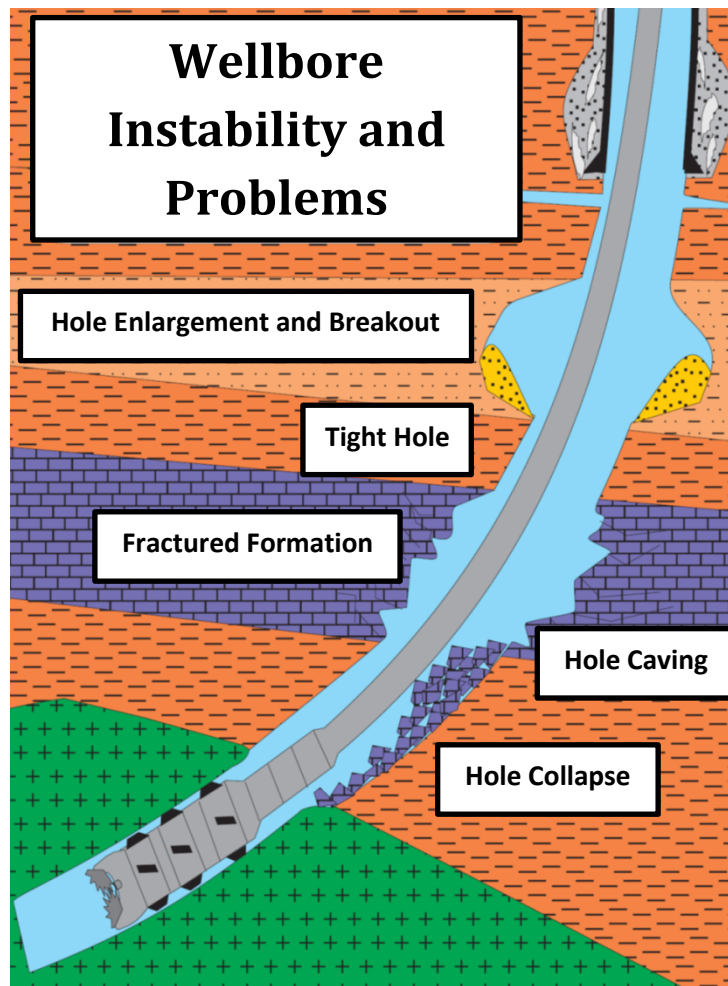
Figure 2-1. Wellbore Instabilities and problems [45]

Mechanism of mechanical wellbore instability can be divided in two main classes:

1. Instability due to failure of intact rock (rock which is unbroken and isotropic in strength)

   Compressional failure or breakout of an intact rock will occur when the compressive stresses around the wellbore exceed the compressive strength of the rock. This results in the enlargement of the borehole from two sides of the wellbore in the circumference of the borehole

2. Instability due to failure of rock containing pre-existence planes of weakness (bedding planes, fractures and etc.).

   Pre-existing planes of weakness such as faults, fractures, and bedding planes may cause instability by the wellbore intersecting the plane at a low angle, causing roof collapse. It is possible to image the planes of weakness prior to wellbore instability. These types of failure mechanism will create enlargement in one area of the borehole or enlargement of the entire hole (Figure 2-2).
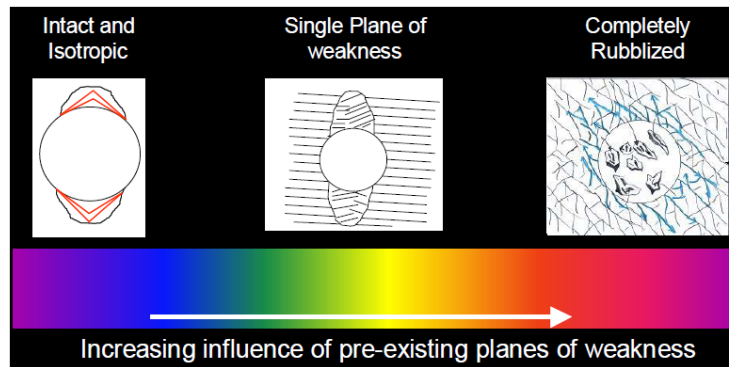
Figure 2-2. Influence of planes of weakness on well bore stability increasing from left to right. The effectiveness of mud weight at controlling instability decreases from left to right. [12]

Types of wellbore instability associated with pre-existing weaknesses can be divided into two classes (Figure 2-3):

1. Failure due to the existence of impermeable pre-existing weaknesses.

   In the case where the pre-existing weaknesses are not preferentially permeable, increase in mud weight will causes to support the wellbore wall. An example of this type might be where a single set of bedding planes is intersected.

2. Failure due to the existence of permeable planes of pre-existing weaknesses.

   Where the mud and filtrate enters pre-existing planes of weakness, increasing the mud weight does not add support to the wellbore wall and may increase instability.

The mechanical action of the drilling assembly can also create enlargement in the wellbore through vibration or hydraulic action in weaker formations and worsening any of the mentioned mechanisms creating instability.
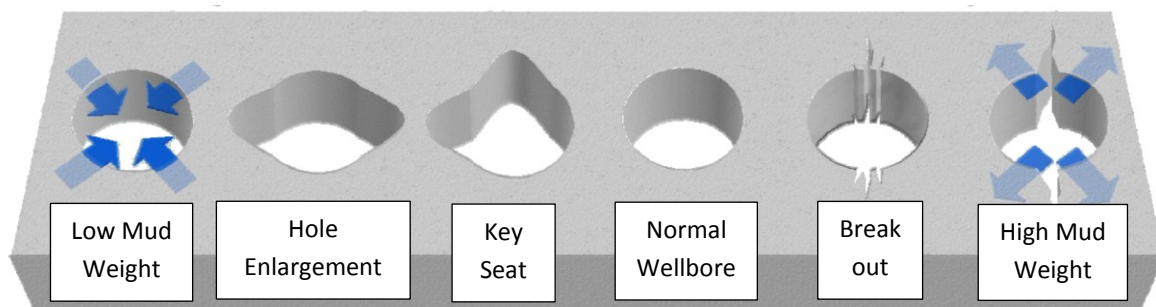
Figure 2-3. Different instabilities on wellbore shape [49]

One of the normal and routine cures for wellbore instability is controlling the mud weight and mud window, so for this reason:

1. The mud weight needed to be high to avoid both breakouts and underbalanced drilling.

2. The mud weight needed to be less than the minimum in situ horizontal stress to prevent mud loss, particularly into the fractured zone.

Prior to drill a well, it is necessary to evaluate the risk posed by each instability:

1. Breakouts are a controllable failure. This type of failure is either self-stabilizing (breakouts tend to stop growing after reaching a certain size) or can be controlled by remedial actions (increasing mud weight prevents breakout development), or both.

2. Destabilized fractured zones are an uncontrollable failure. This type of failure, once initiated, cannot be stopped easily and is expected to become ever more severe. [10], [11], [12]

The nature of the instability can be best seen in the photoelectric factor image in Figure 2-4. The dark areas are where the wellbore wall has failed and the material has been removed. It can be seen that the failed area is largely surrounded by the bedding planes and is located mainly on the wellbore roof, and partly from the wellbore floor. The influence of the bedding planes on the geometry of the hole failure indicates that they are acting as pre-existing planes of weakness. This interval can be seen from the gamma ray to be a shale section which might be expected to be somewhat fissile.
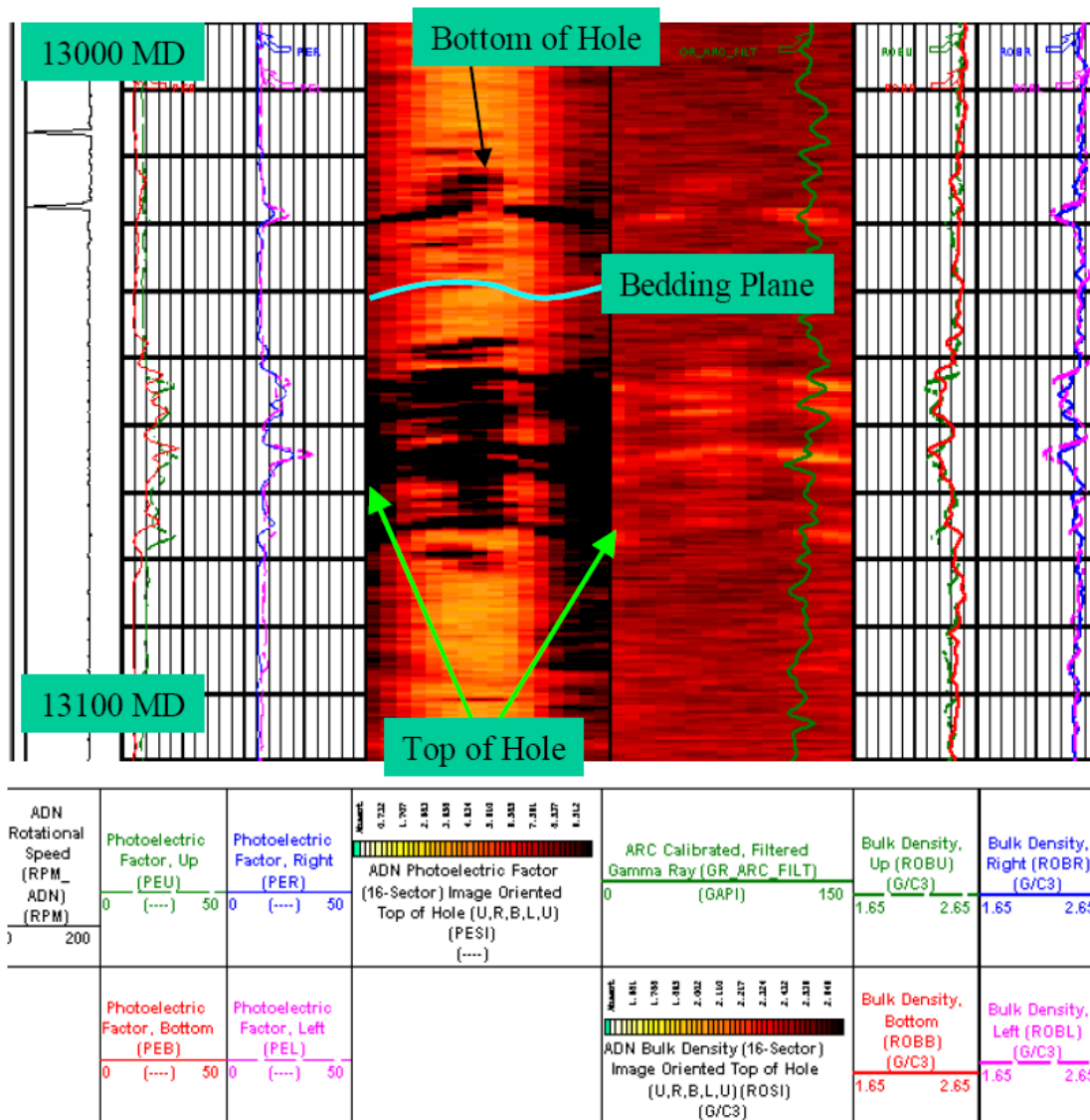
Figure 2-4. Image from wellbore showing wellbore instability on the roof and floor of the wellbore mainly related to bedding planes in this section [14]

Two modes of instability can occur in the same hole at the same time but require different treatments. These modes are:

a. Shear failure of intact rock at the point of maximum stress concentration on the borehole wall.

Increasing mud weight appeared to prevent the shear failure mode but worsen the roof collapse mode. This implies that mud was penetrating the bedding planes or other pre-existing planes of weakness (such as fractures). This mud penetration appears to have been detected from the resistivity tool.

b. Roof collapse due to splitting of weak bedding planes.

Normally, increasing mud weight should add support to the wellbore wall and prevent collapse. However, if the mud is able to penetrate along pre-existing weaknesses the effect of the mud pressure will be to destabilize the wellbore wall rather than support it. [14], [15]

A reliable diagnosis of the instability mechanisms, their severity and their trigger conditions requires a combination of MWD (measurement while drilling) and LWD (logging while drilling) measurements.

LWD measurements can include annular pressure, caliper, gamma ray, and resistivity (phase and attenuation; i.e., shallow and deep, respectively):

1. Annular pressure is an important measurement. It can be used to determine:

   a) The risk of mud losses or shear failure

   b) Assess hole-cleaning effectiveness

   c) Evaluate annular cuttings/gas loading

2. Resistivity measurements can be used to evaluate mud invasion into fractured or permeable zones and faults.

3. Caliper can be used to determine wellbore diameter and shape in real time application.

The evolution of time-dependent instabilities can be measured using the appropriate time-lapse data.

MWD and surface measurements must include deviation, inclination, rate of penetration, pump pressure, rotation rate, downhole torque, down-hole weight on bit, surface torque and hook load, possibly combined with turbine revolutions per minute. The data are principally used to determine the risk of stuck pipe and hole-cleaning effectiveness. [10]

A number of calipers and hole size indicators (by direct measurement or derived) have been introduced with the logging while drilling (LWD) measurements. These include ultrasonic calipers, derived density calipers, and electrical calipers from resistivity tools. The traditional uses of borehole shape measurements have been principally aimed at petro physicists, reservoir engineers, and geologists for completion strategy, hole volume determination, and correction of electrical logs, borehole stability, and borehole size for images.

Hole shape analysis is carried out by processing ultrasonic caliper data into 1D, 2D, or 3D images to illustrate the borehole shape. Processing of images or caliper curve data in real time enables decisions to be made about modification of the BHA or reconsider drilling practice for the remainder of the well. [7]

2.2 Methodology for solving wellbore instability problems

Problems related to wellbore instabilities are a well-known source of additional daily costs. Wellbore instability remains a leading cause of drilling non-productive time (NPT). The development of an efficient industrial methodology to solve these problems is therefore necessary for any operator.

To be successful, this methodology should be used to solve the instability problems in the wellbore in real time. For this reasons the data from an offset well or the data from previous drilled well has to be collected. Afterwards, problems related to the instabilities should be determined and modeling of the problem in order to properly sizing the cure will be performed. To be efficient this process should be performed, not only during the planning phase, but also in real time, directly at the rig site, during drilling.

This methodology is the complete real time logical path that drives the whole wellbore stability package. It establishes the best way of collecting, organizing and reading the needed data and defines a certain number of new techniques for recovering, in real time while drilling, the most important rock parameters. The methodology is divided in three main activities, defined as follows:

a) Modeling
b) Monitoring
c) Understanding

Modeling is the first step that is going to be prepared by using the data from an offset well to determine parameters, organize them in a data base and obtain qualitative solution. The effort is to model the possible scenario in order to quantify the planned cure. By having the model, monitoring and detecting the instabilities in the drilling operation could be performed.

Monitoring is the second step of the whole process and can be simply defined as the real time data collection. The activity is further divided into two main topics, respectively related to:

1. Collection, organization and processing of drilling parameters (ROP, RPM, WOB, mud weight, mud rheology, wellbore diameter and etc.)
2. Formation monitoring (rock strength, porosity, permeability and etc.)

Understanding is the decisional step of the procedure. The modeled, monitored and collected data must be evaluated to identify the most probable mechanism driving the instability. [8]

2.3 Ultrasonic caliper measurements

Ultrasonic calipers are one of a number of borehole size measurements while drilling. The principle of the measurement is a simple broadcast and reflected return of ultrasonic sound pulses. In combination with the sonic transit time of the mud, measuring the time taken for a signal to travel through the mud from source to formation and to return allows calculation of the distance traveled.

When making an ultrasonic measurement it is critical to know the speed of sound within the borehole fluid in the downhole conditions. This is rarely known accurately at the time of drilling. It is therefore important to quality control all readings and to check the accuracy of the caliper by calibration within a known borehole diameter. Alternatively a sample of the mud can be taken and its acoustic properties tested at temperature and pressure to allow the correct inputs. Care must be taken that changes have not been made to the mud properties while drilling the hole, which would require a further check on the mud velocity.

If the distance between the detector and the side of the borehole is too large or the borehole wall has high rugosity or low reflectivity the signal is commonly attenuated. The absolute values for the signal attenuation are difficult to give because this depends on the mud properties as well as the acoustic properties of the borehole wall. The attenuation is the result of echo scattering by increasing solid particles in the drilling fluid, either cuttings or additive particles of the mud.

Understanding the variations in borehole shape allows decisions to be made in drilling the well (fast drilling gives a smaller gauge hole, consistent speed drilling gives a smoother shaped hole, a rotary steerable assembly would remove borehole size variations between sliding and rotating with a mud motor (Figure 2-5)). [7], [47]
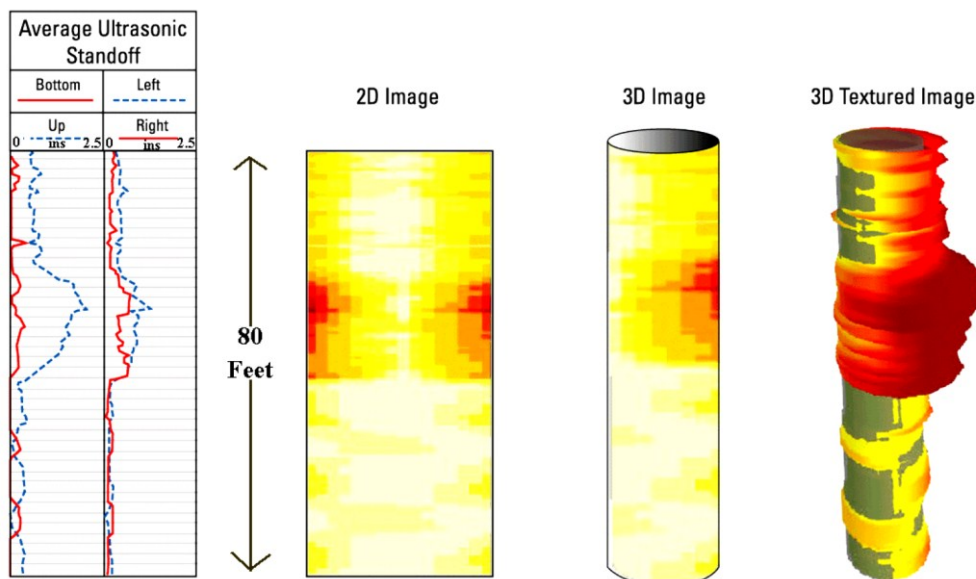
Figure 2-5. Eighty feet of section of ultrasonic caliper data are displayed from a poorly consolidated sandstone interval. The highly rogues section in the middle is a zone where the pipe was worked extensively. [7], [47]

2.3.1 Logging while drilling caliper

In a caliper tool with three set of ultrasonic stand-off measurements at 120 degree spacing around the tool, a borehole caliper can be computed. Figure 2-6 shows a caliper log from the North Sea, with the gamma ray curve in track 1, mirror caliper images in track 2, borehole volume tick marks in track 3, and the three ultrasonic stand-off curves in track 4. In this example it is shown that the shale section from x060 ft to x290 ft is washing out, contrary to what was expected by the operator.

The 3-transducer ultrasonic measurement can be compared to a wireline three-arm mechanical caliper that three measurements are made at 120 degrees around the circumference of the borehole. With mechanical calipers, however, one of the arms tends to track break-outs on the long axis of an oval borehole. Non-contact calipers such as the LWD tool will rotate freely. Mechanical calipers are not available in a LWD tool string. [7], [47]
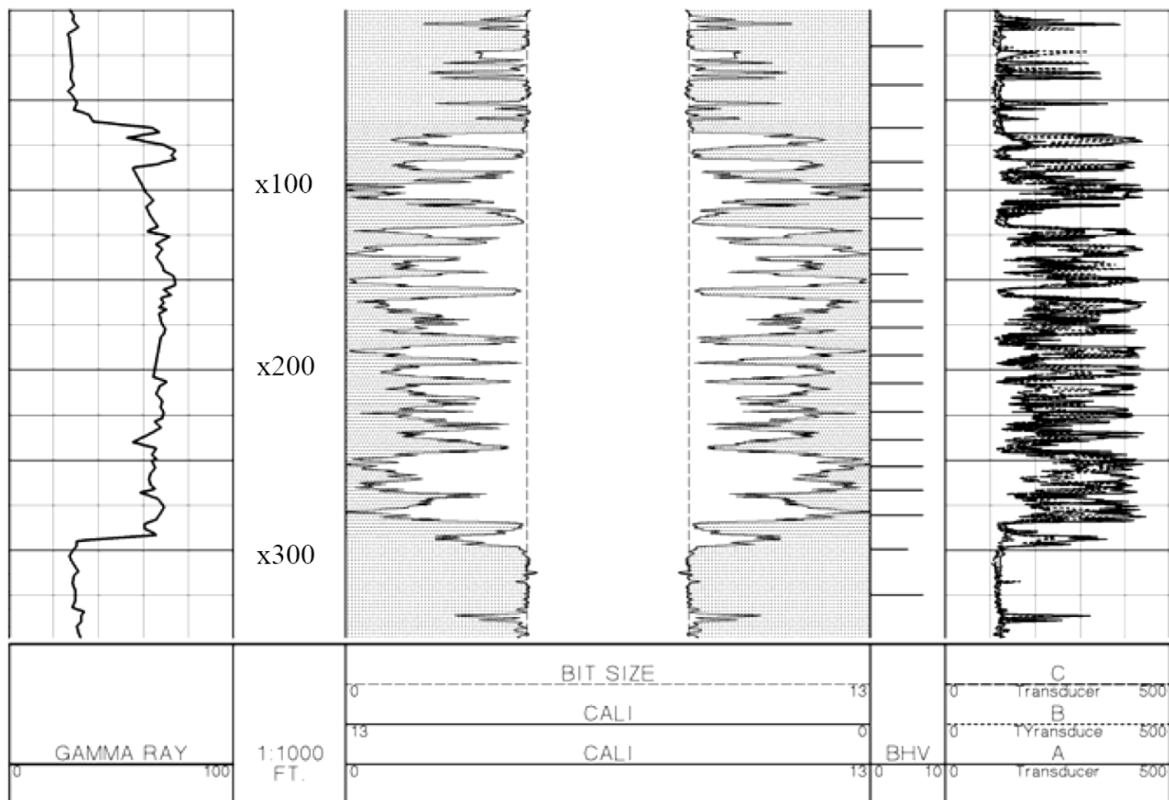
Figure 2-6. LWD Caliper Log Showing Washout in a Shale Section [7]

2.3.2 Borehole break-out

The wellbore profile can be determined by three ultrasonic sensors around the caliper tool. One cannot fit a unique ellipse through three points; however, with three distance measurements from a center point an ellipse can be fitted (Figure 2-7). With a few constraints on the length of the short and long axis of the ellipse, the problem can be easily solved using an error minimization routine. The main constraints are that the short axis cannot be longer than the shortest measured radius and the long axis cannot be shorter than the longest measured radius. When the angle between one of the ultrasonic

transducers, typically the A-transducer in-line with the density and neutron sources and detectors, and the tool face measurement is known, the orientation of the ellipse axes can be computed related to the tool face measurement. The borehole break-out measurement is now oriented in space. When the borehole break-out is related to stress relieve and differences between minimum and maximum horizontal stresses, the orientation of the minimum horizontal stress can be concluded from the direction of the maximum ellipse axis. [13]
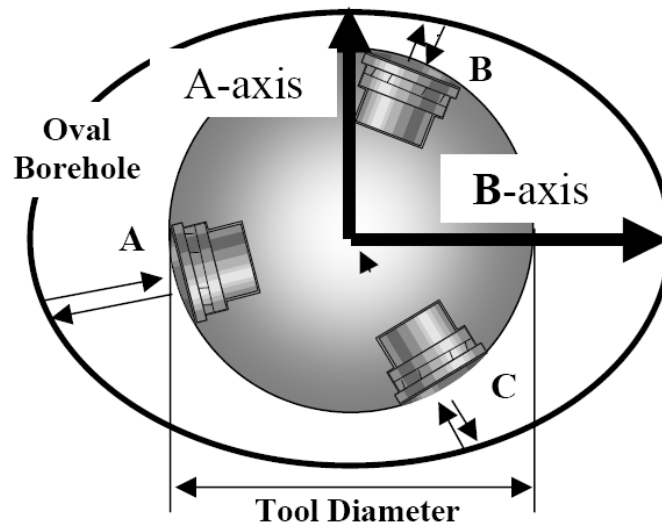
Figure 2-7. Ellipse Fitting through 3 Points [13]

2.3.3 Origin of borehole ellipticity

Under borehole ellipticity we understand a borehole that is not washed out in a circular and/or irregular fashion. The concept of borehole ellipticity assumes a directional aspect of the borehole break-out. Especially in deviated wells oriented borehole ellipticity can be caused by drill pipe wear and key seating, bit tilt or side slip in soft formations.

Highly deviated and horizontal boreholes will commonly not be circular even if no washouts occur. The bit will commonly be drilling with a slight angle to the tangent to the long axis of the borehole (bit tilt). This will cause the borehole to be lightly oval. The direction of the ellipticity will depend on direction of the forces the bit orientation is trying to overcome. However, this effect only creates very slight ellipticity. A more likely cause is the variation in formation hardness. In an inclined well with fairly horizontal formations, when the bit enters soft formations it will trend to drop side slip. If the formation becomes hard it will tend to build when it hits the soft hard interface. These changes in direction create ellipticity in the well bore. A similar well bore profile may also be caused by slide-rotate-slide-rotate drilling.

The side slip will vary with the hardness of the formation and the side force and a stepping type of profile maybe created. This can be seen in Figure 2-8 where the minimum measurement increases and decreases periodically. Although this effect is slight in comparison to the breakout at the top of this section, it is visible in Figure 2-9 that the circularity increases and decreases periodically (looks like beads) in the bottom three quarters of the section where the hole is not washing out. [13]
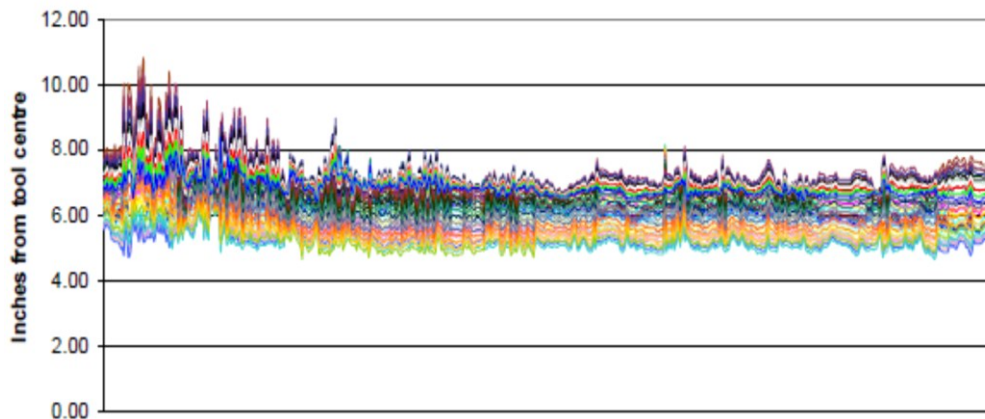
Figure 2-8. Standoff interpolation [13]
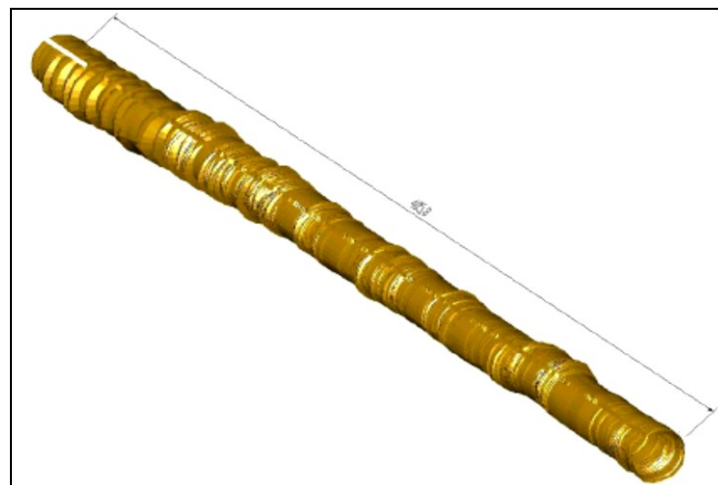
Figure 2-9. Borehole caliper image [13]

2.4   Wellbore stability monitoring

Prior to drilling, all the elements of the wellbore stability monitoring have to be configured. An expert in optimization and wellbore stability should be located at the well site. The responsibilities of the expert are to:

1. Operate the real-time pore pressure and geomechanical models identifying any differences between the predrilled and real-time results
2. Compare the pressure while drilling measurements and static mud weights to the calculated upper and lower bounds from these models
3. Plot the actual torque and drag against the expected modeled values and identify any deviation between the two as an indicator of changing hole condition
4. Monitor drilling parameters and cuttings and carvings for signs of wellbore instability
5. Finally, to communicate all findings to the drilling team to anticipate drilling surprises and recommend appropriate actions

Using the mentioned method, to develop the workflows and processes to deliver information that would impact non-productive time through the integration of the

information from the wellbore stability monitoring with the imaging and caliper information.

Figure 2-10 illustrates the image and caliper measurements taken within an in-gauge 12 ¼-in. hole, showing both real-time and memory images.
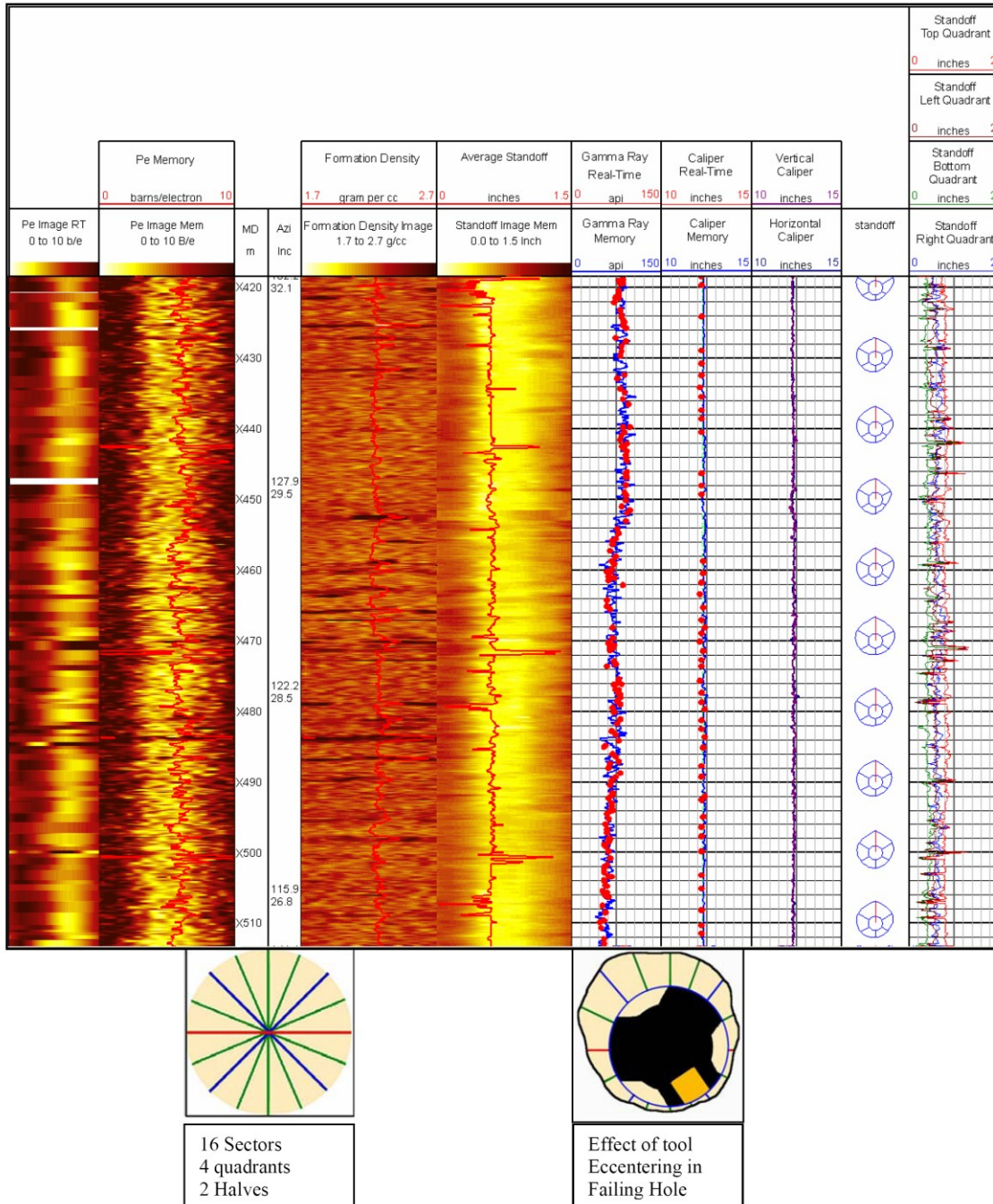
Figure 2-10. Example image and caliper measurements. 1:500 Scale [12]

The color gradation is used to show the changing measurement at the respective orientation around the wellbore. In certain configurations, the diameter of the tool at the measurement point is slightly less than the hole diameter. In any deviated hole, this difference causes the tool not to be perfectly centralized through gravity and BHA side

forces leading to an eccentering effect where the measurement point is closer to the formation when facing in one direction than the other. In this instance and where hole angle is being built, the standoff measurement and correspondingly the volume of mud and barite when the tool is facing the low side of the hole is less than the measurement when the tool is facing the high side of the hole.

There are limits to the distance from the transceiver that the caliper can measure. Once the distance between the transceiver and the wellbore becomes too large, the acoustic signal becomes too attenuated to be detected. The amount of attenuation also increases with increasing mud density. Another potential effect is as follows:

If the wellbore begins to break down and the wellbore surface is not parallel or sub parallel to the transceiver face, a deflection of the acoustic energy away from the transceiver face can occur causing a loss of return signal. If attenuation or deflection of the signal occurs, the response can be used quantitatively to establish excessive hole enlargement as a value is returned that is less than the normal standoff in an in-gauge hole. [12]

Real-time LWD image data quality have been traditionally low because of the inability to transmit the large amount of high definition image data to surface through limited channel bandwidth offered by mud-pulse telemetry systems. However, recent advancements in mud-pulse telemetry technology mark a step-change improvement in providing faster data rates as well as from greater depths. The industry leading system is achieving up to and even beyond 20 bits/sec, which is more than 500% faster than the 3 bits/sec industry standard. Combining advanced high speed mud-pulse telemetry with state of the art image compression technology allows transmission of high quality images that are available in real time and are suitable for determining fine scaled geological features such as thin lamination, fractures (natural and induced), cross bedding, vugs, concretions, accurate breakout definition, etc.

The introduction of wired-pipe technology (WPT) communication systems offers even wider real time bandwidth, allowing reliable, bi-directional data transmission at speeds up to 57,600 bits per second. Data transmission rates of up to 2 Mbps have been achieved in testing facilities. This new communication channel provides full, real time memory access to most of the formation evaluation measurements, essentially eliminating the distinction between real time, memory and post-acquisition analysis.

The high definition electrical imaging service is benefiting to a large extent from this increase in bandwidth. The large volume of data acquired downhole still dictates image compression before transmitting the data to surface. However, image compression ratios achieved with wired pipe systems are significantly lower compared to ratios achieved with mud-pulse telemetry systems. As a consequence, real time images transmitted through wired-pipe systems are yielding unmatched resolution of close to memory image definition. The gain in real-time image resolution greatly reduces uncertainty when interpreting geomechanical features such as drilling induced fractures and borehole breakout. Wellbore

integrity can now be monitored during the drilling process to facilitate drilling and completion decisions to reduce or eliminate NPT (Figure 2-11). [6]
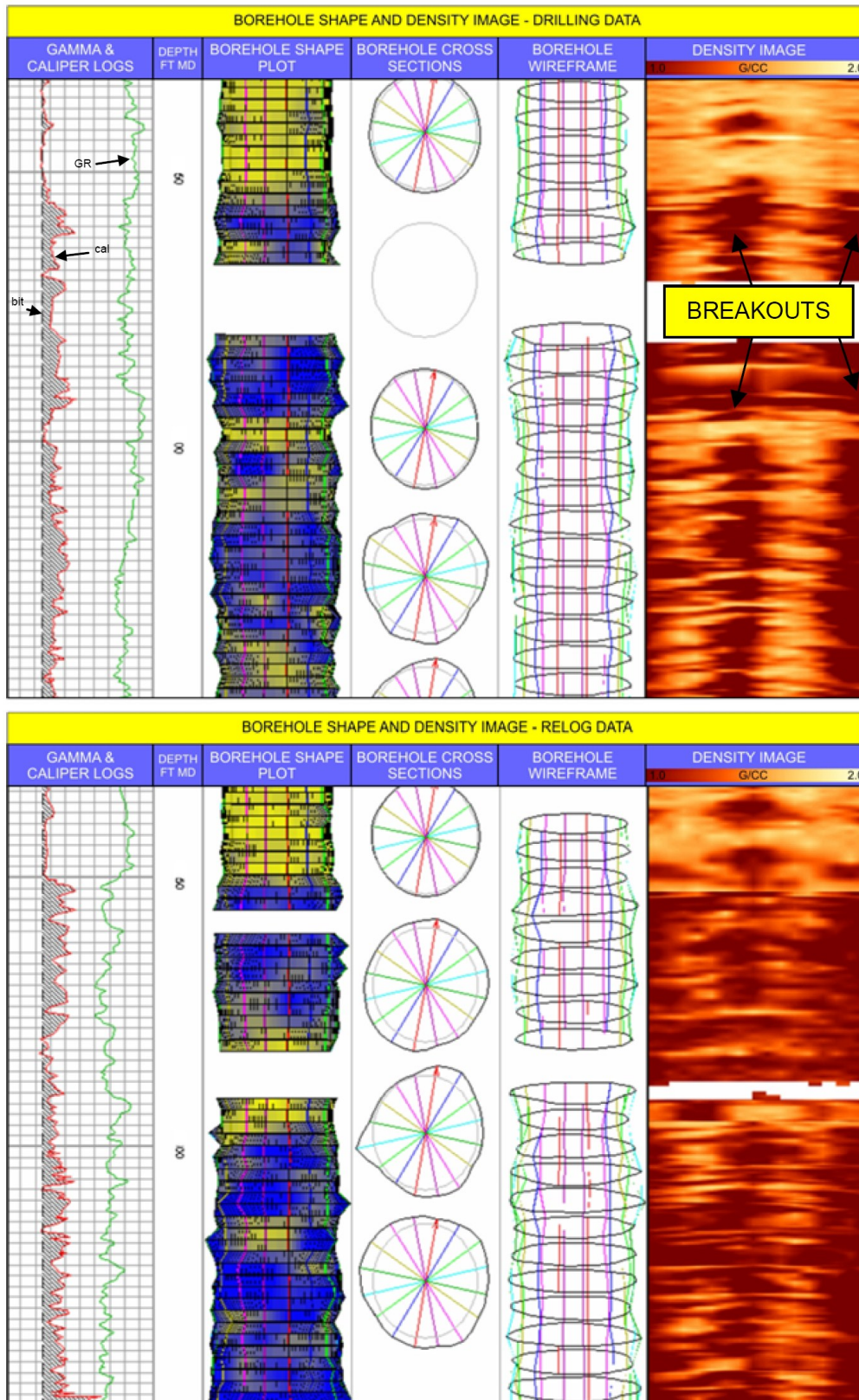
Figure 2-11. Density images and borehole shape plots showing borehole condition 95 hours after penetration by the bit (drilling images) and after a time lag of 63 hours (re-log images). The borehole widening also affects the quality of other logs. [6]

2.5 Comparing the LWD and wireline logging environment

There are three fundamental differences between LWD and wireline electrical image logs:

- **Time of acquisition**: wireline logs are usually acquired 2-10 days after drilling whereas LWD logs are acquired minutes to hours after drilling. With increasing time, filter cake build up and invasion increase as do the likelihood and potential severity of breakout and other types of wall damage. In addition, induced fracture aperture will not be at a maximum and is likely to be masked by filter cake. LWD data can be acquired again on tripping out of hole, up to a few days later, in which case the borehole environment may be closer to that of wireline.

- **Physical environment**: image acquisition on a dynamic platform (e.g. rotating) is subject to vibration with dynamic pressure and temperature changes, whereas wireline images are acquired at equilibrium with a static fluid column and tool motion determined largely by the logger.

- **Method of measurement**: wireline electrical image logs are made using a series of buttons on pads pressed onto the borehole wall, providing high resolution but only partial borehole coverage (Figure 2-12). Conversely, LWD electrical images use drill string rotation to scan the borehole wall using a single sensor providing full borehole coverage and the ability to interpret non sinusoidal and discontinuous features on the borehole wall. [9], [43]
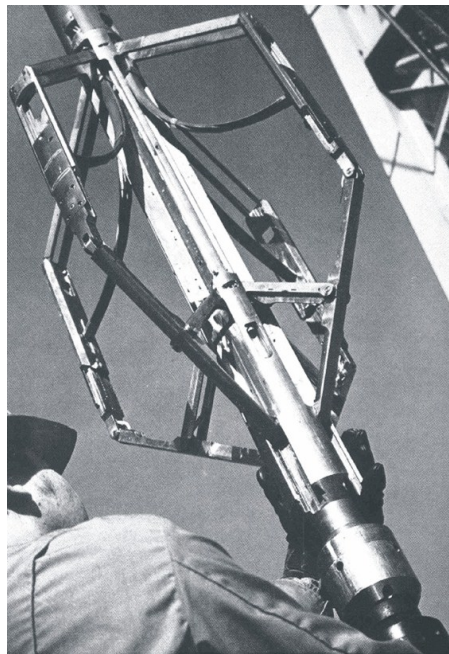
Figure 2-12. Wireline caliper log [46]

2.6 Using images in real time

Wellbore instability problems while drilling range from slight (vibration, stick-slip, irregular weight transfer) to severe (stuck pipe, lost circulation, wellbore collapse). Determining a real time solution is a challenge as the indications are often the same but the remedial action

different. Before the beginning of high resolution LWD images, insufficient information in real time meant certain features (ledges, spiraling, chemical disequilibrium and unconsolidated sandstone) may have been misinterpreted as borehole stress indicators.

This difficulty has been seen by the availability of high resolution images while drilling, which can be used in three main ways to aid interpretation:

1. **Structural interpretation**: accurate dip selection in all wellbore orientations can be used to examine the relationship of bedding to the wellbore, with reference to the pre-well model and to check that geometry dependent mechanical assumptions are correct. Dips can be used to confirm surface orientations in a seismic model, allowing prediction of pressure and mechanical changes.

2. **Sedimentary interpretation**: identification of lithology and fabrics allows comparison with similar environments. Successful identification of thin beds or inter sandstone mud rock layers will enhance the understanding of potential pressure compartmentalization and differentiating them from borehole problems (ledging and spalling).

3. **Geomechanical features**: the identification of breakout, drilling induced fractures DIFs, enhancement of natural fractures and shear plane failures indicate how the formation (and the borehole) is reacting to the drilling process (Table 2-1) and their magnitude can be compared to the pre-well model. These features are the most critical for determining changes to drilling parameters.

Table 2-1. Image features and means of identification while drilling, from near-time re-logging and from post-drilled logging [9]

Feature	Visibility			Relative Importance	When Important
	Real Time	Near Time	Post Drill		
Breakout	moderate	high	high	high	real time
DIF	moderate	high	poor	low*	real time
Shear plane failure	low	moderate	high	high	real time
Natural fracture	high	high	high	low	post-well
Ledging	high	high	high	moderate	post-well
Key seating	low	moderate	high	moderate	post-well
Debris / filtercake	low	moderate	high	moderate	post-well
Washout	low	moderate	high	moderate	both

During drilling, a graphical guide (well profile plot marked with a history of geomechanical criteria) serves as a practical tool for hazard avoidance at the rig site. This summary guide can then be updated with major boundaries, lithology, relevant dips and instability features, with comments on severity and recommendations for qualification as drilling proceeds. Therefore, the following methodology is proposed when using high resolution images in real time (Figure 2-13):

- **Bedding dip direction identification**: if not in agreement with the pre-well model then the breakout model may need recomputed to define acceptable limitations of angular width. The new dips should be checked against proposed well path in case

the relative angle between the well and the formation exits the limits imposed by the stability model.

- **Lithology Evaluation**: high resolution images allow update to lithology interpretation in real time. In addition, features such as cemented nodules, rubble zones and cross-bedding present unique hazards that may require specific changes to drilling practice.
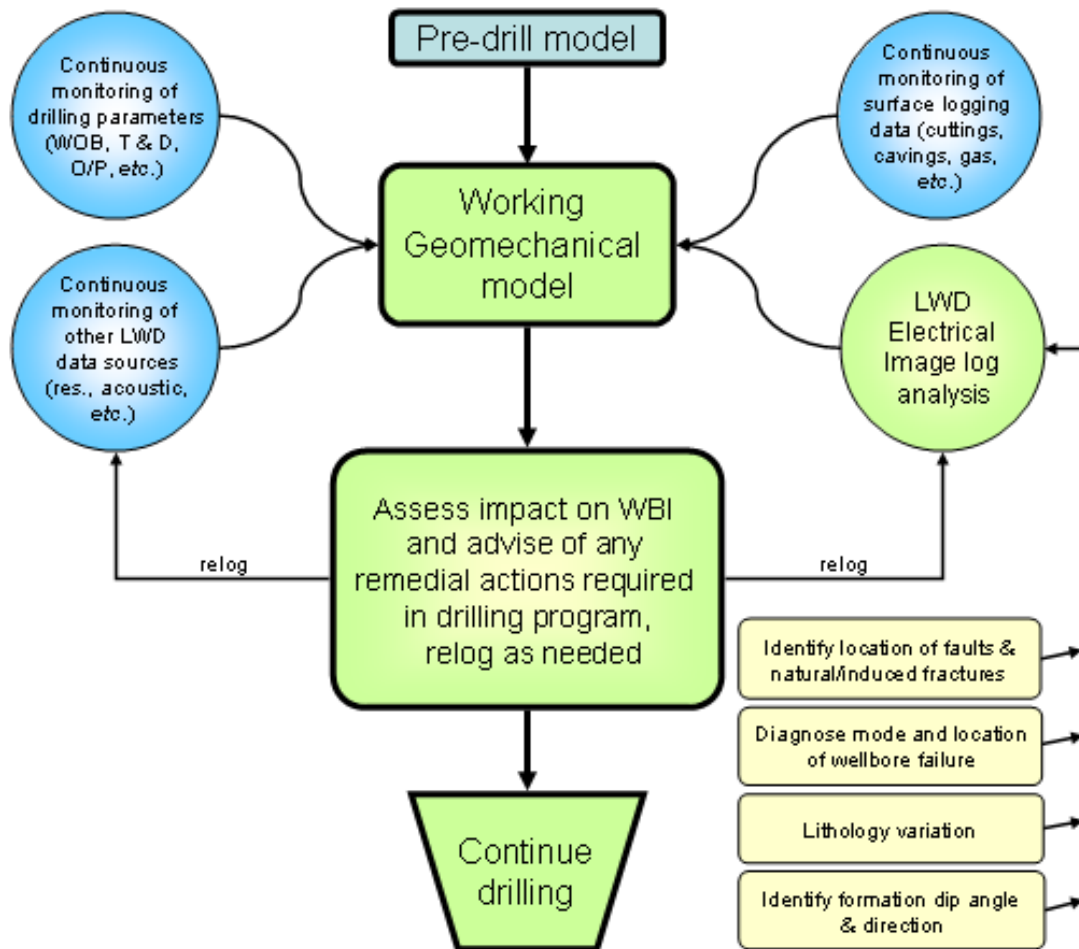
Figure 2-13. Real time wellbore integrity operations flowchart incorporating LWD images. [9]

- **Wellbore instability issues analysis**: the presence and orientation of DIFs and breakout define the upper and lower limits of the drilling stability window. There are several causes of features that appear as borehole breakout therefore the selection of correct remedial action is critical.
- **Faults and fractures**: these indicate weaknesses within the rock and local variations in the stress field. Features, not directly related to pressure or stability, should also be noted, including ledges, key-seating and other borehole asperities. The combination of resistivity and caliper images will be useful for identifying these features and differentiating them from critical wellbore instability features. [9]

2.7 Conclusion

By using all the information and experiments that have been performed to detect wellbore instabilities, ultrasonic caliper could be used to determine the diameter and the shape of the borehole. By using these data in real time, a 3D image of the wellbore could be sketched. However by increasing the number of ultrasonic caliper sub along the drill string 4D image of the borehole could be monitored in real time and any changes in wellbore shape or deviation from the borehole diameter could be an indication of the instabilities in the wellbore.

Ultrasonic sensor could be used to determine the speed of sound in the drilling fluid at the desired depth with the pressure and temperature condition downhole. The accuracy of sound velocity in the drilling fluid will causes to increase the accuracy of the distance measured by the ultrasonic caliper.

3- Ultrasonic Sensor

3.1 Ultrasonic sensor

Ultrasonic sensors are based on measuring the properties of sound waves with frequency above the human audible range.

Ultrasonic sensors emit a sound pulse that reflects off of objects entering the wave field. The reflected sound, or echo is then received by the sensor (Figure 3-1). Detection of the sound generates an output signal for use by an actuator, controller, or computer. The output signal can be analog or digital.

Ultrasonic sensing technology is based on the principle that sound has a relatively constant velocity. The time for an ultrasonic sensor's beam to strike the target and return is directly proportional to the distance to the object. [18]
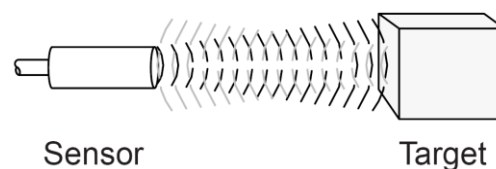
Figure 3-1. Sending echo towards target and received it back [18]

Ultrasonic sensors can be used for several different applications, for example [21]:
- Diameter detection
- Height detection

- Level measuring
- Counting

Ultrasonic sensors are utilized for many purposes. For examples of these applications, please refer to the examples in Table 3-1. Level detection of continuous wave signals (example 1) is used for counting machines and approximate switches due to the simple circuit construction of these devices. Example 2 is used in devices such as automatic doors where the environment is very changeable. The system is arranged so that the instrument may actuate only when a certain number of reflected pulses is detected. Example 2 is also used for measuring distance to an object, such as the backup sensors of cars. Example 3 is an application utilizing the phenomenon by which the Doppler Effect produces a modulated signal as an object moves closer or farther away. This is often used for intruder alarm systems. Example 4 is an application utilizing the change of sound velocity according to the density and the flow speed of a gas. Example 5 is a method used to count the number of Karman vortex generated against flow speed and utilize phenomena that ultrasonic signals level are reduced as Karman vortex passes into the sensor. [19]

Table 3-1. Application example [19]

No.	Function Method	Performance Principle ($\boxed{S}$: transmitter / $\boxed{R}$: receiver)	Applications
1	Detection of Signal level of continuous wave		Counting instruments Access switches Parking meters
2	Measurement of pulse reflection time		Automatic doors Level gauges Automatic change-overs of traffic signals Back sonars of automobiles
3	Utilization of Doppler effect		Intruder alarm systems
4	Measurement of direct propagation time		Densitometers Flowmeters
5	Measurement of Karman vortex		Flowmeters

Sound waves are propagated through a medium by the vibration of molecules. Within the wave, regular pressure variations occur with alternating areas of compression, which

correspond to areas of high pressure and high amplitude, and with areas of low pressure zones where widening of particles occurs. Sound waves are expressed as sine waves with the following properties:

$$v = \lambda \times f$$

<div align="right">**Equation 3-1**</div>

Wavelength (λ) is the distance between two areas of maximal compression. The importance of wavelength is that the penetration of the ultrasound wave is proportional to wavelength Figure 3-2.
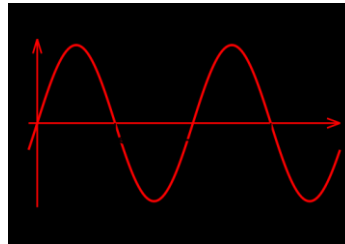
Figure 3-2. Wave length [18]

Frequency (f) is the number of wavelengths that pass per unit time. It is measured as cycles (or wavelengths) per second and the unit is Hertz (Hz). It is a specific feature of the crystal used in the ultrasound transducer. It can be varied by the operator within set limits - the higher the frequency, the better the resolution, but the lower the penetration.

Propagation Velocity (v) is the speed that sound waves propagate through a medium and depends on medium density and compressibility. [18], [48]

3.2 Cycle period

A short ultrasonic pulse is transmitted at the time 0, reflected by an object. The sensor receives this signal and converts it to an electric signal. The next pulse can be transmitted when the echo is faded away. This time period is called cycle period. (Figure 3-3) [21]
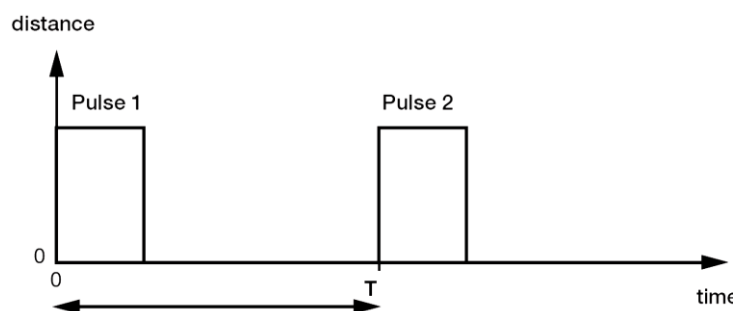
Figure 3-3. Cycle period [21]

Sensors with [21]:

- Long sensing ranges have long cycle periods and slow reaction time
- Short sensing ranges have short cycle periods and fast reaction times

3.3 Angle of beam

The energy of the ultrasonic pulse is transmitted in form of a cone along the transducer axis. The highest intensity is on the axis and decreases with rising angles. The angle of beam is defined by the angle through which the energy of the ultrasonic pulse is reduced by 33% of its maximum value. The best detection is given by an object that stands vertical to the transducer axis. To give a save detection, the object should not have a greater angle than half of the angle of beam ($\alpha/2$). (Figure 3-4) If the object is canted at a greater angle, there is no reflection of the ultrasonic pulses. An object with a flat surface and canted at an angle of 45° to the transducer axis refracts the ultrasonic pulse in an angle of 90°. An ultrasonic pulse can be compared to a light beam. [21]
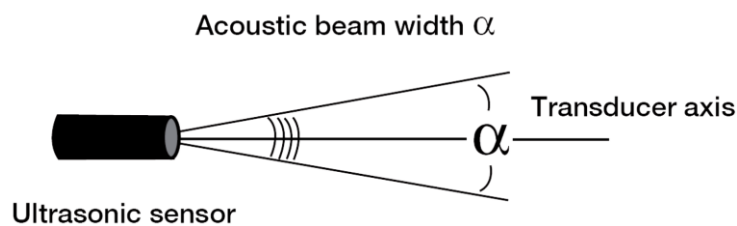
Figure 3-4. Acoustic beam angle [21]

3.4 Voltage amplitude

During the transmission the voltage amplitude of the ultrasonic pulse is changing. The pulse period of the ultrasonic pulse depends on the duration of the transmission pulse and on the ringing time of the transducer (Figure 3-5). [21]
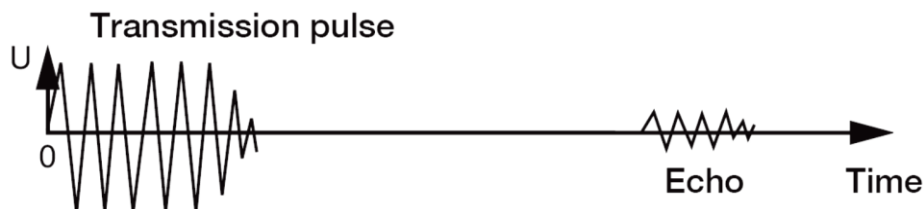
Figure 3-5. Amplitude of signal voltage [21]

3.5 Sensing range and effective beam

The sensing range of an ultrasonic sensor is the area between the minimum and the maximum sensing limits.

Ultrasonic sensors have a small unusable area near the face of the sensor. If the ultrasonic beam leaves the sensor, strikes the target, and returns before the sensor has completed its transmission, the sensor is unable to receive the echo accurately. This unusable area is known as the blind zone. (Figure 3-6)
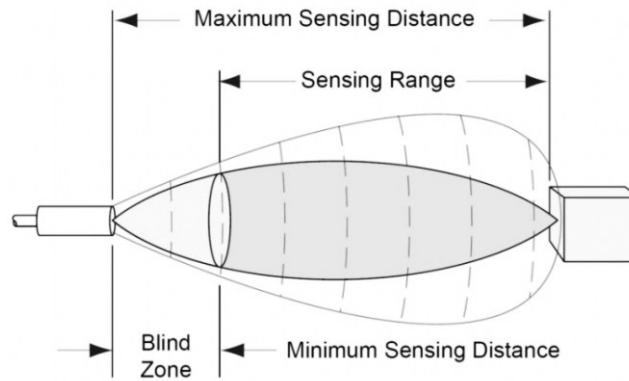
Figure 3-6. Blind zone and maximum range of the sensor [18]

Three different properties of the received echo pulse may be evaluated, for different sensing purposes. They are [18]:

- Time of flight (for sensing distance)
- Doppler shift (for sensing velocity)
- Amplitude attenuation (for sensing distance, directionality, or attenuation coefficient)

3.5.1 Maximum sensing distance

Target size and material determine the maximum distance at which the sensor is capable of seeing the object. The harder an object is to detect, the shorter the maximum sensing distance can be. Materials that absorb sound (foam, cotton, rubber, etc) are more difficult to detect than acoustically reflective materials, like steel, plastic, or glass. If detected at all, these absorbent materials can limit maximum sensing distance. (Figure 3-7) [18]
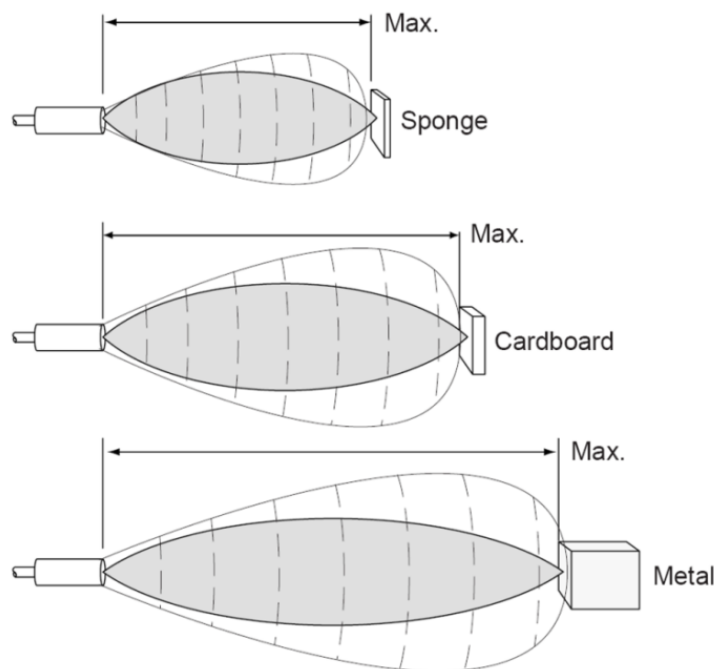
Figure 3-7. Maximum sensing range of the sensor [18]

3.5.2 Effective beam

When the transducer vibrates, it emits ultrasonic pulses that propagate in a cone-shaped beam. This cone can be adjusted, usually via the use of a potentiometer, to widen or extend the sensing range (Figure 3-8). [18]
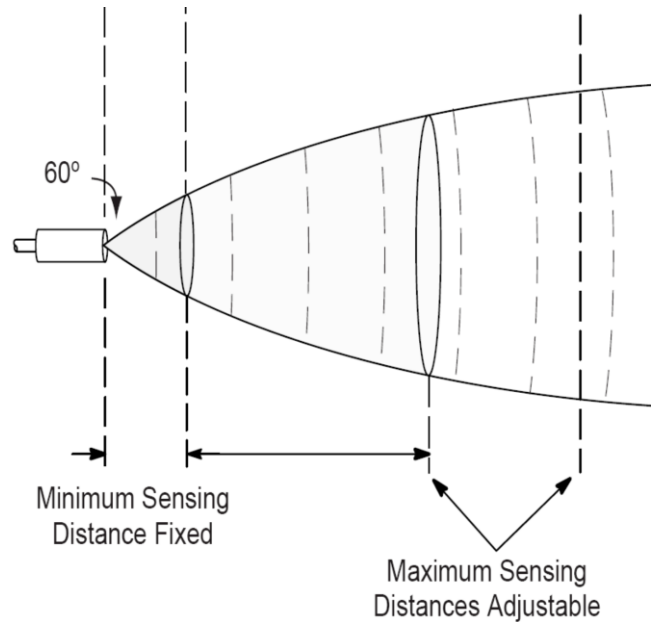
Figure 3-8. Effective beam of the sensor [18]

3.6 Modes of operation

There are two basic modes of operation: opposed mode and diffuse (echo) mode.

In opposed mode, one sensor emits the sound wave and another, mounted opposite the emitter, receives the sound wave. (Figure 3-9)
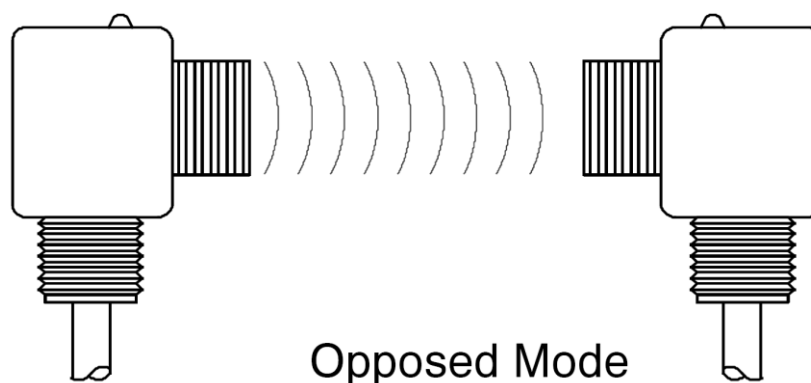
Figure 3-9. Opposed mode of the sensors [20]

In diffuse mode, the same sensor emits the sound wave and then listens for the echo that bounces off an object (Figure 3-10). [20]
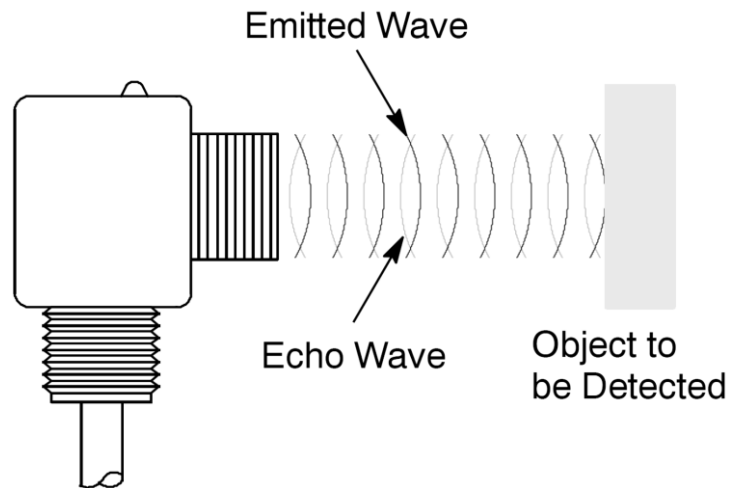
Figure 3-10. Diffuse mode of the sensor [20]

3.6.1 Echo ranging

In echo ranging mode, an ultrasonic transmitter emits a short burst of sound in a particular direction. The pulse bounces off a target and returns to the receiver after a time interval t. The receiver records the length of this time interval, and calculates the distance travelled r based on the speed of sound v:

$$r = v \times \frac{t}{2}$$ **Equation 3-2**

(Note that in many applications; since the transmitter and receiver are at the same location, this distance r will be twice the distance from the sensor to the target). (Figure 3-11) [22]
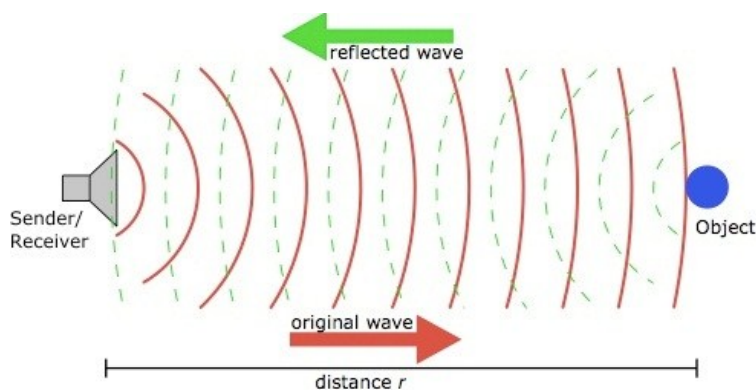
Figure 3-11. Distance of the sensor to the object [22]

3.7 Doppler shift

When a wave reflects off of a moving object, its frequency is shifted by an amount proportional to the velocity of the object. This fact can be exploited in ultrasonic sensing by having the receiver measure not the time of flight but the frequency of the returning echo pulse. Knowing f_L and f_S, the frequency of the listener and source, respectively, the velocity of the wave V, velocity of listener V_L and velocity of the source V_S:[22]

$$f_L = \frac{V+V_L}{V+V_S} f_S$$

<div align="right">**Equation 3-3**</div>

3.8 Signal attenuation

Ultrasonic sound attenuates much faster than audible sound when propagating through air. By measuring the intensity of the returning pulse, an estimate of the distance travelled can be made using the following equation:

$$I = I_0 e^{-ax}$$

<div align="right">**Equation 3-4**</div>

where I and I_0 are the received and the original intensities, respectively, and where a is the attenuation coefficient (a property of the medium) and x is the distance travelled by the wave. Attenuation may also be caused by an increased angle between the target and receiver, which may even deflect the echo somewhere else and not be heard at all. The effect of distance and angle on the amplitude of the received signal is illustrated in Figure 3-12. [22]
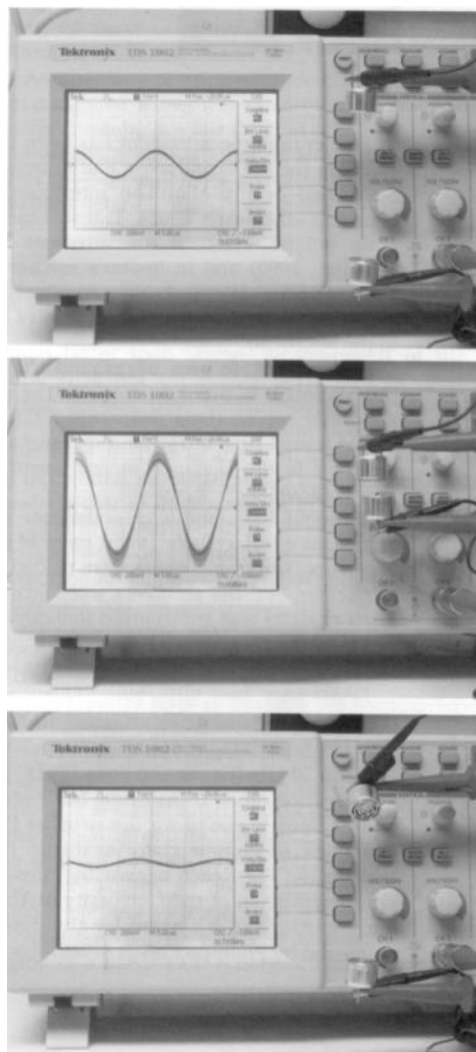
Figure 3-12. Effect of distance and angle on the amplitude of received signal [22]

3.9 Generating the ultrasonic signal

Ultrasound is most commonly generated as a direct conversion from electrical energy. This is accomplished by applying a rapidly oscillating electrical signal to a piezoelectric crystal attached to a mounting. The charge causes the crystal to expand and contract with the voltage, thereby generating an acoustic wave. The waves are later detected by a piezoelectric receiver, which converts the waves back into voltage using the same method.

3.9.1 Single versus separate units

Separate transmitting and receiving transducers are placed immediately next to each other and housed as a single unit. A single transducer may be used for transmission and receiving, but it takes time for the transducer to change modes, presenting a challenge to short-distance measurement. Another strategy is to place transmitters and receivers on independent bodies.

3.9.2 Pulsed versus continuous measurement

Time-of-flight-based sensing requires emitting a pulse and waiting for it to return. These waiting time limits the speed with which successive measurements can be made, without risking confusion. However, Doppler- and attenuation-based sensing devices do not have the same restrictions: a constant wave of ultrasound may be emitted, and the received wave's attenuation or frequency continuously analyzed. [18]

3.10 Sensor spacing considerations

Spacing between sensors is determined by their beam angles. Sensors must be spaced so they do not interfere with each other. This interference is called crosstalk (Figure 3-13).
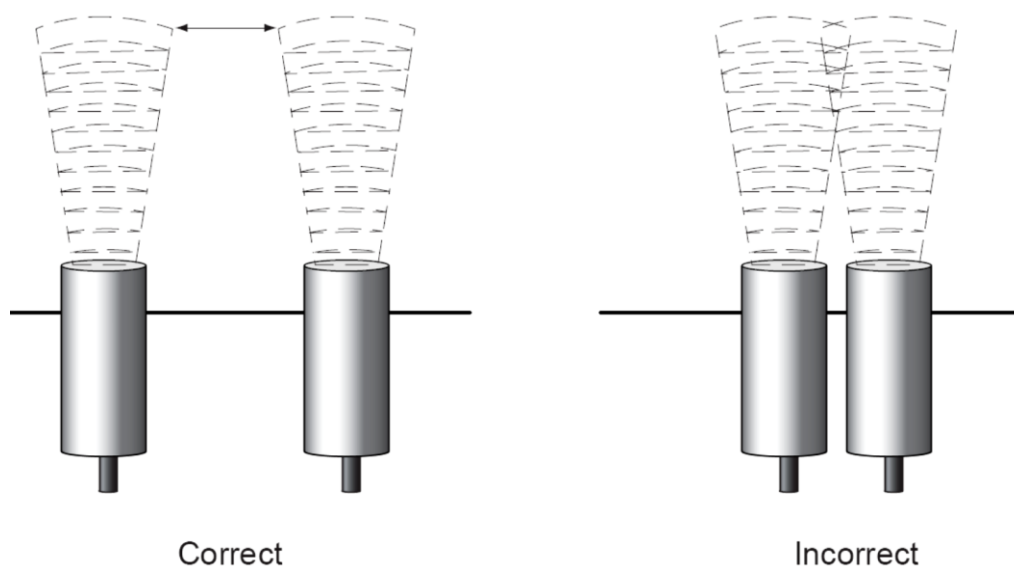
Figure 3-13. Spacing between sensor and crosstalk problem [18]

When more than one ultrasonic sensor is in use, spacing's should be considered as an important rule. However, many factors such as temperature, angle, and material may affect measurements.

Weather. Temperature and humidity affect the speed of sound in air. Therefore, range finders may need to be recalibrated to make accurate measurements in a new environment.

Currents. The surface temperature of a target can also influence the sensing range. Radiated heat from high temperature targets distorts the sound beam, leading to shortened sensing range and inaccurate readings. (Figure 3-14)
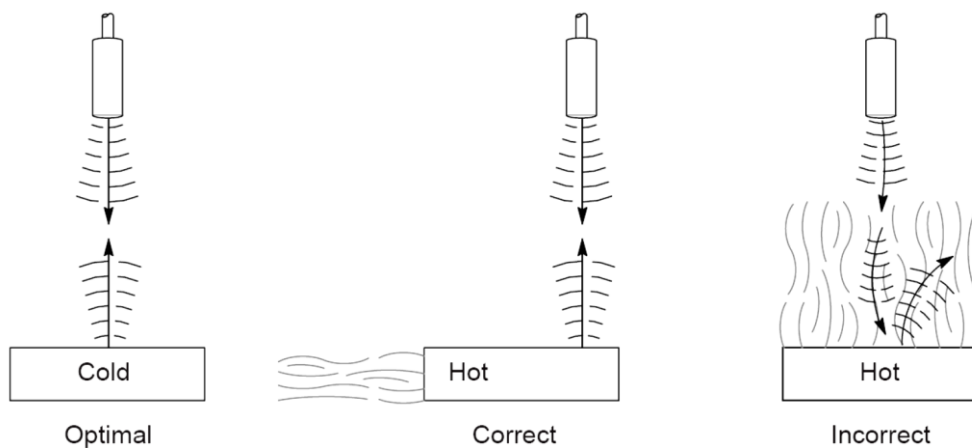
Figure 3-14. Effect of temperature on the reflected echo [18]

Angle. For the transmitted wave to echo back to the receiver, the target surface must be perpendicular to the transmitter. Round objects are therefore most easily sensed since they always show some perpendicular face. When targeting a flat object, care must be taken to ensure that its angle with respect to the sensor does not exceed a particular range. (Figure 3-15)
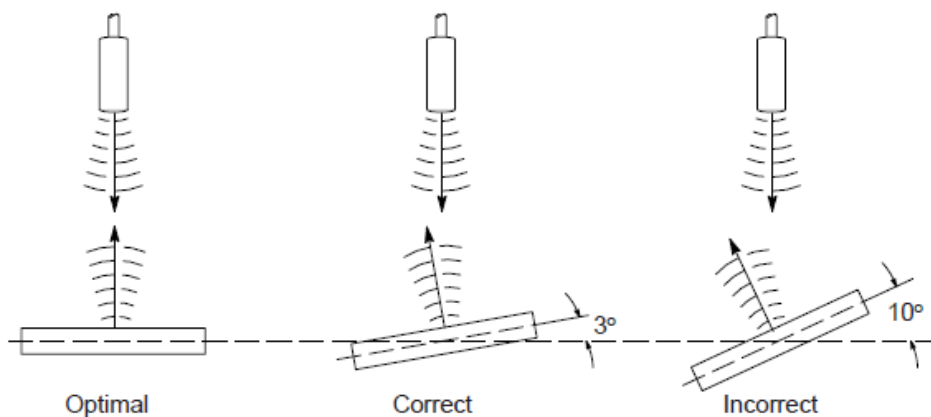
Figure 3-15. Effect of target angle with respect to sensor's face [18]

When sensing the sound-scattering surfaces of irregularly shaped targets, the approach angle becomes less critical. (Figure 3-16) [18]
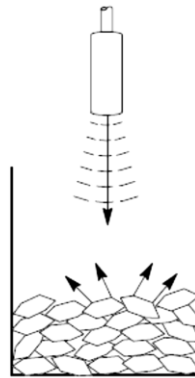
Figure 3-16. Effect of irregularly shaped targets on reflected echo [18]

3.11 Construction and operation principles

When voltage is applied to piezoelectric ceramics, mechanical distortion is generated according to the voltage and frequency. On the other hand, when vibration is applied to piezoelectric ceramics, an electric charge is produced. By applying this principle, when an electric signal is added to a vibrator, constructed of two sheets of piezoelectric ceramics or a sheet of piezoelectric ceramics and a metal sheet, an electric signal is radiated by flexure vibration. As a reverse effect, when an ultrasonic vibration is added to the vibrator, an electric signal is produced. Because of these effects, piezoelectric ceramics are utilized as ultrasonic sensors.

3.11.1 Open structure type ultrasonic sensors

As shown in the diagram of an ultrasonic sensor (Figure 3-17), a vibrator is fixed elastically to the base. This vibrator is a combination of a resonator and a vibrator which is composed of a metal sheet and a piezoelectric ceramics sheet. The resonator is conical in order to efficiently radiate the ultrasonic waves generated by the vibration and also in order to effectively concentrate the ultrasonic waves at the central part of the vibrator.
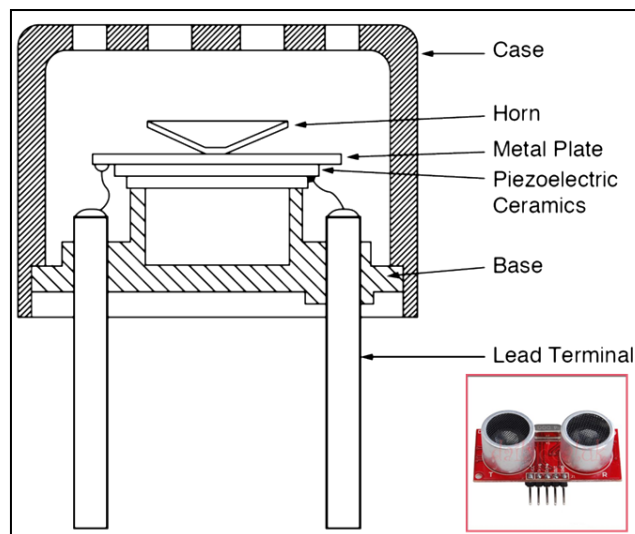
Figure 3-17. Open structure type ultrasonic sensor [19]

3.11.2 Enclosed type ultrasonic sensor

Ultrasonic sensors for outdoors use are sealed to protect them from dew, rain and dust. Piezoelectric ceramics are attached to the top inside of the metal case. The entrance of the case is covered with resin. (Figure 3-18) [19]
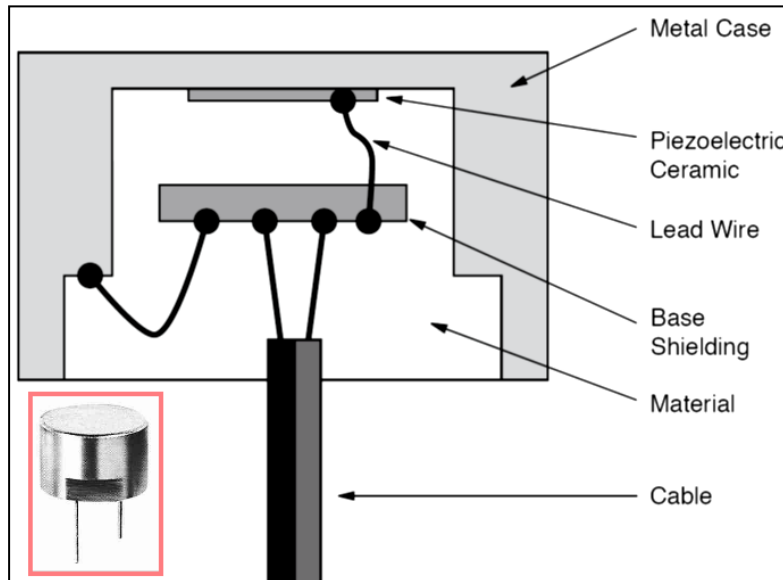
Figure 3-18. Enclosed type ultrasonic sensor [19]

3.12 Hardware configuration of distance measurement

Figure 3-19 show the hardware installation for measuring distance and it is called the "pulse reflection method" which makes it possible to count the number of reference pulses. This method is used to measure reflection time up to the object between transmitting pulse and receiving pulse of the ultrasonic wave. [20]
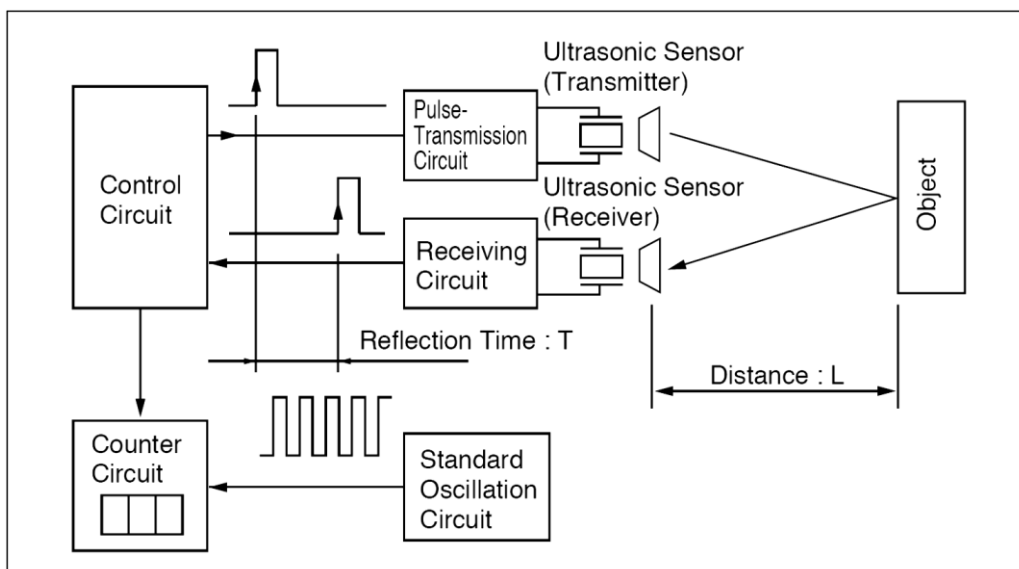
Figure 3-19. Principles of measuring distance [20]

4- Ultrasonic Caliper Development

4.1 Ultrasonic caliper

An ultrasonic sensor has been developed for MWD (measurement while drilling) and LWD (logging while drilling) applications that perform real time borehole caliper measurements and also wellbore stability monitoring. The caliper determines the shape of the borehole with a defined accuracy and resolution. These measurements are transmitted to the surface and used to compensate MWD and LWD measurements. Furthermore, with early and accurate real-time caliper measurements, borehole instability can be detected. For example, an elliptical wellbore can indicate the maximum and minimum stress directions. Borehole enlargement or washout can indicate that the mud is too heavy or too reactive with the formation. An under-gauge borehole might indicate bit wear.

Another use of ultrasonic caliper tools is to offer a method for calculating borehole volumes. On the final bit run, the sensor may collect the caliper data while tripping out of the borehole for determining borehole size for the estimation of cement volumes. [4], [16], [44]

Real-time usage of ultrasonic caliper causes the early detection of borehole instability. The caliper supports the driller in making proper decision such as reaming a critical zone, changing the flow rate to reduce borehole erosion, or modifying the string RPM to reduce shocks with the formation. [24, [36]

Other applications of ultrasonic caliper tools might include real-time detecting of casing wear and borehole stability, evaluation of borehole cleaning, and determination of tight spots or formation ledges. [4], [37], [38]

4.2 Simulating drill string movement

To simulate different positions and geometries of an ultrasonic sensor inside a borehole, a special test robot was built to simulate drill string movements as well as drill string rotation with the sensor attached. This robot has the capability to move with controlled speed in three directions (x, y and z) and also to rotate with different revolutions per minute up to 220 RPM. The limitations for the directional movements are ±20 cm for the horizontal x- and y-axes and 40 cm for the vertical z-axis (Figure 4-1). [5]

Figure 4-1. Test robot used to simulate drill string movement

4.3 Simulating wellbore

A cemented wellbore was built to simulate the borehole for different ultrasonic experiments. The wellbore has a diameter of 40 cm and the depth of 50 cm. The wellbore was mounted at a metal plate with holes in it so that the drilling fluid could be filled in and dumped out easily (Figure 4-2). In addition, gas can be injected through these holes into the drilling fluid for special experiments. [5]
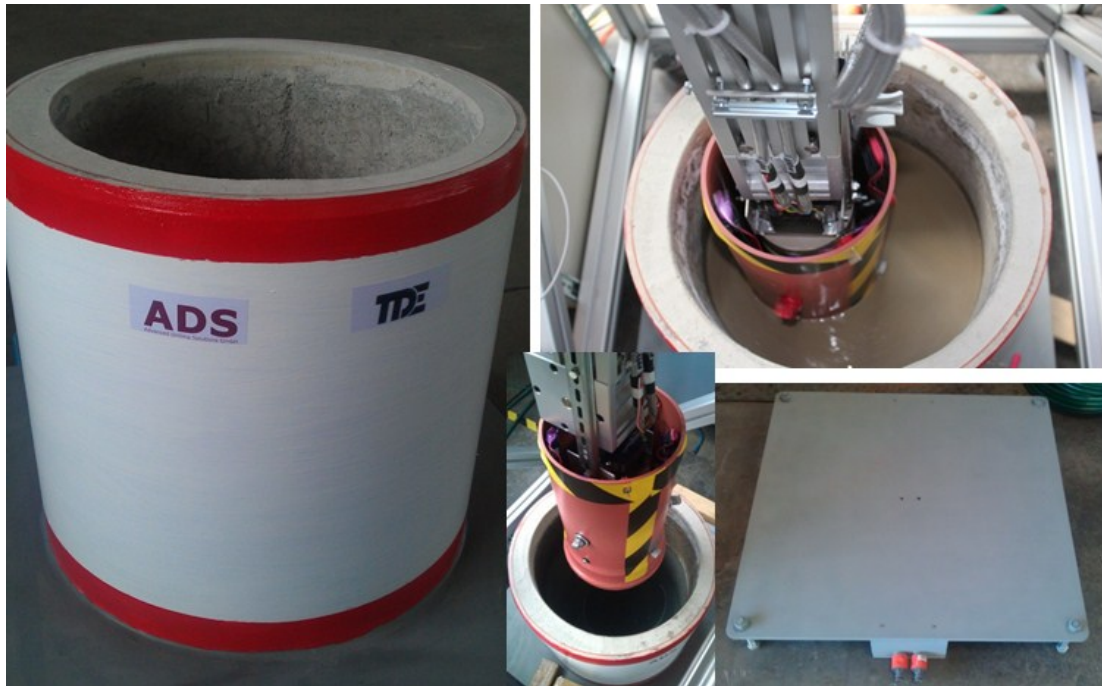
Figure 4-2. Cemented wellbore used to simulate borehole

4.4 Ultrasonic sensor measurement principle

Ultrasonic sensors are based on measuring the travel time of sound waves, usually with frequencies above the human audible range. Such sensors emit a sound signal which will be reflected by objects entering the wave field. If the reflected signal – also denoted as echo – propagates towards the receiving component of the sensor, it is picked up by that component; the measured component thereby is usually the travel time (Figure 4-3).
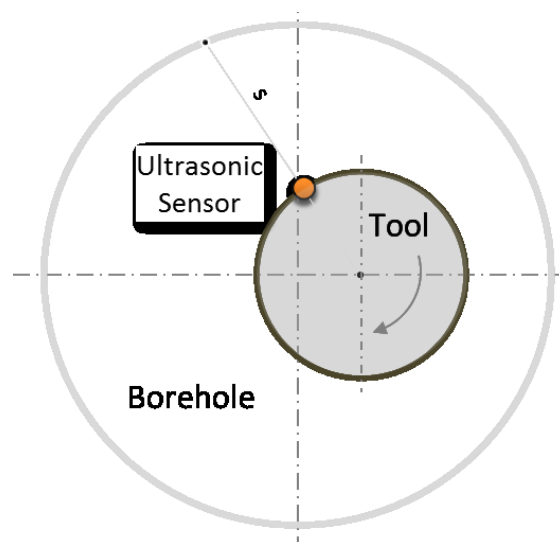
Figure 4-3. Distance of the sensor from the wellbore wall

The sensor's main component is a piezoelectric ceramic. During the electrical excitation, that ceramic sends an acoustic signal – normally a pulse or a sequence of pulses. This signal travels further through the mud, hits the borehole wall and returns back to the receiver

following wave propagation rules. If that signal touches the receiver, an electrical signal is generated by the ceramic. The sensor electronics amplifies that signal and measures the travel time – the time of flight – of the acoustic wave from the transmitter across a reflector – in the current case the borehole wall – back to the receiver. This measured time of flight which is also denoted as two-way travel time, enables the computation of the distance between the sensor at its current position and the borehole wall. If, in addition to the travel time, the signal amplitude is measured, the acoustic attenuation can be calculated. [23], [39]

Based on that pulse-echo technique, the distance from the sensor to the borehole wall can be calculated with the two-way travel time by

$$S = v_m \frac{t}{2}$$

Equation 4-1

S denotes the standoff, v_m the mud's acoustic velocity and t the two-way travel time, the time difference between pulse emission and echo arrival, or in other words, the time difference between transmitter firing and echo detection of the borehole wall signal. [4], [17], [26], [41]

4.5 Ultrasonic caliper package

Three sets of ultrasonic caliper package mounted at the test robot have the diameter of 16.5 cm (6.5 inch), 20 cm (7.8 inch) and 16 cm (6.2 inch). The package consists of a sender and a receiver, a battery package, a micro controller and a counter switch. A separate sensor package is used to determine the acoustic properties of the drilling fluid (Figure 4-4). The reason for that is to estimate the speed of sound of the drilling fluid in-situ, since in real world downhole pressure and temperature are high and thus different compared to surface conditions. Normally correction graphs are used for the evaluation of such high pressure - high temperature conditions.

Figure 4-4. Referenced package, measures speed of sound in mud at different Pressure and temperature

When the sensor distance to the reflector is close to the blind zone or the distance from the wellbore wall is too large, indicating that the calculated distance is not valid for that particular point. In the opposite case, when the measurement is valid, the micro controller calculates the distance using the two-way travel time and sound velocity of the mud.

The sensors which have been used in these experiments have the following specifications. The first ultrasonic sensor was used to do tests in air only (Figure 4-5). The specifications are:

- Voltage: DC 5V
- Ultrasonic frequency: 40 kHz
- Maximal range: 400 cm
- Minimal range: 3 cm

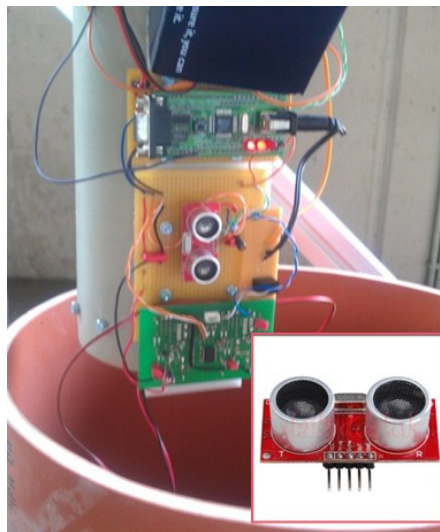**Figure 4-5. Ultrasonic sensor used to test in air**

The second ultrasonic sensor was used to perform experiments in air, water and bentonite mud (Figure 4-6). The specifications are:

- Voltage: +48V to -24V
- Ultrasonic frequency: 40 kHz
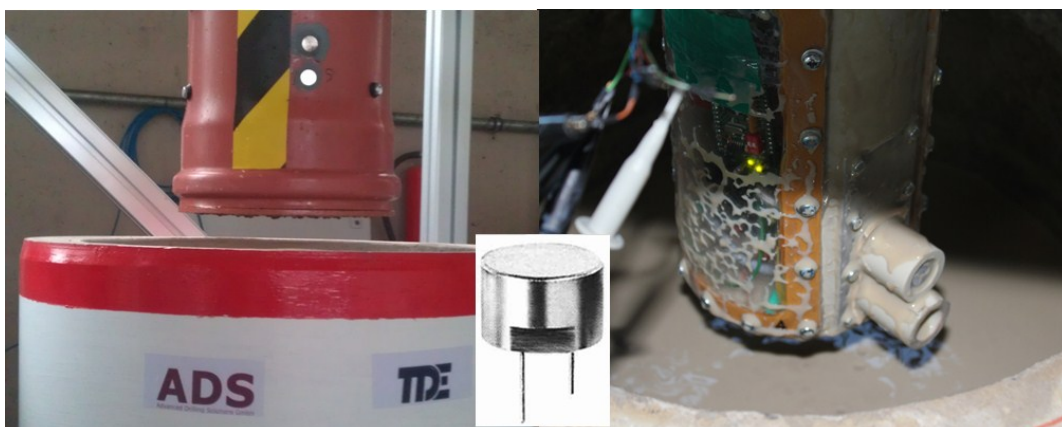- Operating Temperature: -40°C to +80°C

Figure 4-6. Ultrasonic sensor used to test in air, water and bentonite mud

4.6 Ultrasonic electronics – hardware description

Ultrasonic electronics, hardware, consist of six different modules (Figure 4-7):

Power Supply: Main power is provided by a 7 VDC rechargeable battery.

Power Distributer: 7 VDC from main power supply is converted into 5 VDC, 48 VDC and -24 VDC. 5 VDC is used for logic components and the amplification module. To get appropriate acoustic power at the sender +48 VDC and -24 VDC are used to pulse.

Microcontroller: Main logic controller where the software is running. It sends an adjustable number of 40 KHz pulses to the Pulser Module and evaluates receiving signal by the Amplification Module. Measured data are sent via serial line to the Communication Module. Configuration and adjustments can also be done by serial communication.

Communication Module: Via the serial Bluetooth module a wireless connection in between the control logic and a PC/Laptop can be set up. At these external terminal measurement data is received and settings for the control logic can be done.

Pulser Module: The Ultrasound Pulser IC HV748 is generating High Voltage pulses (-24 VDC - +48 VDC) out of a 5 VDC pulsed signal by the microcontroller.

Amplification Module: As the received signal is very small an amplifier is necessary. In this case an amplification module is used which includes three sub-circuits: 1.) AC-Amplifier, 2.) Envelope creator, 3.) Threshold detector. The amplification can be changed by the microcontroller to adjust the signal for the transmission medium. The envelope creator is needed for the threshold measurement. The threshold detector sends a digital signal when the envelope reaches a configurable threshold.
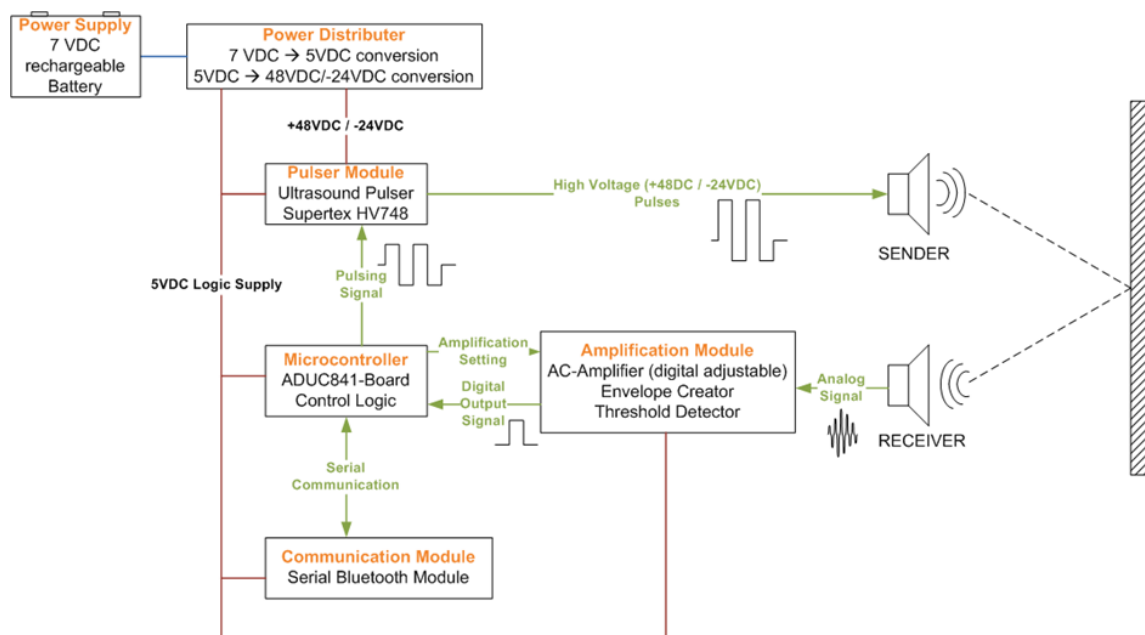

Figure 4-7. Ultrasonic hardware principle

4.7 Ultrasonic software description

The controller software consists of a simple state machine. After the power on reset the hardware is initialized. The state machine starts with incrementing the angle variable and sending a burst signal to the Pulser Module. Afterwards two timers are started. The measurement timer is used to measure the time from pulsing to the received threshold signal. If a delay time is configured, the system delay's the start of the measurement timer. The timeout timer is used to resume the program if nothing is received.

In the second state the measurement timer is stopped when the threshold is detected. When the timeout timer is finished, a jump to the next step is done. To ensure a fixed repetition rate independent of a valid or invalid measurement, the timeout has to be expired before the next state is jumped in, in the software. If the timeout expires before the threshold measurement is done, the measurement timer is stopped, and the measurement value is reset to zero. Afterwards the measurement timer is read out and the current angle value, the delay time and the measurement value is sent to the Communication Module via the serial interface. Another wait cycle ensures that the whole system is working with a repetition rate of 100 Hz (Figure 4-8).
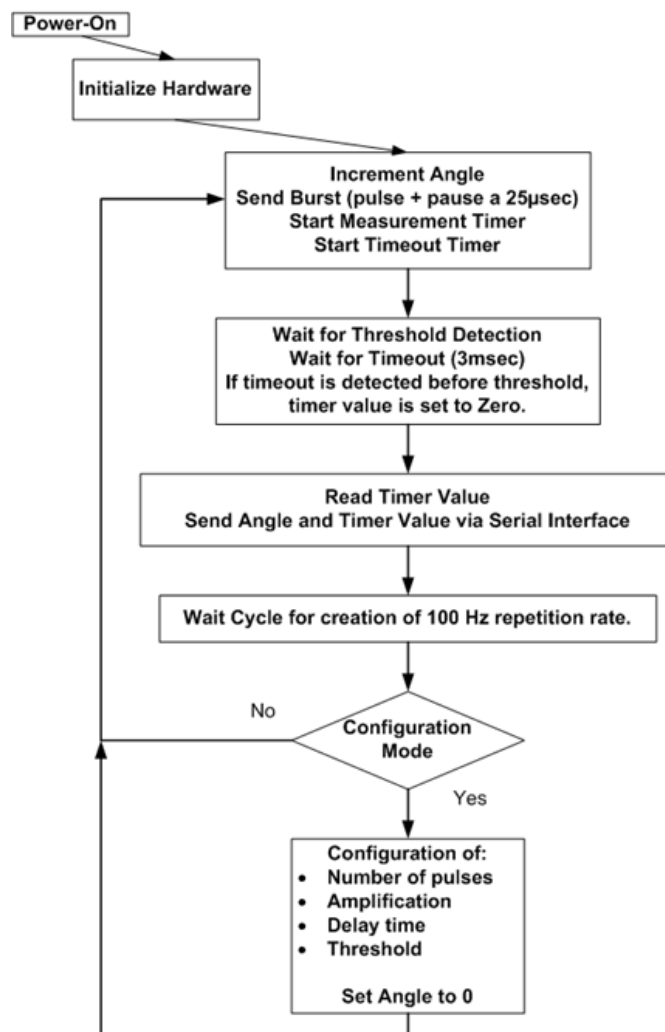

Figure 4-8. Software algorithm of the distance measurement

If the Configuration mode is entered, the measurement stops and following parameters can be adapted:

- Number of pulses: Number of pulses is related to the amount of energy which is sent out by the sender. (More pulses = more energy)
- Amplification: Receiving amplification to overcome the damping of the medium.
- Delay time: A delay can be set to overcome a possible cross talk.
- Threshold: The threshold can be adapted in order to the used medium.

4.8 Blind zone detection test

Ultrasonic sensors have a small unusable area for distances, measures close to the face of the sensor. If the ultrasonic wave returns before the sensor has completed its transmission, the sensor is unable to receive the echo accurately. This area is known as the blind zone [4]. To estimate the blind zone of the senor, a wooden plate was placed in front of the ultrasonic sensor at a distance of 20 cm (Figure 4-9). In this experiment the plate was moved towards the sensor and the distance was recorded in intervals of 1 cm until a final distance of 1 cm. According to Figure 4-10, blind zone for the ultrasonic sensor extends to about 3 cm in air. Distances below cannot be measured with appropriate accuracy. [27]

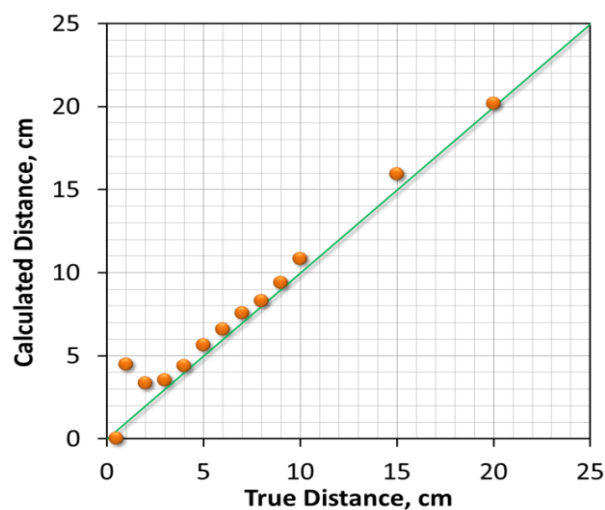

Figure 4-9. Testing for the blind zone area

Figure 4-10. Blind zone detection result

4.9 Numerical simulation

The simulation takes the principles of wave propagation – Snellius, Huygens and Fermat [25] – and the (circular) borehole geometry as well as the tool position and orientation within the borehole into account.

In theory there are two points in the borehole which can act as reflector for the transmitted signal. If the tool is strictly centralized – the rotational center of the tool equals the center of a circular borehole – one reflection point is at the borehole wall in toolface direction and the second one is in the opposite direction behind the tool's sensor. In practice the signal is of course only reflected by the first reflector in that case, but if the tool is not centralized as shown in Figure 4-11, no direct reflection back to the sensor occurs from the borehole wall. Since the reflector in toolface direction is not perpendicular to the wave path, the signal is reflected to somewhere in the borehole, but not back to the sensor.
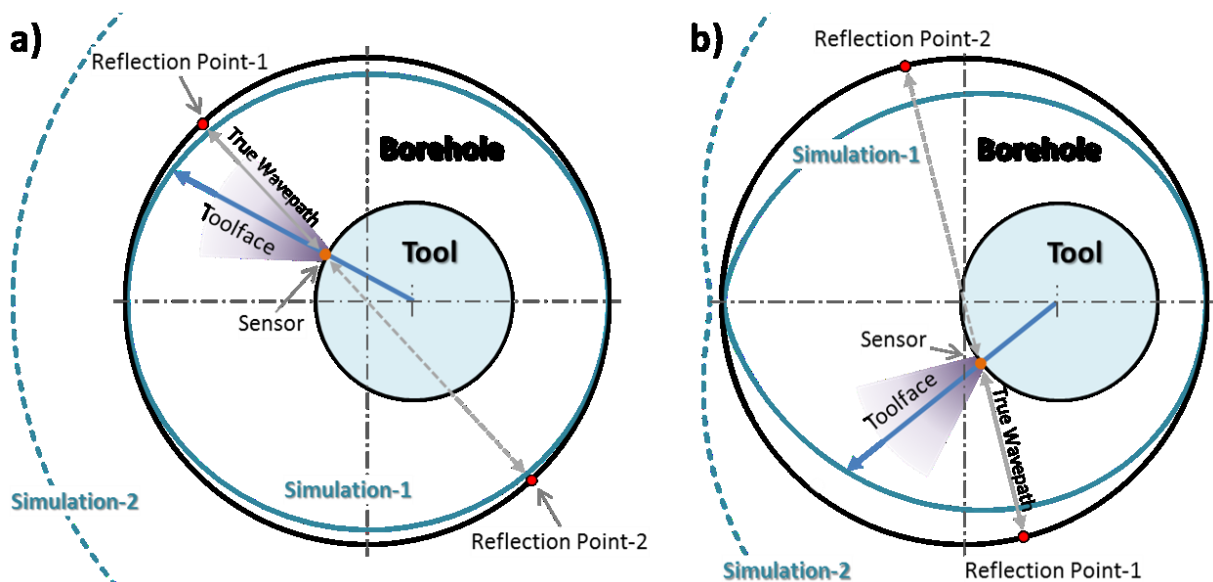

Figure 4-11. Simulating the wellbore by considering two reflection points

The only two points which are possibly reflecting the signal back to the receiver are denoted in Figure 4-11 as reflection point-1 and -2. Depending on the aperture of the ultrasonic sensor – which is in the actual case about ±25 degree and indicated as dark purple cone – the signal might hit such a reflection point or not. Both reflection points can be easily calculated for a circular borehole; only a line through the borehole center will intersect the borehole wall perpendicular, thus the coordinates of the reflection points can be easily written as

$$x_p = \pm R \times \frac{x_t - r\cos\alpha}{\sqrt{r^2 - 2rx_t\cos\alpha + x_t^2}}$$

Equation 4-2

$$y_p = \pm R \times \frac{r \sin \alpha}{\sqrt{r^2 - 2r\, x_t \cos \alpha + x_t^2}}$$

Equation 4-3

In above equations R denotes the true borehole radius, r the radius of the tool – or to be more precise the distance of the sensor from the tools rotation axis. The distance of tool center to the borehole center is denoted by x_t, and α stands for the toolface angular position. Positive signs in both equations denote reflection point-2 and negative signs – the more likely – reflection point-1.

The true length d of the wave path is simply the distance from the sensors position to the particular reflection point and can be written as

$$d = R \pm \sqrt{r^2 - 2r\, x_t \cos \alpha + x_t^2}$$

Equation 4-4

The positive sign denotes the path length via reflection point-2 and the negative sign via reflection point-1. The simulation takes that two reflection points into account, it calculates the true wave path length and projects the results into toolface direction resulting in the two simulation curves. The simulation based on the more likely wave path is in Figure 4-11 and all subsequent figures denoted as simulation-1 and drawn as solid blue line; vice versa, the less likely one is denoted as simulation-2 and drawn as dashed blue line.

The reflection apertures are the angles Θ_1 & Θ_2 between the sensor's toolface direction and the reflection points (cp. Figure 4-12) and vary with the toolface' angular position x_t and the lateral tool position x_t. In the case shown in Figure 4-11a, the reflection aperture is less than the aperture of the ultrasonic transmitter and thus appropriate to create reflections whereas in Figure 4-11b this is not the case, thus no signal will be directly reflected back to the sensor and the recoded data will be invalid in that case.

The reflection apertures can be written as

$$\Theta_1 = +\arccos\left(\frac{r - x_t \cos \alpha}{\sqrt{r^2 + x_t^2 d - 2rx_t \cos \alpha}}\right)$$

Equation 4-5

$$\Theta_2 = -\arccos\left(\frac{r - x_t \cos \alpha}{\sqrt{r^2 + x_t^2 d - 2rx_t \cos \alpha}}\right) + \pi$$

Equation 4-6

In mentioned equations Θ_1 denotes the aperture angle of the more likely reflection. In Figure 4-12 Θ_1 is displayed as radar plot in combination with a 25° reference aperture angle.
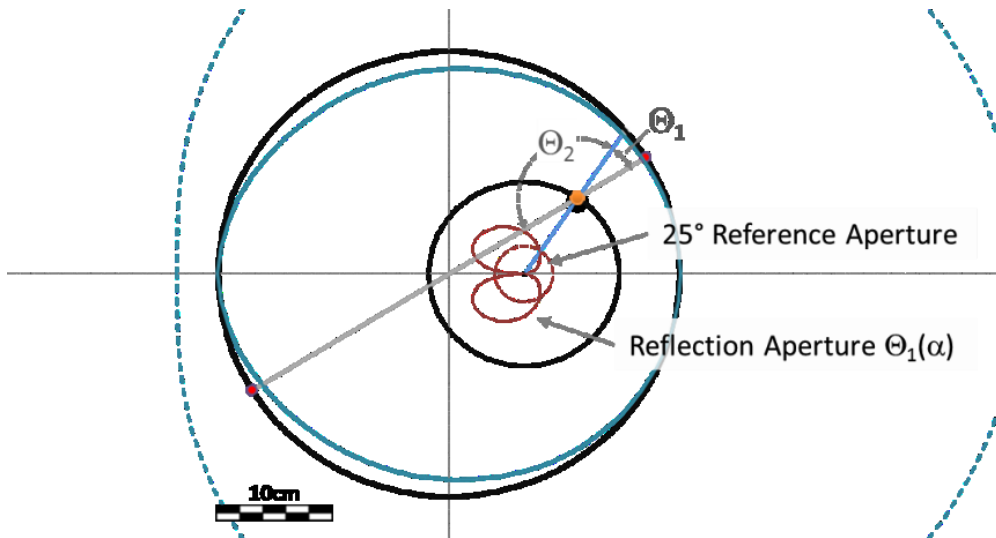
Figure 4-12. Apertures is the angle between the sensor location and the reflection point

4.10 Ultrasonic caliper experiments

To perform the experiments, ultrasonic sensor was mounted on the rotating machine. Tests performed in wellbore with different drilling fluids. The recorded data during experiments were sending to the computer by blue-tooth connection (Figure 4-13).
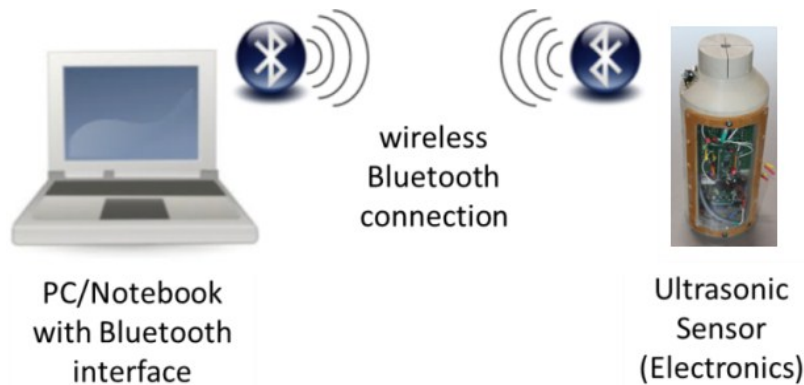

Figure 4-13. Data transferring by Bluetooth [29]

The ultrasonic caliper package consists of a transducer and a transceiver, battery package, micro controller and the counter switch. An extra transducer and transceiver sensor is used to determine the acoustic properties of drilling fluid. By considering the RPM, for each point 4 different numbers were recorded. These four numbers are counter number, validity number, measured distance and finally speed of sound in the drilling fluid. When the tool turns one full round (360°) the counter number becomes zero. So as the drill string RPM is low the number of recorded data by the ultrasonic sensor in one full round (360°) is more than the time when the RPM of the drill string is high. When the sensor passing the blind zone or the distance from the wellbore wall is large the validity number becomes zero and the calculated distance is not valid for that point. When the pulse sent by the sender and received by the receiver the distance calculation will be processed by the micro controller and finally the result will be seen on the screen. The experiments were categorized by the

wellbore geometry and the position of the tool in the wellbore as well as by the applied drilling fluids. The experiments were conducted at room temperature in:

- Air
- Water
- Mud (Bentonite)

All of above mentioned drilling fluids were used to perform several experiments based on the position of ultrasonic caliper in the wellbore including different wellbore geometry, more precisely:

- Centralized position of the tool in the wellbore
- Decentralized position of the tool in the wellbore
- Simulation of squeezed formation

Recorded data of each experiment that was mentioned above was transferred to the software for more analysis. Each recorded data for a full round (360°) was analyzed accurately to find out the weak points so that the upgrade could be done both for software and hardware (Figure 4-14).
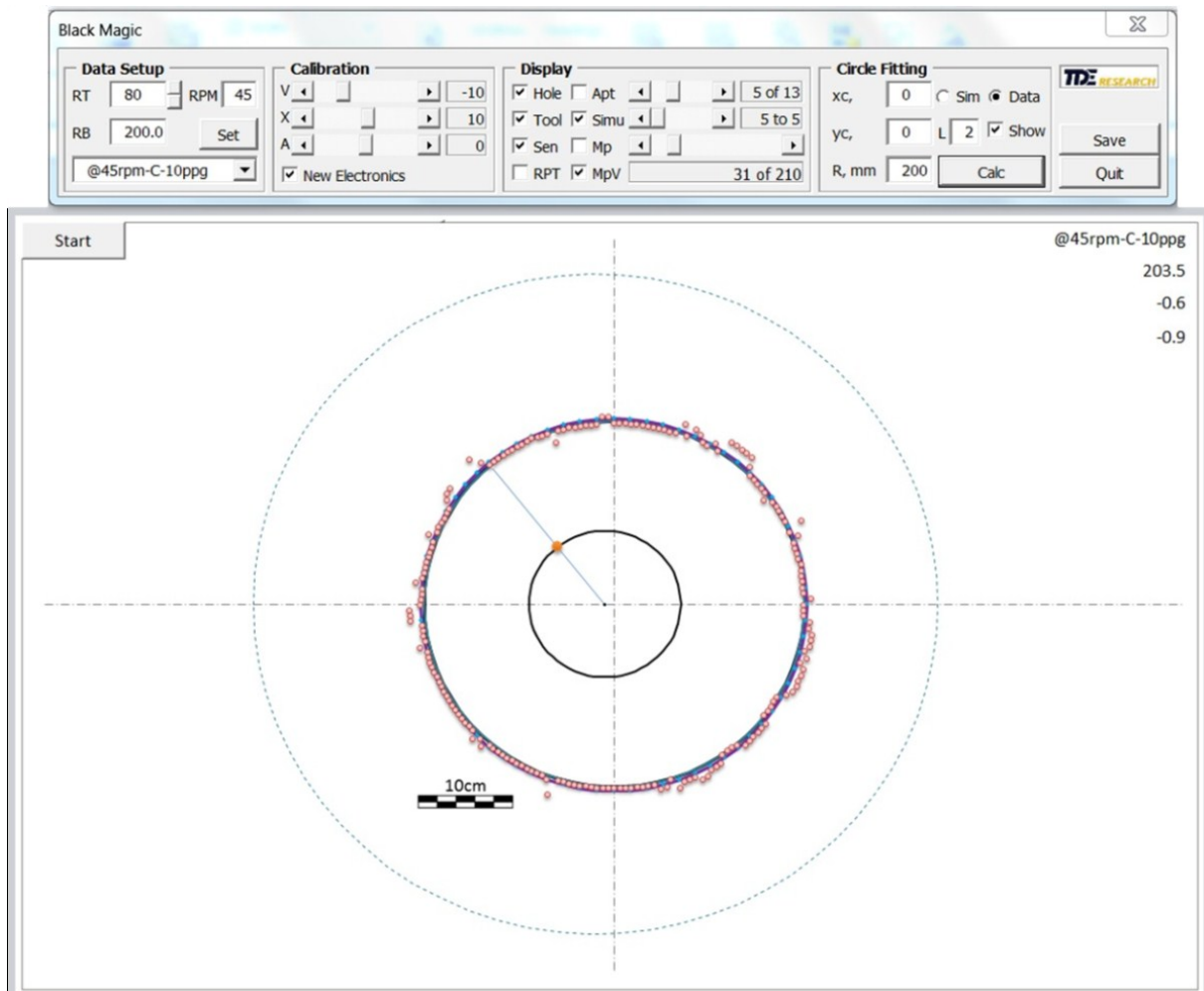
Figure 4-14. Ultrasonic caliper software that recorded data were analyzed

There are four parts in this software which the test information could be adjusted, these four sections are:

- **Data Setup**: in this section radius of the tool (caliper), wellbore radius and also RPM of the caliper could be adjusted. There is also another section that the recorded data of each test was read by the software (Figure 4-15).
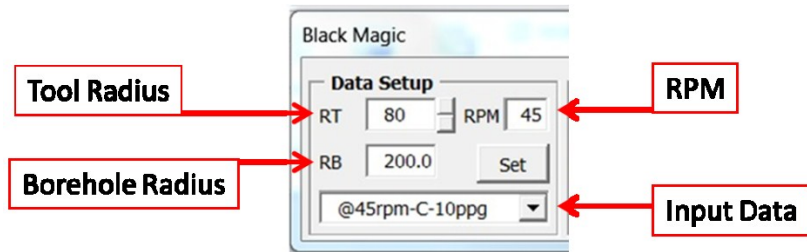

Figure 4-15. Data setup

- **Calibration**: In this part the wellbore and data position could be calibrated and also the size of data could be corrected (Figure 4-16).
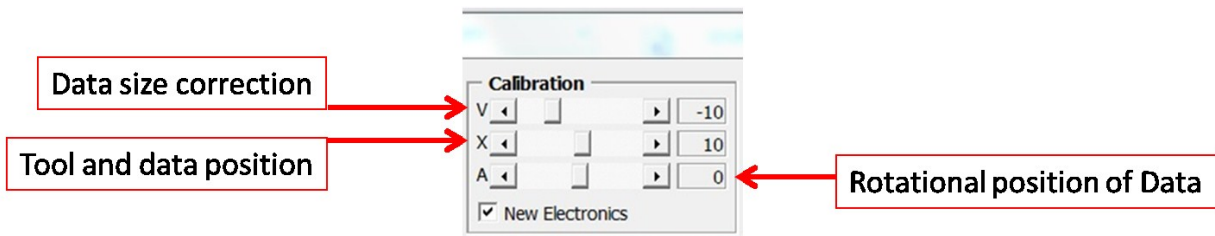
Figure 4-16. Calibration section

- **Display**: In this section borehole, tool, simulated data, sensor and etc. could be displayed. In other parts the data of each round could be shown (Figure 4-17).
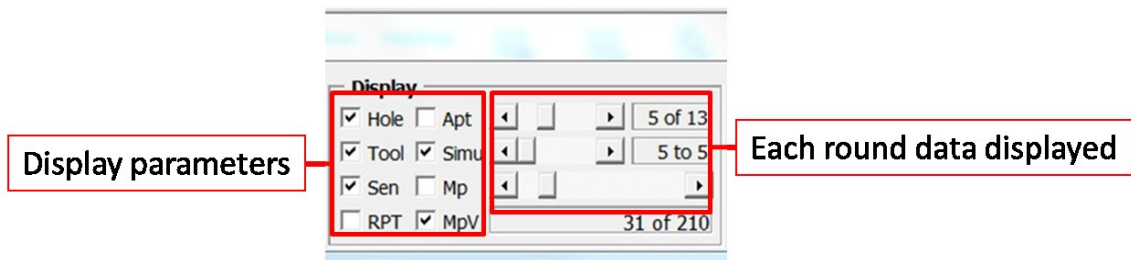

Figure 4-17. Display parameter

- **Circle** In this section the circle fitting is applied to the data for each round (Figure 4-18).
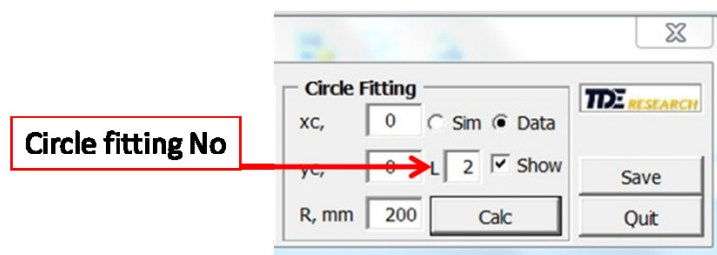

Figure 4-18. Circle fitting section

- **Graph**: Drawing recorded data

4.11 Testing in air

When the ultrasonic sensor was mounted on the rotating machine, tool diameter becomes 16.5 cm (6.5 inch). Tests performed in the wellbore with the diameter of 40 cm (15.7 inch). All tests performed in room pressure (atmospheric pressure) and temperature (16 to 18°C). The speed of sound in air was measured by the referenced package; it was 340 m/sec. Based on the speed of sound in air the input energy for sending pulses and receiving echoes, 8 pulses were sent into air so that reflected echo has the energy to be detected by the ultrasonic sensor (Figure 4-19). The wave length of ultrasonic sensor pulses in air based on formula 3-1 is 8.5 mm. it means that the sensor could not detect objects smaller than 8.5 mm in air. So the resolution is 8.5 mm in air.
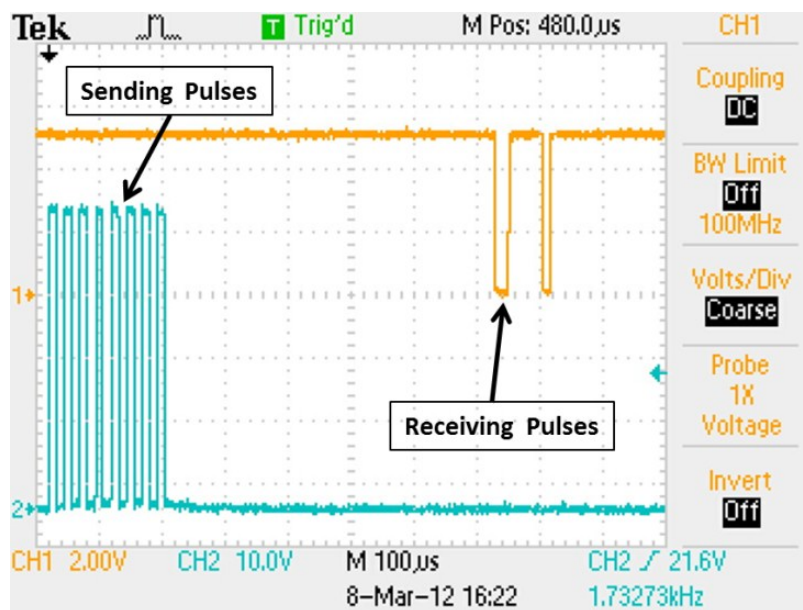

Figure 4-19. 8 pulses sent in air and received signals were shows after treatment

4.11.1 Centralized position of the tool in the wellbore (Air)

The caliper centralized in the borehole with 40 cm diameter and the tests performed with this parameter. During the test ultrasonic caliper recorded the data with different RPMs which are 5, 15, 30, 60, 100 and 180 RPM.

As mentioned before a simulation of the particular experiments was performed. The simulation takes the principles of wave propagation (principles of Huygens and Fermat) [6] into account and uses borehole geometry, tool position and orientation as input. In this simulation regarding the position of the tool in the borehole and the position of the sensor, when the signals are sending towards the wellbore, two points could be found that both sending and returning echoes are perpendicular to the wellbore wall. As shown in Figure 4-20 when the tool is decentralized (or even centralized) and the position of the sensor is changing as the tool rotate, there are two points that the sending and receiving echoes are perpendicular to the wellbore wall (point 1 and 2).
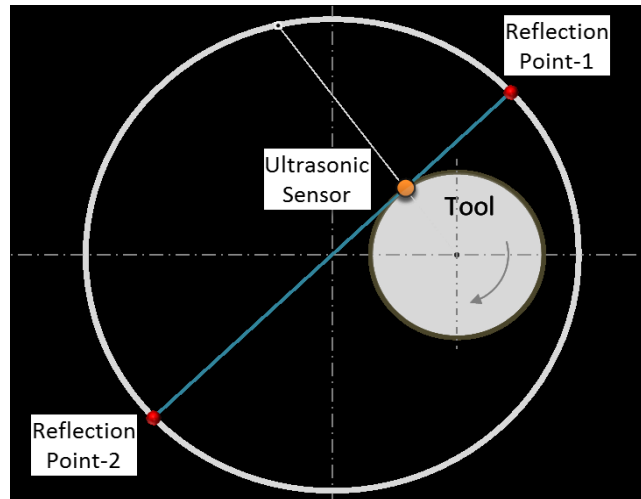
Figure 4-20. Two points which the sending and receiving signals are perpendicular to the wellbore wall

So the signals which are received at any time could be either from point 1 or point 2. For this reason both distances were calculated and two simulated wellbore based on the position of points 1 and 2 and also the tool, were plotted (simulation 1 is the plot of calculated data of point 1 and simulation 2 is the plot of calculated data of point 2). The simulated results are drawn as blue lines in the figures and are compared to the real borehole geometry and also to the measured data (orange dots).

Figure 4-21 shows the result of the experiment with rotational speed of 5 RPM. The result of all other rotational speed was shown in appendix. For all rotation rates the measured data and simulated wellbore are similar and reflect the true wellbore diameter in an appropriate shape. Some deviations of few data points from the true wellbore profile may be caused by the borehole roughness due to irregular cement surface.
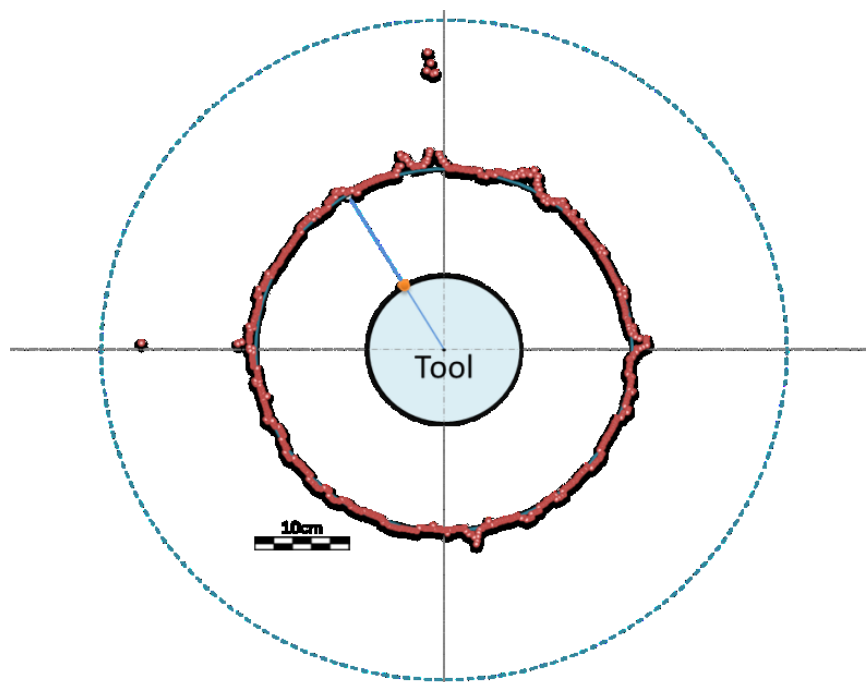

Figure 4-21. Sensor rotates in air with 5 RPM in 40 cm diameter wellbore (centralized position)

4.11.2 Decentralized position of the tool in the wellbore (Air)

In this experiment a similar procedure, as mentioned in previous tests, was performed. The only difference was the position of the tool. The ultrasonic caliper (tool) was positioned in one side of the wellbore but not too close to pass the blind zone. The experiments were performed in different rpms 15, 30, 60, 100 and 180 RPMs. There are some points that are out of the wellbore range and the reason for that might be multiple reflections or cycle skipping phenomena. There are some areas that the sensor could not record any data, it could be that the sensor does not receive any reflection back during the recording time. The reason for that is the angle between the sensor and the wellbore wall. Figure 4-22 shows the result of the experiment with rotation speeds of 5 RPM in room temperature and pressure. The result of other rotational speed tests was shown in appendix.
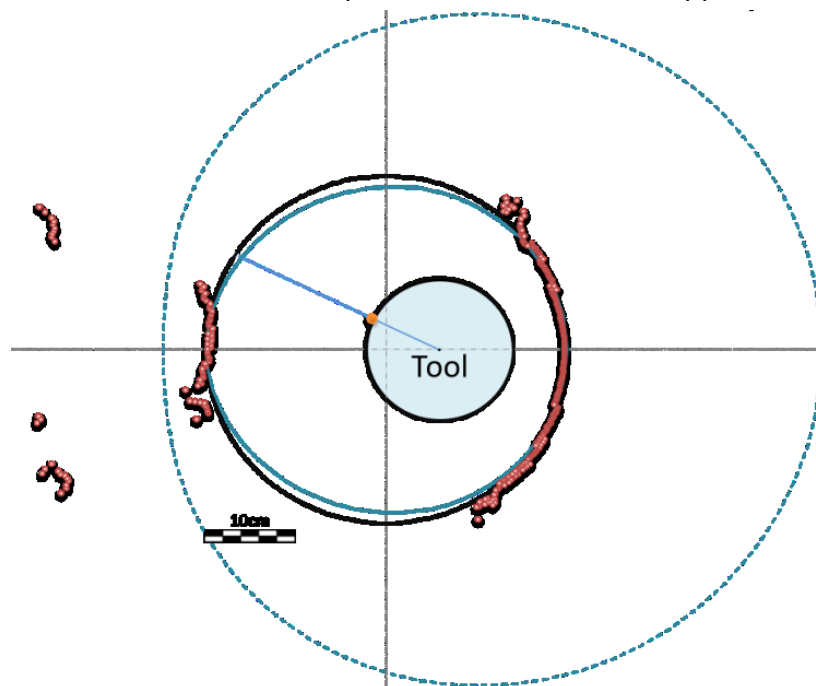

Figure 4-22. Sensor rotates in air with 5 RPM in 40 cm diameter wellbore (decentralized position)

4.11.3 Simulation of squeezed formation (Air)

In this experiment it is tried to simulate the squeezed formation. For this reason an artifact were placed in the wellbore and at the same time the tool is centralized and rotates with different rpms (5, 15, 30, 60, 100 and 180 RPM). Figure 4-23 shows the result of the experiment with 5 RPM, squeezed formation could be detected by the sensor and the only abnormal parts are the edge of the artifact where scatting and reflection of the echoes might causes the recorded data does not match the borehole or the artifact. The result of the tests with all other RPM were performed and presented in appendix.
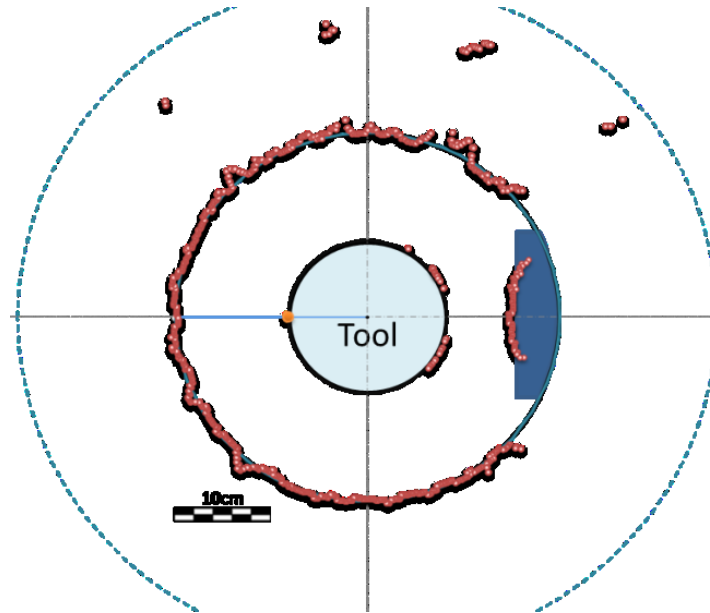
Figure 4-23. Sensor rotates in air with 5 RPM in 40 cm diameter wellbore (simulating squeezed formation)

4.12 Testing in water

The experiments have been performed with different positions and geometry in wellbore where the drilling fluid is water; they have been categorized based on geometry of the tool in wellbore. These experiments are similar to those one which have been done in air, the speed of sound is the only parameter which has changed. The speed of sound that was recorded in these experiments was about 1460 m/sec. The amount of energy that is needed to put into water for sending an echo and receiving it is 2 pulses, because the speed of sound in water is faster than in air and also water is an incompressible liquid. If 8 pulse system were used in water then reflected echo will be received before sending all 8 pulses and measurements will become wrong (Figure 4-24). The wave length of the signal in water regarding to the formula 3-1 is 36 mm and it means the resolution of the sensor in water is 3.6 cm and it could not detect objects smaller than 3.6 cm.
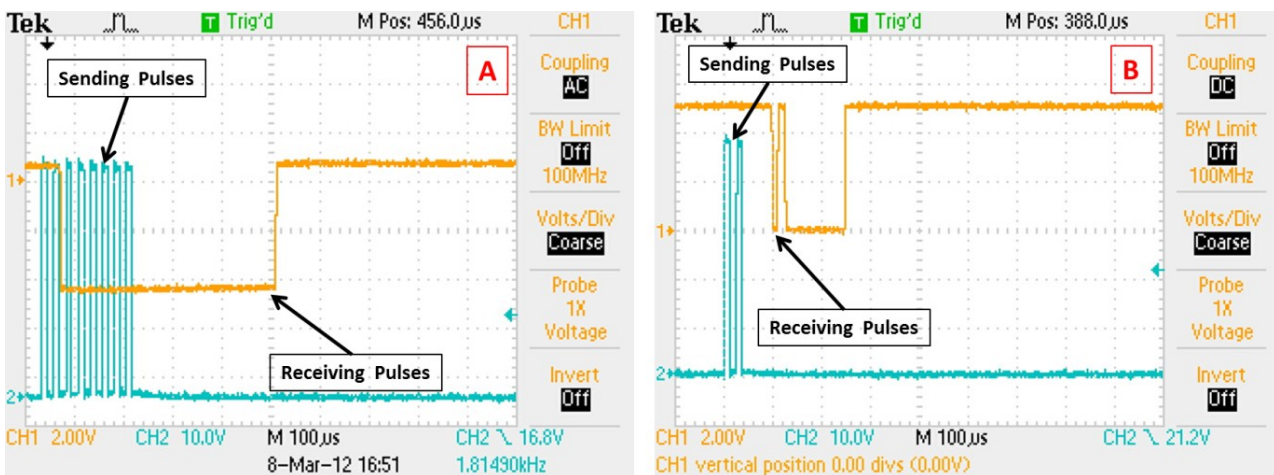

Figure 4-24. a) 8 pulses sent in water and reflected echo received before all 8 pulses were sent so measurement could not be done, b) 2 pulses sent in water and reflected echo detected after pulses were done so the measurement could be performed

4.12.1 Centralized position of the tool in the wellbore (Water)

During the experiment the ultrasonic caliper recorded the data with different rpms –15, 30, 45, 60 and 100 RPM – and the recorded data for each revolution were plotted. Figure 4-25 shows the result of experiment in water with different 15 RPM and central position of the tool in wellbore. With the centralized position of the tool and different rpms measured data and simulated wellbore are the same. So simulated wellbore, recorded data and real wellbore size are the same and fitted together. The results of the tests with other RPM were plotted in appendix.
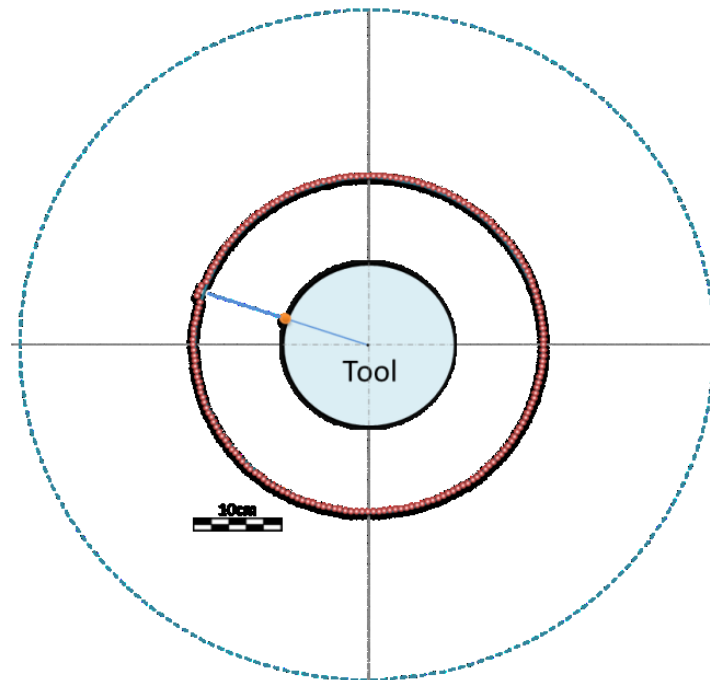
Figure 4-25. Sensor rotates in water with 15 RPM in 40 cm diameter wellbore (centralized position)

4.12.2 Decentralized position of the tool in the wellbore (Water)

In this experiment the tool is decentralized in the wellbore but not passing the blind zone area. Water is the fluid that was used during the experiment. The experiments were performed with different rpms 15, 30, 45, 60 and 100 RPM. Figure 4-26 shows the result of experiment in water with 15 rpm while the tool is decentralized in borehole. The numbers of recorded data in decentralized position of tool are more detected in water rather than in air. The results of experiments with other RPM are plotted in appendix.
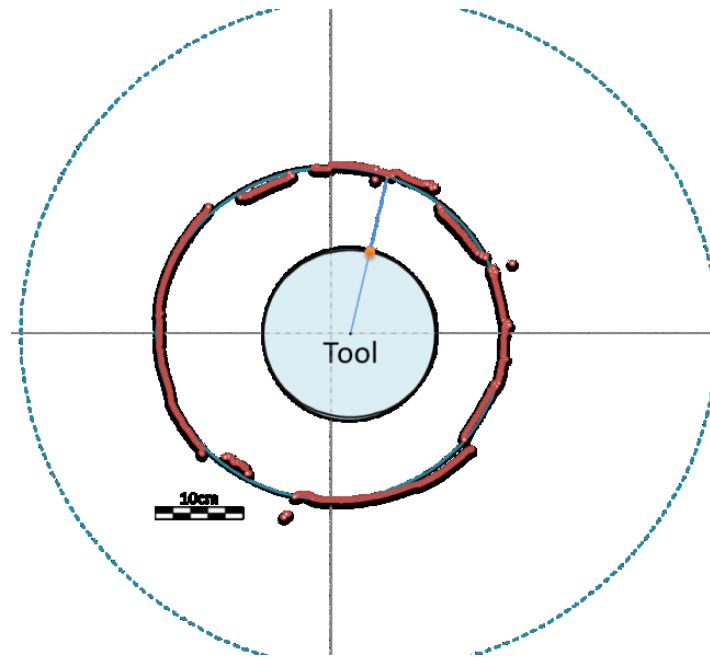
Figure 4-26. Sensor rotates in water with 15 RPM in 40 cm diameter wellbore (decentralized position)

4.12.3 Simulation of squeezed formation (Water)

In this experiment an artifact is placed inside the borehole to simulate a squeezed formation in water. Experiments were performed with different tool RMPs (15, 30, 45, 60 and 100 RPM). Figure 4-27 shows the result of the experiment with 15 RPM and squeezed formation could be detected by the sensor. The reason that some of the data are fitted the circle and some not could be the reason of resolution of the sensor in water (3.6 cm) or because of the borehole roughness. The result of the experiments with other rpm was plotted in appendix.
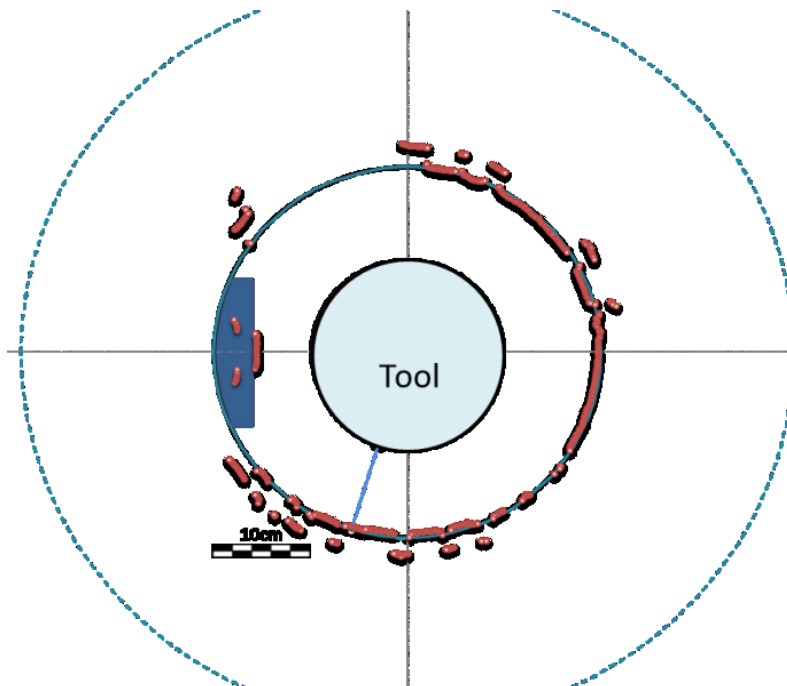
Figure 4-27. Sensor rotates in water with 15 RPM in 40 cm diameter wellbore (simulating squeezed formation)

4.13 Testing in bentonite mud

In this experiment bentonite mud is used as a drilling fluid to perform different tests regarding to the position and geometry of the tool in the borehole. Experiments have been performed in room temperature and pressure, so the properties of bentonite mud are as follows. Mud weigh is 8.5 ppg with rheological properties of 2 cp plastic viscosity and the yield point of 7 lb/100ft^2. The speed of sound in bentonite mud with the specifications which were mentioned is about 1370 m/sec. The resolution of sensor in bentonite mud is 34.2 mm which the sensor can detect objects bigger than this size. The number of pulses that send into bentonite mud is 2 pulses.

4.13.1 Centralized position of the tool in the wellbore (Bentonite Mud)

In this experiment again the tool is centralized in the borehole and sensor rotates with different rpms (15, 30, 45, 60 and 100 RPM). Recoded data were matched with the simulated and real borehole size. There are some few data where they were not recorded. Scattering of the echoes by the bentonite particles and also mud cake on the wellbore wall could be the reasons of not recording some few points. Figure 4-28 shows the results of experiment in bentonite mud while the tool is rotating with 15 RPM. The result of the tests with other rpm was shown in appendix.
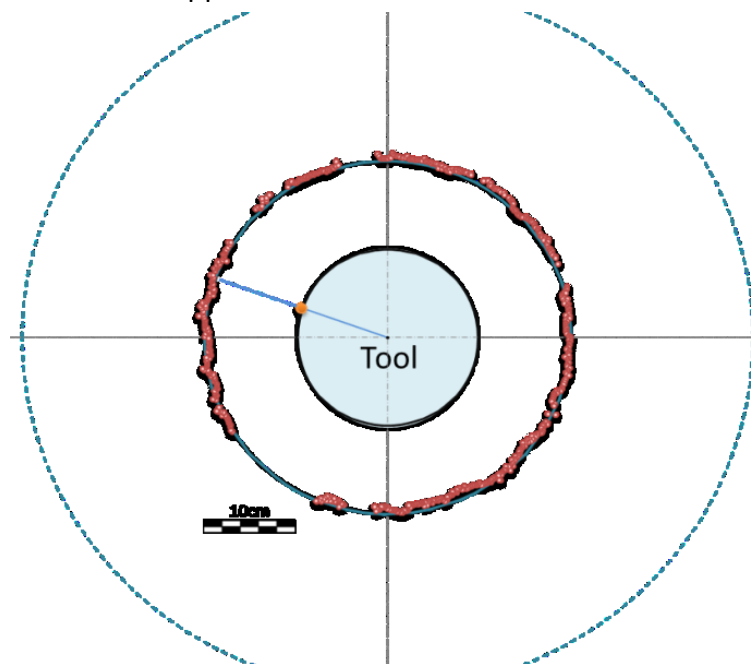
Figure 4-28. Sensor rotates in bentonite mud with 15 RPM in 40 cm diameter wellbore (centralized position)

4.13.2 Decentralized position of the tool in the wellbore (Bentonite Mud)

In this experiment the tool is decentralized in the wellbore by considering the blind zone area. The experiments were performed with different rpms – 15, 30, 45, 60 and 100 RPM – in bentonite mud. The recorded data are nearly covered the wellbore profile and also matches the simulated wellbore. In comparison with the experiments which have performed in air the experiment in bentonite mud recorded more data rather than in air.

Figure 4-29 shows the results of experiment in bentonite mud while the tool is rotating with 15 RPM. In appendix results of the experiment with other rpm were plotted.
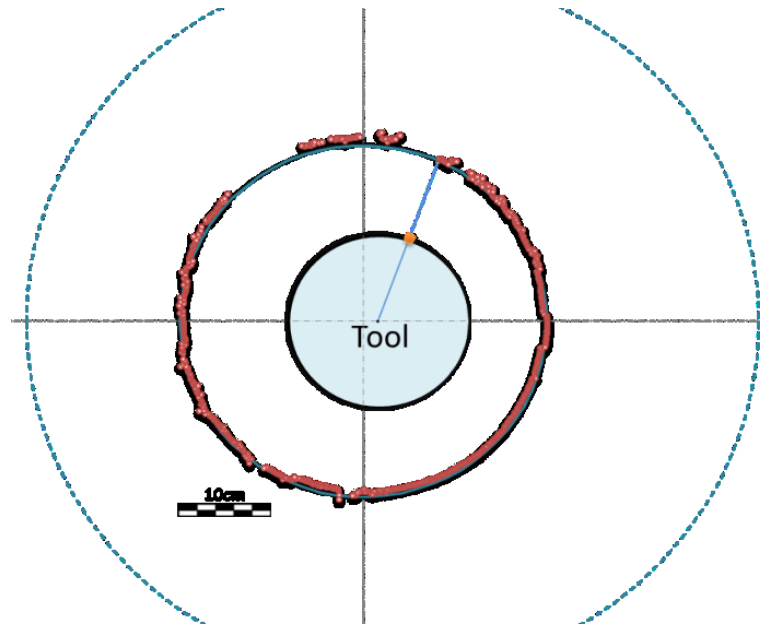

Figure 4-29. Sensor rotates in bentonite mud with 15 RPM in 40 cm diameter wellbore (decentralized position)

4.13.3 Simulation of squeezed formation (Bentonite Mud)

In this experiment an artifact is placed inside the borehole to simulate squeezed formation in bentonite mud. Experiments were performed with different tool rpms – 15, 30, 45 and 60 RPM. Figure 4-30 show the results of the experiment with 15 RPM, it can be see that the squeezed formation could be detected by the sensor. In appendix the result of the tests with other rpm were plotted.
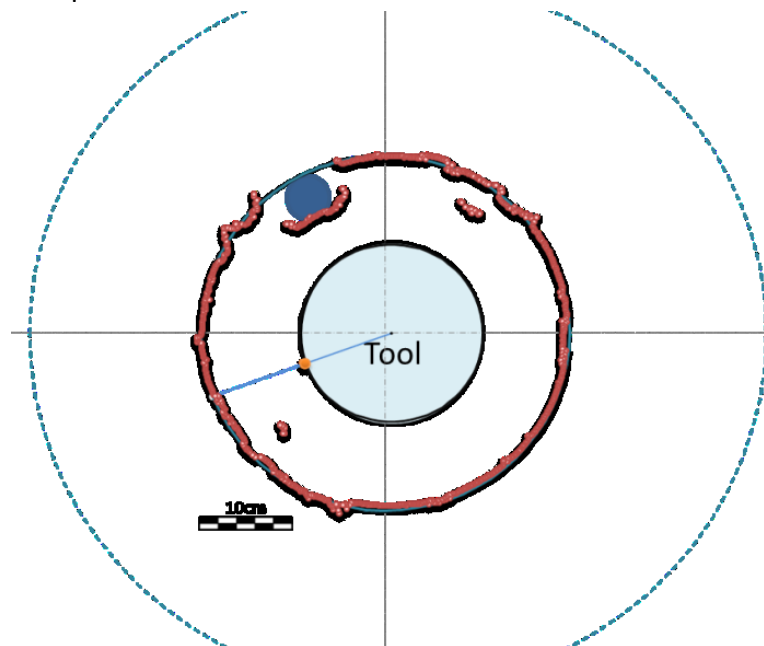
Figure 4-30. Sensor rotates in bentonite mud with 15 RPM in 40 cm diameter wellbore (squeezed formation)

4.14 Effect of mud weight

In this experiment salt water is used as a drilling fluid to perform different tests regarding to the position and geometry of the tool in the borehole. Experiments have been performed in room temperature and pressure. Tests performed in three different mud weight 8.65, 9 and 10 ppg. Salt with different concentration added to the water, so rheological properties of saltwater with different concentration has the plastic viscosity of 2 cp and the yield point of 1 lb/100ft^2. The speed of sound in salt water varies with different densities of the liquid. [42]

4.14.1 Salt water with 8.65 ppg density

In this experiment the tool (caliper) is placed in the wellbore with different position and geometry. Caliper rotates with different RPM (30, 60 and 100 RPM) in the wellbore and records diameter of the borehole. The speed of sound in 8.65 ppg salt water is recorded 1565 m/sec. Figure 4-31, Figure 4-32 and Figure 4-33 show the result of experiment with different tool position and geometry in 8.65 ppg salt water. Results of other tests with different RPM were plotted in appendix.
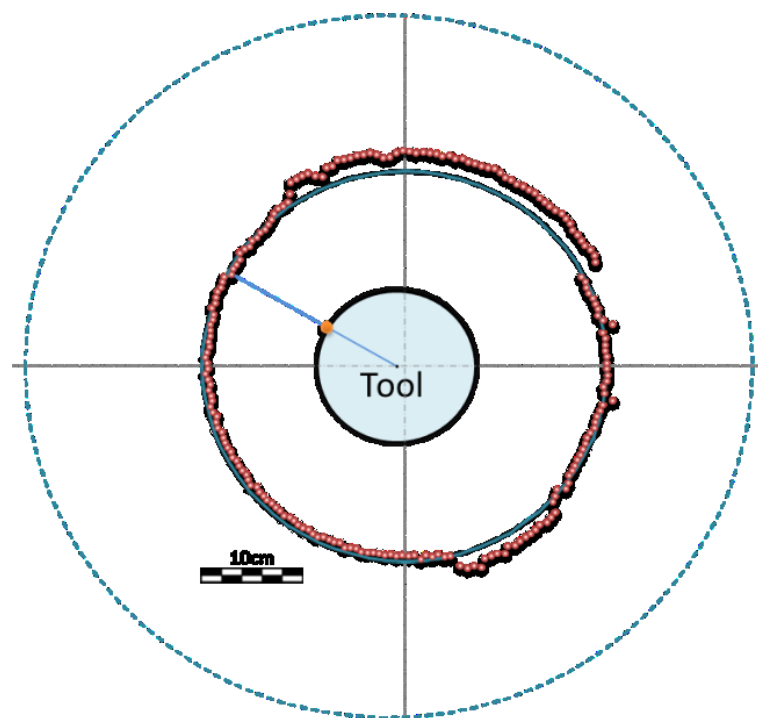
Figure 4-31. Sensor rotates in salt water, 8.65ppg, with 30 RPM in 40 cm diameter wellbore (centralized position)
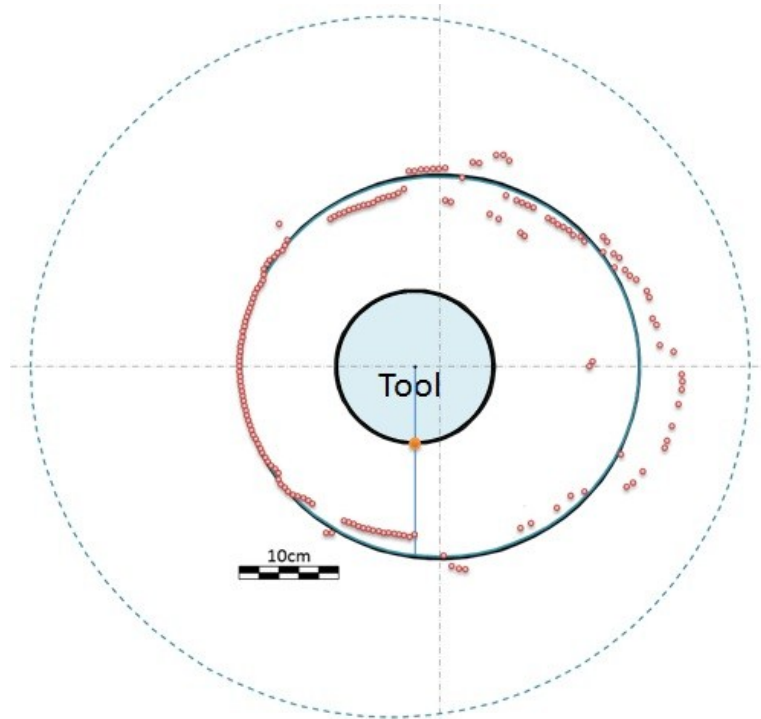
Figure 4-32. Sensor rotates in salt water, 8.65ppg, with 30 RPM in 40 cm diameter wellbore (decentralized position)
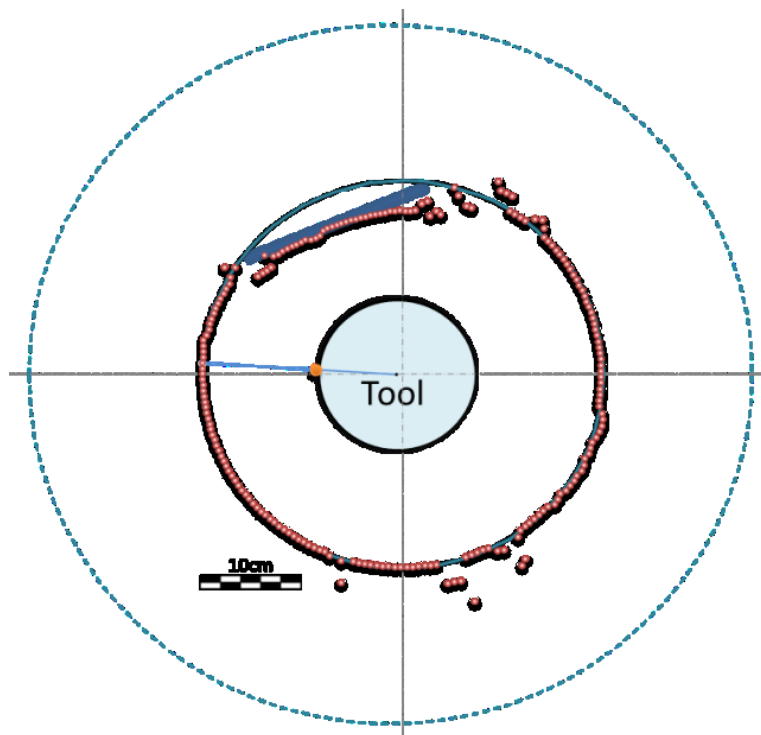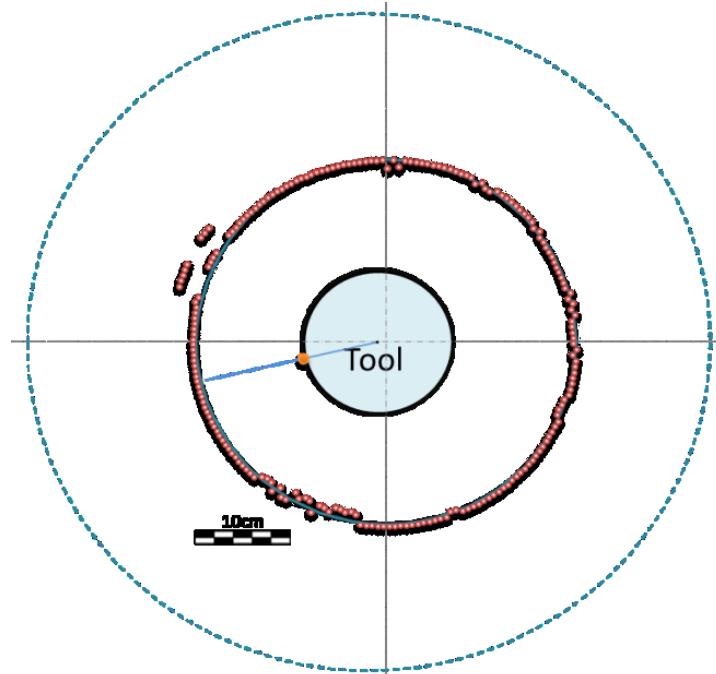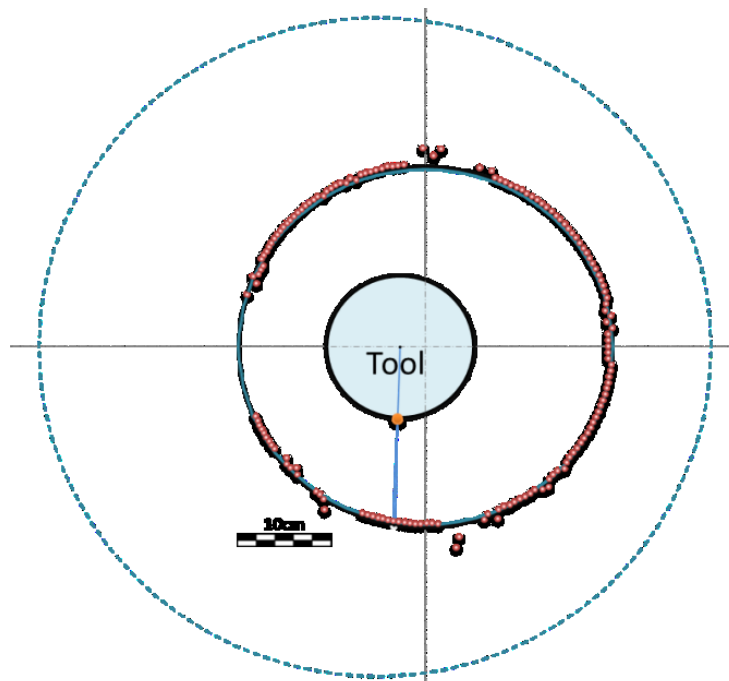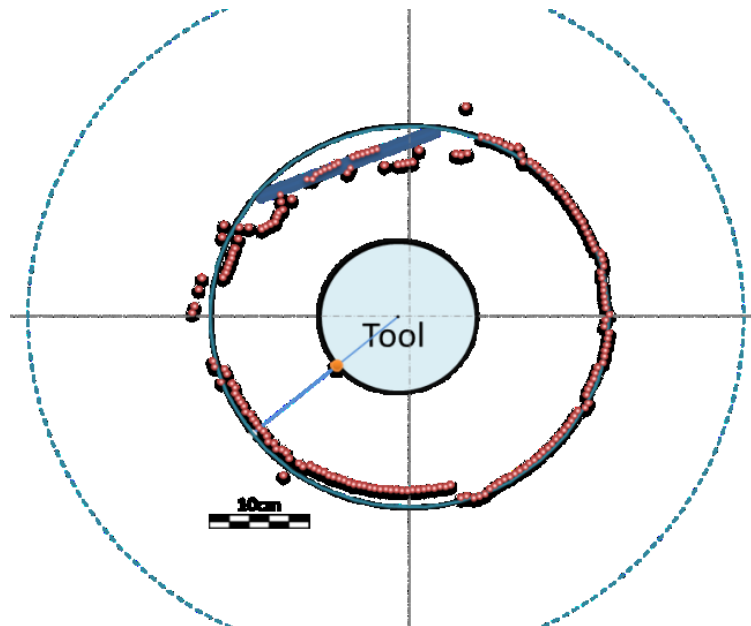

Figure 4-33. Sensor rotates in salt water, 8.65ppg, with 30 RPM in 40 cm diameter wellbore (squeezed formation)

4.14.2 Salt water with 9 ppg density

In this experiment all tests performed in salt water with the density of 9 ppg. The same procedure just like 8.65 ppg drilling fluid regarding to the geometry and position of the tool was used to perform all the tests. Caliper rotates with different RPM (30, 45, 60 and

100 RPM) in the wellbore and records the diameter of the borehole. 1680 m/sec is the speed of sound that was recorded in 9 ppg salt water. Figure 4-34, Figure 4-35 and Figure 4-36 show the result of experiment with different tool position and geometry in 9 ppg salt water. In appendix the result of the tests with other rpm were plotted.
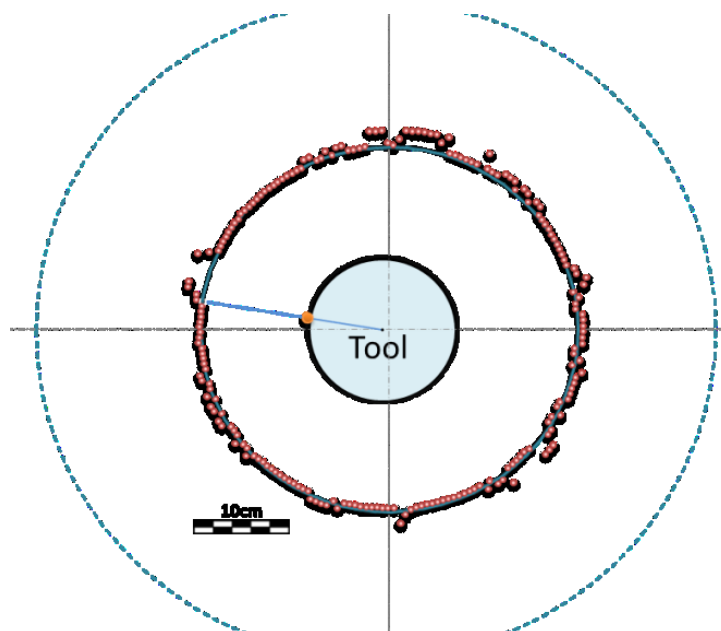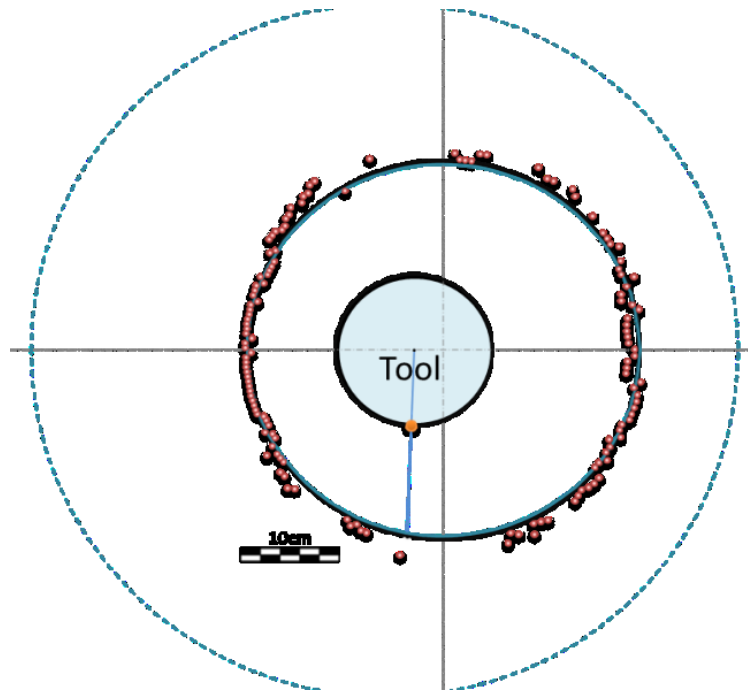

Figure 4-34. Sensor rotates in salt water, 9 ppg, with 30 RPM in 40 cm diameter wellbore (centralized position)

Figure 4-35. Sensor rotates in salt water, 9 ppg, with 30 RPM in 40 cm diameter wellbore (decentralized position)
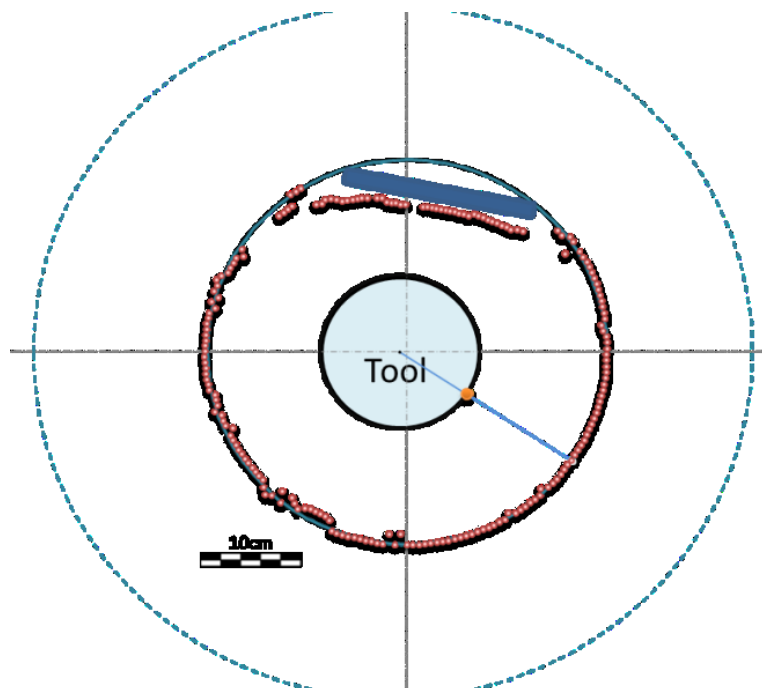
Figure 4-36. Sensor rotates in salt water, 9 ppg, with 30 RPM in 40 cm diameter wellbore (squeezed formation)

4.14.3 Salt water with 10 ppg density

In this experiment the same procedure like 8.65 and 9 ppg drilling fluid regarding to the geometry and position of the tool was used to perform all the tests in 10 ppg density salt water. Tool rotates with different RPM (30, 45, 60 and 100RPM) in the wellbore and records wellbore diameter. 1920 m/sec is the speed of sound that was recorded in 10 ppg salt water. Figure 4-37, Figure 4-38 and Figure 4-39 show the result of experiment with different tool position and geometry and different RPM in 10 ppg salt water. Results of other tests with different RPM were plotted in appendix.

Figure 4-37. Sensor rotates in salt water, 10 ppg, with 30 RPM in 40 cm diameter wellbore (centralized position)

Figure 4-38. Sensor rotates in salt water, 10 ppg, with 30 RPM in 40 cm diameter wellbore (decentralized position)

Figure 4-39. Sensor rotates in salt water, 10 ppg, with 30 RPM in 40 cm diameter wellbore (squeezed formation)

4.15 Crosstalk problem

Spacing between sensors is determined by their beam angles. The sensors must be spaced so they do not interfere with each other. If the beam of sensors interferes with each other the crosstalk problem happens [18]. This phenomenon could be monitored by oscilloscope (Figure 4-40).
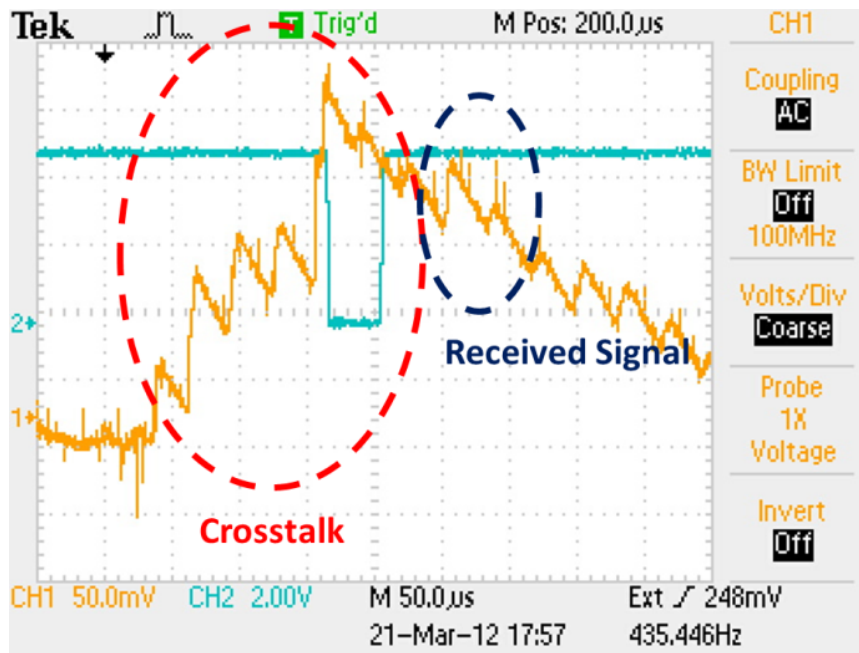
Figure 4-40. Crosstalk phenomenon detected by the oscilloscope

For solving this problem the position of sender and receiver was fixed in a way that the beam shape of each sensor was not overlapped the other one. Figure 4-41 shows the final design of the tool for reducing crosstalk and eliminating it while performing the test.
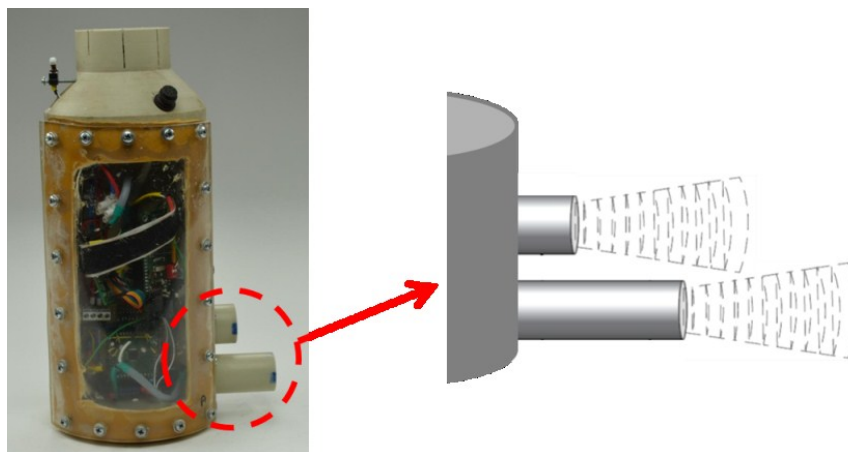
Figure 4-41. Tool design for solving crosstalk problem

4.16 Data transmission to surface

Performing all ultrasonic tests and experiment is the reason of developing a tool (ultrasonic caliper sub) so that it could measures the diameter of the wellbore and detects instabilities like squeezed formation, key seats and etc. The caliper sub as shown in Figure 4-42 has three sets of ultrasonic sensor for measuring wellbore diameter and one set of ultrasonic sensor for measuring speed of sound in drilling fluid. For sending all these amount of data in real time drilling application to the surface, caliper sub needs to be connected to the wired pipe. The amount of data that could be transferred by wired drill pipe is 57600 bit per second [6]. Ultrasonic sensor that is used in all these experiments has the measurement

frequency (repetition rate) of 100 Hz (each 10 milisec one measurement). By considering three sets of ultrasonic sensor that measures borehole diameter (3 x 40 bits), one set of sensor that measures sound velocity (1 x 30 bits), one set of magnetometer detecting position (1 x 30 bits) and semicolons that separate data (5 x 10 bits) totally 230 bits needed (Table 4-1). With the repetition rate of 100 Hz, total amount of data that a caliper sub sends to the surface is 23000 bit per sec. As wired drill pipe transferring 57600 bit per second so the number of caliper sub that could be used in series are 2 (57600/13000 = 2.5).

It is assumed that the data is sending to the surface in ASCII format. It is possible to increase the amount of data to be transferred by using a different protocol than ASCII or compress the data and then send it in real time. For the start the data is transferred in ASCII format because it can be evaluated easily without any special software to decompress the data.

Table 4-1. Amount of data per sensor that record in ASCII format

Position	Semicolon	Velocity of Sound	Semicolon	Sensor 1 recording distance	Semicolon	Sensor 2 recording distance	Semicolon	Sensor 3 recording distance	End signs
3 Byte	1 Byte	3 Byte	1 Byte	4 Byte	1 Byte	4 Byte	1 Byte	4 Byte	1 Byte
30 Bit	10 Bit	30 Bit	10 Bit	40 Bit	10 Bit	40 Bit	10 Bit	40 Bit	10 Bit

Figure 4-42. Ultrasonic caliper sub

4.17 Effect of gas on recording data

Ultrasonic caliper records borehole diameter in different drilling fluids with different tool geometry and position in the wellbore. During the tests drilling fluid condition was stable and only one phase liquid was used to perform the experiments. In this experiment it is tried to monitor the effect of gas bubbles in the drilling fluid as the ultrasonic caliper recorded the diameter of the borehole or measuring the distance from the sensor to the wellbore wall. The wellbore filled with water and the caliper submerged in the fluid. It is placed in the wellbore with a specified distance from the wall. Afterwards ultrasonic caliper starts sending

echoes to the wall for measuring two way traveling time to determine the distance. Meanwhile air bubbles with the compressor are injected from the base plate (Figure 4-43).

Figure 4-43. Wellbore condition before and after air injection to the water

Before injecting air received signal was recorded and monitored by oscilloscope. And then when air injected to the wellbore the received signal was recorded and also compared with the time when no bubbles were injected to the water (Figure 4-44).
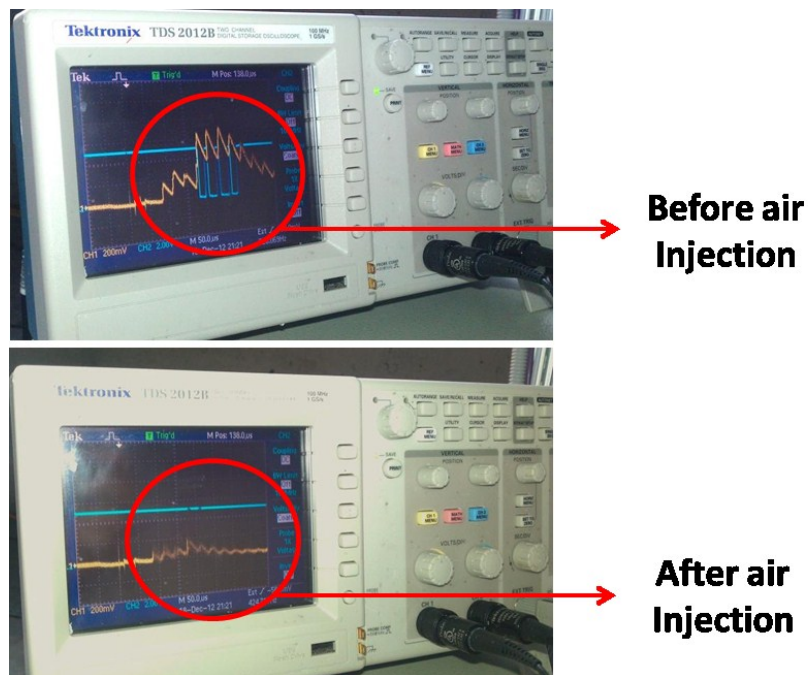

Figure 4-44. Oscilloscope reading received signal before and after air injection

As the air bubbles comes to the area between ultrasonic sensor and wall, received signals become weak and no distance measurement could be done during injection time. However when the injection is stopped the received signal is detected by the oscilloscope again. [50]

After performing the test, sound velocity measurement package was constructed. As shown in Figure 4-45 two ultrasonic sensors are placed in front of each other (opposed mode) and as the distance between the sensors is fixed so the speed of sound could be calculated by measuring the traveling time of echo from the sender to the receiver. With this design it is possible to detect the speed of sound downhole at the desired depth with high pressure and temperature. It is also a device to detect the gas kick in real time drilling operation.
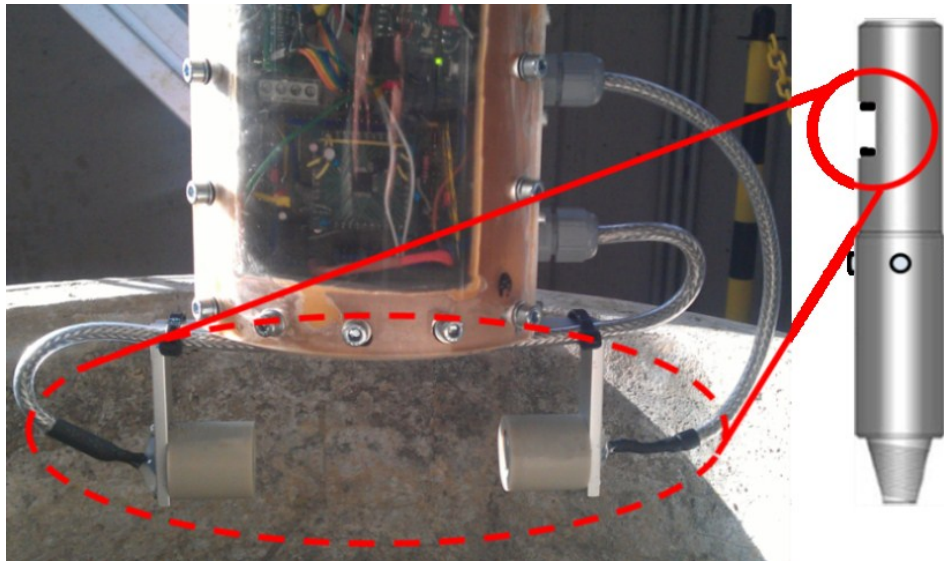
Figure 4-45. Referenced ultrasonic sensor for measuring sound velocity in the downhole condition

4.18 Circle fitting

The intersection of an ideal borehole is usually a circle which might be approximated by incorporation of the ultrasonic measurements to estimate the borehole diameter with more or less appropriate accuracy. That accuracy is influenced by geometrical aspects of the tool like (de)centralization and diameter of the tool compared to the real borehole diameter. In addition the accuracy is of course influenced by the measurement errors caused by inaccurate sound velocities applied to transform two-way travel times to distances as well as by erroneous picked first arrival times. Furthermore drilling phenomena, like wash outs and squeezing formations, can strongly affect the results. Assuming the wellbore shape is or parts of it are approximately circular, fitting a circle to the measured data might support the estimation of the true borehole shape.

The ultrasonic caliper tool provides data in the form $P_k=(\alpha_k, d_k)$ with α_k denoting the tool face directional angle and d_k the measured distance from the sensor to the reflection point. The index k indicates a particular survey out of n measurements. With r denoting the radius of the tool – in tool face direction projected – the coordinates of a particular reflection can be written as

$$x_k = -(r+d)\cos\alpha \quad y_k = +(r+d)\sin\alpha$$

Equation 4-7

whereby x_k, y_k are relative to the center of the ultrasonic tool. A mapping of a circle to those points can be formulated by using the equation of the circle,

$$(x - x_c)^2 + (y - y_c)^2 = R^2$$

Equation 4-8

In above equation the parameters x_c, y_c and R denote the center and the radius of the circle respectively. Circle fitting provides solutions for those unknowns in minimizing the distance of the measured values x_k, y_k to the circle by some error norm. The least squares fit is based on minimizing the squared distance, the objective function is thereby defined as

$$E = \sum_{k=1}^{n} |R_k - R|^2$$

Equation 4-9

The term $(R_k - R)$ denotes the distance from the measured values to the circle and

$$R_k = \sqrt{(x_k - x_c)^2 + (y_k - y_c)^2}$$

Equation 4-10

denotes the distance of a measure k to the center of the circle. Unfortunately the minimization of equation 4-9 incorporating equation 4-10 is a nonlinear problem that has no closed solution and all known algorithms are either iterative and costly or approximative by nature [31]. Modifying the objective function to

$$E = \sum_{k=1}^{n} |R_k^2 - R^2|^2$$

Equation 4-11

results by use of equation 4-10 in

$$E = \sum_{k=1}^{n} |(x_k - x_c)^2 + (y_k - y_c)^2 - R^2|^2$$

Equation 4-12

Introducing the new variables

$$A = -2x_c \quad B = -2y_c \quad C = x_c^2 + y_c^2 - R^2$$

Equation 4-13

equation (4-12) results in

$$E = \sum_{k=1}^{n} |(x_I^2 + y_I^2) + A x_k + B y_k + C|^2$$

Equation 4-14

Above equation provides a closed form solution for A, B and C and thus for x_c, y_c and R in a least square sense (L^2-norm). This method for fitting a circle is known as the Kasa method [34] and mentioned by Chernov and Ososkov [1984] as linear regression method (LRM). The

advantage of the Kasa method is its closed and easy form, but a major disadvantage is its low stability – a superfluous sensitivity to even small errors in measurements [32].

Rewriting the objective function 4-14 in matrix form results in

$$\begin{vmatrix} x_1 & y_1 & 1 \\ x_2 & x_2 & 1 \\ \vdots & \vdots & \vdots \\ x_n & y_n & 1 \end{vmatrix} \times \begin{vmatrix} A \\ B \\ C \end{vmatrix} = -\begin{vmatrix} x_1^2 + y_1^2 \\ x_2^2 + y_2^2 \\ \vdots \\ x_n^2 + y_n^2 \end{vmatrix}$$

Equation 4-15

which is a system of equations with the unknowns A, B and C. Solving that system by conventional solvers like LSQR in combination with the least squares error model obtains the same result as obtained by the closed form solution of the Kasa method [30], [35]. To reduce now the superfluous sensitivity of the Kasa method to erroneous data, we simply replaced the L^2-norm error function by the more general L^p-norm, resulting in the slightly modified objective function

$$E = \sum_{k=1}^{n} \left| R_k^2 - R^2 \right|^p = \sum_{k=1}^{n} \left| (x_1^2 + y_1^2) + A x_k + B y_k + C \right|^p$$

Equation 4-16

Using p=2 results in the least squares solution, using p=1 results in a robust solution (L^1-norm). In any case, for arbitrary values of p, equations 4-15 & 4-16 can be solved by application of iteratively reweighted least squares (IRLS) method [33]. Figure 4-46 shows an example of the proposed method (black solid circle) compared to the conventional Kasa method (dashed black circle) applied to 7 regular points at a circle and 1 outlier. That outlier influences strong the least square results – radius and position of the circle are strong biased, whereas the robust circle is highly unimpressed from the outlier.
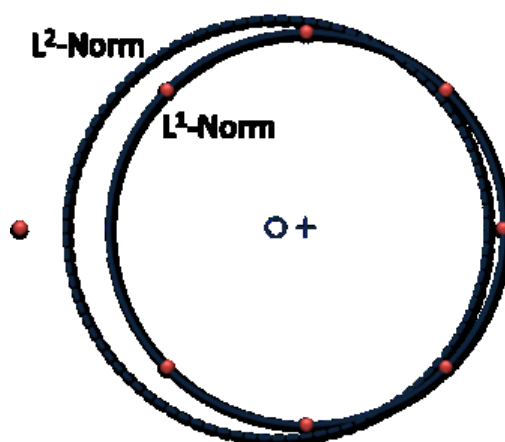
Figure 4-46. Example for Robust Circle Fitting [28]

4.18.1 Application of the method

The proposed method is applied to all recorded data for fitting circles on a revolution base. Data measured in different drilling fluids as well as with different tool positions were selected for testing the proposed method with two different error functions. Figure 4-47 to

Figure 4-50 show the results of circle fitting with both, the L[1] and the L[2]-norm. By comparing those results, the data which are out of the borehole range can be detected, the difference between L[2] and L[1] results prove the advantage of the robust method. Figure 4-47 shows the results of the test performed in air with two artifacts inside the borehole to simulate squeezed formation. Figure 4-48 shows the results of the test performed in water with the tool decentralized, the data were recorded with 60 RPM.
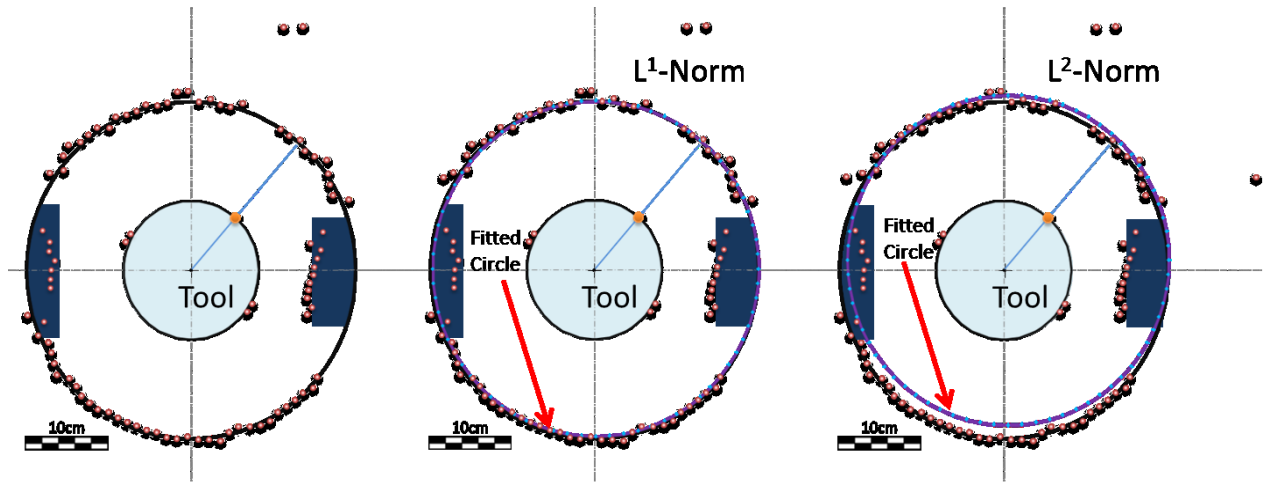
Figure 4-47. Simulating Squeezed Formation in Air (45 RPM, R=40 cm) [28]
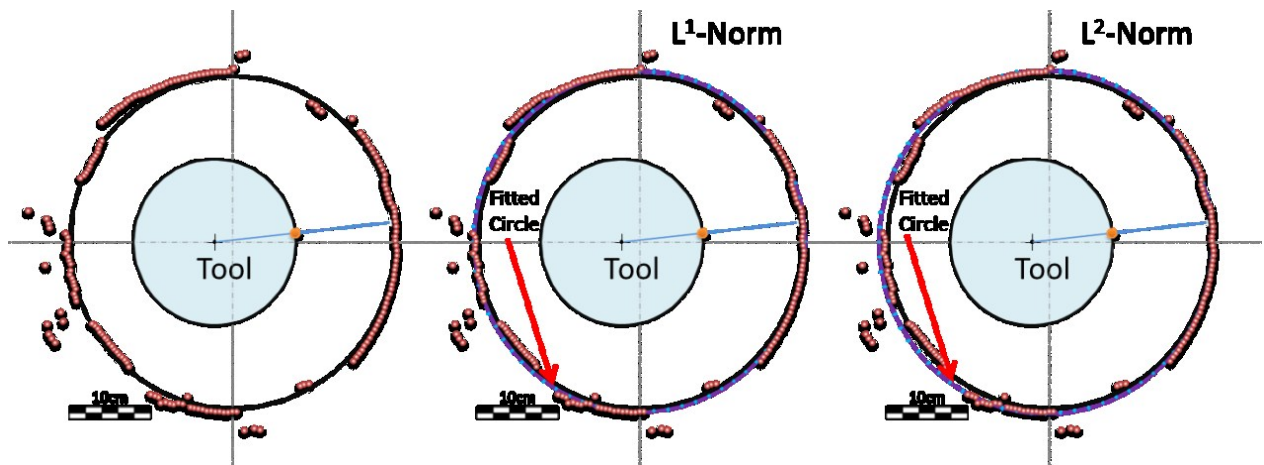
Figure 4-48. Decentralized Position in Water (60 RPM, R=40 cm) [28]
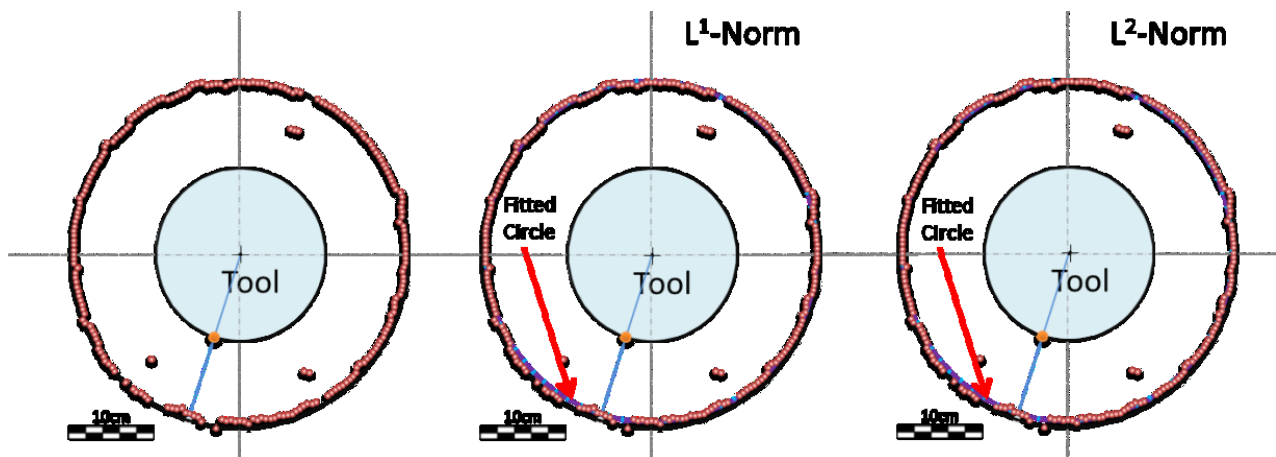
Figure 4-49. Centralized Position in Bentonite Mud (60 RPM, R=40 cm) [28]
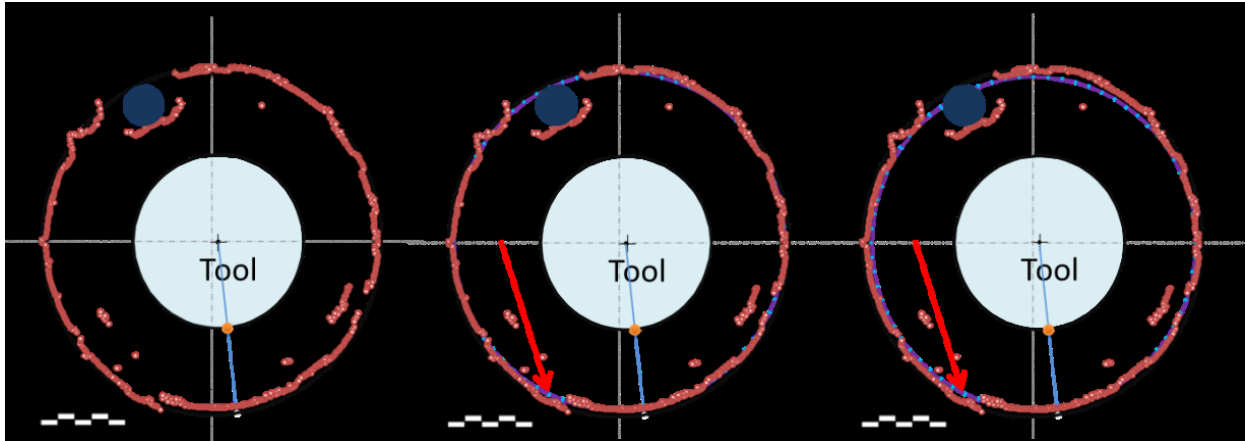
Figure 4-50. Simulating Squeezed Formation in Bentonite Mud (15 RPM, R=40 cm) [28]

Tests have also been performed in bentonite mud; the results are shown in Figure 4-49 and Figure 4-50. Figure 4-49 shows the results of the test with the tool centralized and rotating with 60 RPM. In Figure 4-50 the results of simulating squeezed formation recorded with 15 RPM are shown. In all figures the purple circle shows the result of circle fitting method with both L^1 and L^2-norm error function.

In Figure 4-47 to Figure 4-50 the implemented L^1 and L^2-norm error functions provide different results of circle fitting. In the right part of all figures, the circle with L^2-norm error function fitted is shown. In that case the circle was affected by the data out of the regular range; the results do not match the wellbore profile and also the majority of recorded data. The middle part of the figures shows the results with the L^1-norm error function applied, these results prove that the circle fits the majority of recorded data and also the wellbore; these circles are not affected by the data out of range. In Figure 4-47 and Figure 4-50 squeezed formations are simulated. Although parts of the recorded data are inside the borehole, it does not have any effect on the fitting circle. In Table 4-2 the fitted circle radiuses based on the L^1 and L^2 error functions are shown, the regular borehole radius is 200 mm, errors are shown absolute and in percent. In all those experiments the errors of the L^1-norm approximation are less than those using the L^2-norm error function.

By using the proposed method the circles fitted to the recorded data are not affected by the out range data. Different drilling fluids, the position and the geometry of the tool inside borehole do not seriously affect the results.

Table 4-2. Comparison of the Circle Fitting Results using L^1- and L^2-Norm Error Functions

	L^1-Norm	L^2-Norm	L^1-Norm	L^2-Norm
	Radius of Circle, mm		Error, %	
Figure 47	198.58	195.67	0.7% smaller	2.2% smaller
Figure 48	204.66	206.22	2.3% larger	3.1% larger
Figure 49	196.45	195.92	1.8% smaller	2.0% smaller
Figure 50	194.77	191.27	2.6% smaller	4.4% smaller

When drilling formations – with different characteristics – are affected by different phenomena like hydrostatic pressure or effect of mud cake among others, in case of wash out, squeezed formation or other instabilities, diameter and shape of the wellbore might change. For detecting such anomalies in the wellbore, robust circle fitting seems to be an appropriate method. All experiments were performed with a single set of ultrasonic sensors, future work will emphasize in increasing the number to at least three concurrently operating sensors. With that configuration it is expected to monitor the wellbore shape with enhanced accuracy in real time and automatically compensate decentralization of the tool in the borehole.

5- Conclusions

Based on all the experiments performed it can be concluded that geometry and position of the ultrasonic caliper tool have a great impact on the results. If the diameter of the caliper tool is small compared to the wellbore diameter or if the tool is strongly decentralized within the borehole, the accuracy of the results may decrease dramatically. That challenge can be tackled by some constructional constraints applied to the design of such a tool. The usage of stabilizers of course leads to a rather stable and centralized position of the tool in the borehole; in combination with appropriate tool diameters the geometrical conditions provide short and comprehensible wave paths.

However, viscosity and density of the drilling fluid also has a great impact on the results. With increasing viscosity of drilling fluids the number of recorded data increases; the most number of valid data points were recorded in bentonite mud rather than in water and air. But as the viscosity of the bentonite mud increases by adding more bentonite into the fluid, attenuation of the signals increases and also scattering of the echoes causes few amount of data recorded.

When the density of drilling fluid increases from air, water to bentonite; ultrasonic sensor parameters should be changed so that data could be recorded. Number of sending pulses (input energy) and amplification of the received signal should be changed in different liquid. Performing ultrasonic tests in air needs eight pulses so that enough energy was input into air and then reflected echo could be detected by the sensor. But when tests performed in water two pulses are enough because the speed of sound in water is nearly 4 to 5 times

greater than in air. If more than two pulses were sent into water then the reflected echo will be receive before sending all pulses so the measurement will not correct.

For different drilling fluids appropriate signal amplification was necessary to justify the received signals for correct travel time detection; the maximum amplification was necessary in air. Improper amplification leads to inaccurate results caused by cycle skipping in case of insufficient amplification. If the gain is oversized, noise in the signal may be identified misleadingly as signal arrival.

Blind zone has a great impact on the recording results. Entering to this area means the recorded data are not correct because as the distance between sensor and the wellbore wall is very short so ultrasonic wave returns before the sensor has completed its transmission and the sensor is unable to receive the echo accurately.

In real-world drilling, pressure and temperature will usually increase with depth, implying in many cases a dramatic change of the properties of the drilling fluid. Thus, the properties of the mud measured at surface will not reflect the downhole properties. For that reason, a separate ultrasonic reference sensor system was used to gain experience in recording in-situ the sound velocity of mud. In all experiments velocities were determined accurately in air only; the results obtained are promising so that in future work the package will be installed for ultrasonic caliper sub. Figure 5-1 sketch how such a reference system could be realized in practice. In a slot in the sub transmitter and receiver of the reference ultrasonic package are arranged in proper position. The travel time is measured at a reference distance and transformed into in-situ velocity values of the mud.

Figure 5-1. Referenced ultrasonic sensor, measures the speed of sound in mud at different Pressure and temperature

Referenced ultrasonic sensor is capable of determining speed of sound in the mud with downhole pressure and temperature. This part could be used as a gas kick detector in real time drilling application. The speed of sound in drilling mud is constant value at a desired depth but when the condition of the mud changes, gas kick happened, the speed of sound in gas or in the mixture will drop dramatically. This is the sign of gas kick in real time drilling by using referenced ultrasonic sensor (Figure 5-2).
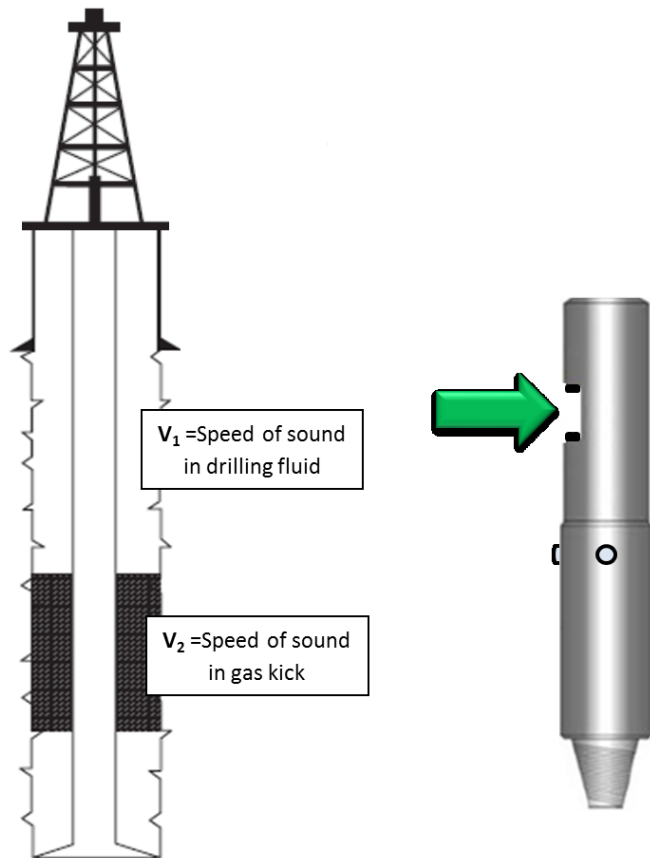
Figure 5-2. Gas kick detector

Ultrasonic test results show that in some cases and situations like decentralized position of the tool or when there is an artifact in the wellbore to simulate the squeezed formations, there are some area's in the wellbore that the sensor could not detect them and record any kind of data. The reason for that might be the distance between the sensor and the wall is very short or out of the sensor's range. Another reason might be the angle between the sensor and wall of the wellbore which causes scattering of the echoes or multiple reflections of the echoes. By increasing the number of sensors, minimum three, this problem could be covered and other two sensors could be compensate the parts that was not recorded by the first sensor (Figure 5-3).
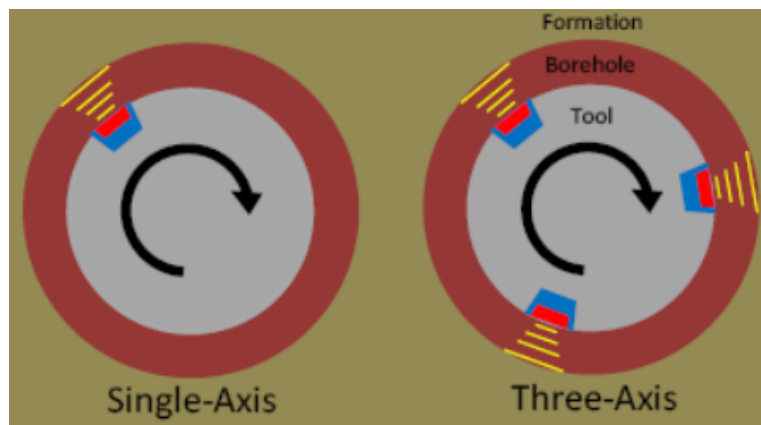
Figure 5-3. Increasing the number of sensor to cover the wellbore with receiving data [26]

During drilling operation, borehole will be affected by different phenomena and some instability like wash out, squeezed formation or etc. which causes the diameter and shape of the wellbore might change. For detecting such anomalies in the wellbore, robust circle fitting seems to be an appropriate method. By increasing the number of ultrasonic sensor and using the robust circle fitting method, it is expected to monitor the wellbore shape with enhanced accuracy in real time and automatically compensate decentralization of the tool in the borehole.

Performing all these tests for developing an ultrasonic caliper is the reason to use multiple of them along the drill string to monitor the wellbore diameter, shape and wellbore stability in real time drilling application (Figure 5-4).
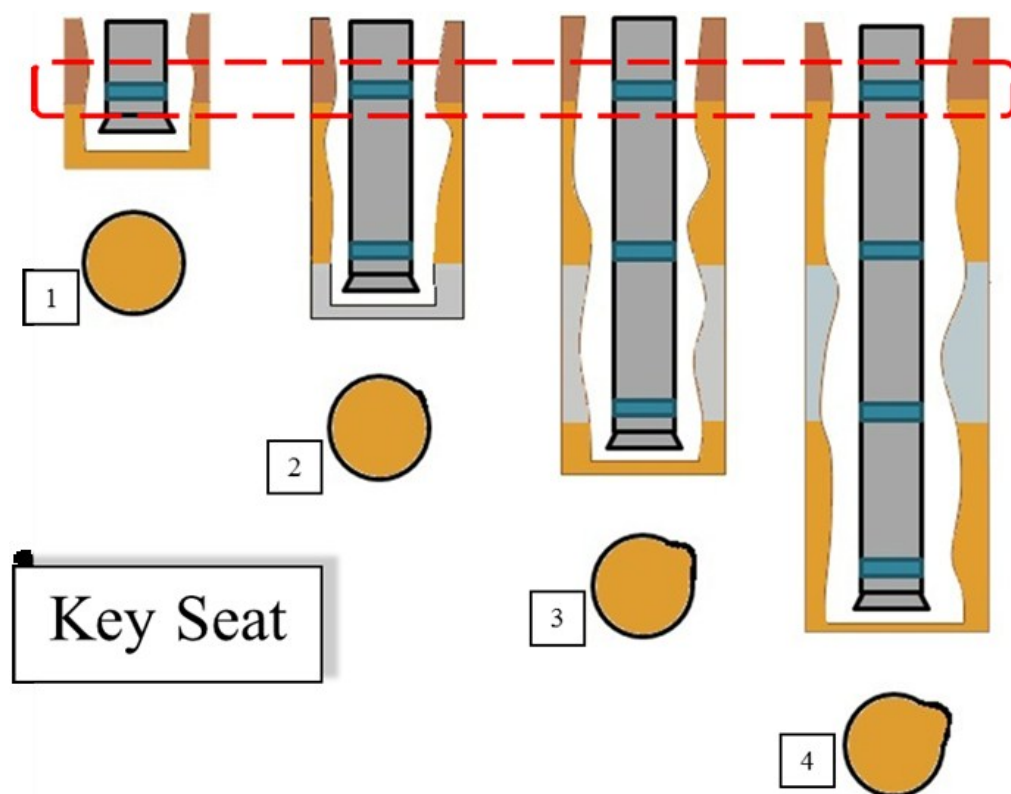
Figure 5-4. Using multiple ultrasonic calipers along the drill string

Depending on the sensors density along the drill string, a 4D image of the borehole with more or less resolution can be created. Such images will reflect the evolution of a borehole in terms of shape and diameter. Since the creation of key-seats for instance will be observable during drilling, this could be a good monitoring tool for the driller to tackle arising problems in an early stage.

6- References

[1].   I.D.R. Bradford, W.A. Aldred, J.M. Cook, E.F.M. Elewaut, J.A. Fuller, T.G. Kristiansen, T.R. Walsgrove. 2000. When Rock Mechanics Met Drilling: Effective Implementation of Real-Time Wellbore Stability Control Paper SPE 59121, Presented at IADC/SPE Drilling Conference held in New Orleans, Louisiana, 23–25 February.

[2].   Bradley, W. 1978. Bore Hole Failure near Salt Domes, paper SPE 7503 presented at the 53th Annual Fall Technical conference and Exibition of the SPE of AIME, 1-3 October, Houston, Texas.

[3].   B. Pasic, N. G. Medimurec, D. Matanovic. 2007. Wellbore Instability: Causes and Consequences, Vol. 19, Page. 87 – 98, Zagreb.

[4].   C. Maranuk, 1997. "Development of an MWD Hole Caliper for Drilling and Formation Evaluation Applications" SPE 38585, San Antonio, Texas, October.

[5].   Elahifar, B., Esmaeili, A., Fruhwirth, R.K., Thonhauser, G., 2012: Determining the Accuracy of Ultrasonic Caliper Measurements for Real Time Drilling Application. SPE 158160, Asia Pacific Oil and Gas Conference and Exhibition, Perth, Australia, 22-24 October.

[6].   C. Wolfe, S. Morris, and A. Baule, 2009. Enhanced Real Time Wellbore Stability Monitoring Using High Definition Imaging with Wired Pipe Telemetry, Paper SPE 119808, Presented at Conference and Exhibition held in Amsterdam, The Netherlands, 17–19 March.

[7]. Carlos Maeso, I. Tribe, 2001. Hole shape From Ultra Sonic Caliper and Density while Drilling, Paper SPE 71395, Presented at Annual Technical Conference and Exhibition held in New Orleans, Louisiana, 30 September–3 October.

[8]. F. Zausa, L. Civolani, M. Brignoli, F. J. Santarelli, 1997. Real Time Wellbore Stability Analysis at the Rig Site Paper SPE 37670, Presented at Drilling Conference held in Netherlands, 4-6 march.

[9]. G. Lindsay, S. Morris and J. Lofts, 2007. Wellbore Stress Indicators While Drilling A comparison of Induced features From Wireline and LWD high Resolution Electrical Images, Paper SPE 105808, Presented at Drilling Conference held in Amsterdam, The Netherlands, 20–22 February.

[10]. I.D.R. Bradford, W.A. Aldred, J.M. Cook, E.F.M. Elewaut, J.A. Fuller, T.G. Kristiansen, T.R. Walsgrove, 2000. "When Rock Mechanics Met Drilling Effective Implementation of Real-Time Wellbore Stability Control" paper SPE 59121, Presented at Drilling Conference held in New Orleans, Louisiana, 23–25 February.

[11]. J. A. Greenwood, A.Brehm, E. van Oort, D.R Algu, Y.E. Volokitin, 2005. Application of Real Time Wellbore Stability Monitoring on a Deep Water ERD well Paper SPE 00092588, Presented at Drilling Conference held in Amsterdam, The Netherlands, 23-25 February.

[12]. J. Greenwood, P. Bowler, J.F. Sarmiento, S. Willson, S. Edwards, 2006. Evaluation and application of Real Time Image and Caliper Data as Part of a Wellbore Stability Monitoring Provision, Paper SPE 99111, and Presented at Drilling Conference held in Miami, Florida, U.S.A., 21–23 February.

[13]. P. Boonen, G. McElhinney, 2002. Rock Mechanic and Wellbore Stability Analysis While Drilling Using LWD Sonic Density and Caliper Measurement, Paper SPE 78208, Rock Mechanics Conference held in Irving, Texas, 20-23 October.

[14]. S. Edwards, B. matsutsuyu, S. Willson, 2003. Imaging Unstable Wellbores While Drilling, Paper SPE 00079846, Presented at Drilling Conference held in Amsterdam, The Netherlands, 19-21 February.

[15]. Uday A. Tare, et al 2000. Understanding Chemical-Potential-Related Transient Pore-Pressure Response to Improve Real-Time Borehole (In) Stability Predictions, Paper SPE 00065514, Presented at SPE/Petroleum Society of CIM International Conference on Horizontal Well Technology held in Calgary, Alberta, Canada, 6-8 November.

[16]. G. Uswak, N. McLafferty, 1995. Cement Imaging Through Ultrasonics, SPE 95-01-03, Journal of Canadian Petroleum Technology, Volume 34, Number 1.

[17]. Schultz, Ward E., Moake, Gordon L., Jackson, Charles E., 1998. Field Examples of Ultrasonically-Enhanced Density, Neutron-Porosity, and Caliper Logs Obtained While Drilling, SPE 36545-PA, Volume 1, Number 3, June.

[18]. Allen Bradley, 1999. Fundamentals of sensing training manual, publication fsm-900 edition. Rockwell Automation, Inc.

[19]. Murata, Ultrasonic sensor application manual, Catalog No.S15E-5, http://www.symmetron.ru/suppliers/murata/files/pdf/murata/ultrasonic-sensors.pdf [16/2/2013].

[20]. Bradley, Ultrasonic proximity sensor manual, Page 3-3, http://literature.rockwellautomation.com/idc/groups/literature/documents/ca/c116-ca503_-en-p.pdf [16/2/2013].

[21]. EGE, "Ultrasonic Sensor", Elektronik Spezial Sensoren, Page 2, http://www.bibus.es/fileadmin/editors/countries/biesp/product_data/ege/documents/ege_ultrasonic_sensors_catalogue_en.pdf [16/2/2013].

[22]. Eduardo R. Miranda and Marcelo M. Wanderley. New Digital Musical Instruments: Control and Interaction beyond the Keyboard, A-R Editions, Spring 2006. ISBN 0-89579-585-X

[23]. J.J. Orban, M.S. Dennison, M. Jorion, J. Mayes, 1991. New Ultrasonic Caliper for MWD Operations, SPE 21947, Presented at Drilling Conference held at Amsterdam, 11-14 March.

[24]. C. Maeso, I. Tribe, 2001. Hole Shape from Ultrasonic Calipers and Density While Drilling – A Tool for Drillers, SPE 71395, New Orleans, Louisiana, 30 September–3 October.

[25]. J C Kimball, Harold Story, 1998 Fermat's principle, Huygens 'Principle, Hamilton's optics and sailing strategy, European journal of physics, Volume 19 issue 1, page 15-24.

[26]. Market, J., and Parker, T. 2011. Reliable LWD Caliper Measurements. Paper SPE 146245, Presented at European Offshore Conference, Aberdeen, UK, 6-8 September.

[27]. Elahifar, B., Esmaeili, A., Fruhwirth, R. K., and Thonhauser, G. 2012. Accuracy of Ultrasonic Sensor in Caliper Log. IEEE International Instrumentation and Measurement Technology Conference, Graz, Austria, Pape 449-453, 13-16 May.

[28]. Elahifar, B., Esmaeili, A., Fruhwirth, R.K., Thonhauser, G., 2012. Real time Measurement of Borehole Shape and Diameter by Using Ultrasonic Caliper in Different Drilling Fluid and Wellbore Conditions for Detecting Instabilities. SPE Canadian Unconventional Resources Conference held in Calgary, Alberta, Canada, 30 October–1 November.

[29]. F. Fasch, 2012, Development of A Downhole-Sensor-Testbed, Master thesis, Automation Technology – Economy Graz University.

[30]. Bube, K.P., Langan, R.T., 1997: Hybrid lambda1/lambda2 minimization with applications to tomography. Geophysics, 62, 04, 1183-1195.

[31]. Chernov N., Lesort C., 2005: Least squares fitting of circles. Journal of Mathematical Imaging and Vision, 23, 239-251.

[32]. Chernov, N.I., Ososkov, G.A., 1984: Effective algorithms for circle fitting. Journal of Computer Physics Communications, 33, 329-333.

[33]. Gentle, J., 2007: Matrix Algebra: Theory, Computations, and Applications in Statistics. New York: Springer. ISBN 978-0-387-70872-0.

[34]. Kasa, I., 1976: A curve fitting procedure and its error analysis, IEEE Trans. Inst. Meas. 25, 8-14.

[35]. Paige C. C., Saunders M. A., 1982: LSQR: An algorithm for sparse linear equations and sparse least squares, ACM Transactions on Mathematical Software, 8(1), 43-71.

[36]. Nickolay A. Smirnov, Aleksey S. Varykhalov, 2008. Determining the horizontal well profile with acoustic reflected wave method, SPE 117430, Presented at Russian Oil and Gas Technical Conference and Exhibition, 28-30 October.

[37]. Solon Thomaz Coelho de Souza Padilha and Romero Gomes da Silva Araujo, 1997. New Approach on Cement Evaluation for Oil and Gas Reservoirs Using Ultrasonic Images, SPE 38981, Presented at Latin American and Caribbean Petroleum Engineering Conference, 30 August-3 September.

[38]. J. Hayrnan, R. Hutin, P. V. Wright, 1991. High-Resolution Cementation and Corrosion Imaging By Ultrasound, SPE 1991-KK, Society of Petrophysicists & Well Log Analysts.

[39]. G.L. Moake, J.R. Birchak, R.G. Matthews, and W.E. Schultz, 1995. Standoff and Caliper Measurements While Drilling Using a New Formation-Evaluation Tool with Three Ultrasonic Transducers, SPE 26494-PA, Drilling & Completion, Volume 10, Number 2.

[40]. Eric Molz, Duane Canny, Eddie Evans, 1998. Ultrasonic Velocity And Attenuation Measurements In High Density Drilling Muds, SPE 1998-F, Society of Petrophysicists & Well Log Analysts.

[41]. G. Aithoff, A. Arian, A. B. Kavaipatti, G. L. Varsamis, L. T. Wisniewski, 1998. MWD Ultrasonic Caliper Advanced Detection Techniques, SPE 1998-III, Society of Petrophysicists & Well Log Analysts, 26-29 May.

[42]. Alex Q. Chen, S. Freear, D.M.J. Cowell. Measurement of Solid in Liquid Content Using Ultrasound Attenuation 5th World Congress on Industrial Process Tomography, pp.820, September 2007, Norway, Bergen.

[43]. Rao, Rama V. N, Zhu Zheny, Burns Daniel R, Toksoz M. Nafi, 2002. Acoustic Logging While Drilling (LWD): Experimental Studies with Anisotropic Models, Earth Resources Laboratory Industry Consortia Annual Report.

[44]. Eric Brian Molz, 2000. Mud Velocity Corrections for High Accuracy Standoff/Caliper Measurements, SPWLA 2000-P, Society of Petrophysicists & Well Log Analysts.

[45]. Amoco, Wellbore stability Manual

[46]. J. Reinecker, M. Tingay and B. Muller, 2003. Borehole Breakout Analysis from four-arm Caliper Log, World Stress Map Project

[47]. B. S. Adnoy, I. Cooper, S. Z. Miska, R. F. Mitchell and M. L. Payne, 2009. Advanced Drilling and Well Technology, ISBN 978-1-55563-145-1, Society of Petroleum Engineers, Page 378.

[48]. O. Serra, 1984. Fundamentals of Well – Log Interpretation, ISBN 0-444-42132-7, Elsevier Science Publisher, Pages 213 to 225.

[49]. W. Standifird, 2007. A Proposal to Develop an Improved Methodology for Wellbore Stability Prediction, Drilling Engineering Association, http://dea-global.org/wp-content/uploads/2009/10/DEA_161_Presentation.pdf [25/02/2013].

[50]. Elahifar, B., Esmaeili, A., Fruhwirth, R.K., Thonhauser, G., 2013: Wellbore Instability monitoring by using 4D Imaging of Ultrasonic Caliper Logs in Real Time Drilling. SPE

17002-MS, International Petroleum Technology Conference, Beijing, China, 26-28 March.

7- Appendix

7.1 Testing in Air

Figure 7-1 to Figure 7-15 show the results of ultrasonic tests and measurement in air. Test results are categorized based on the tool geometry and position on the wellbore.

7.1.1 Centralized position of the tool in the wellbore (Air)
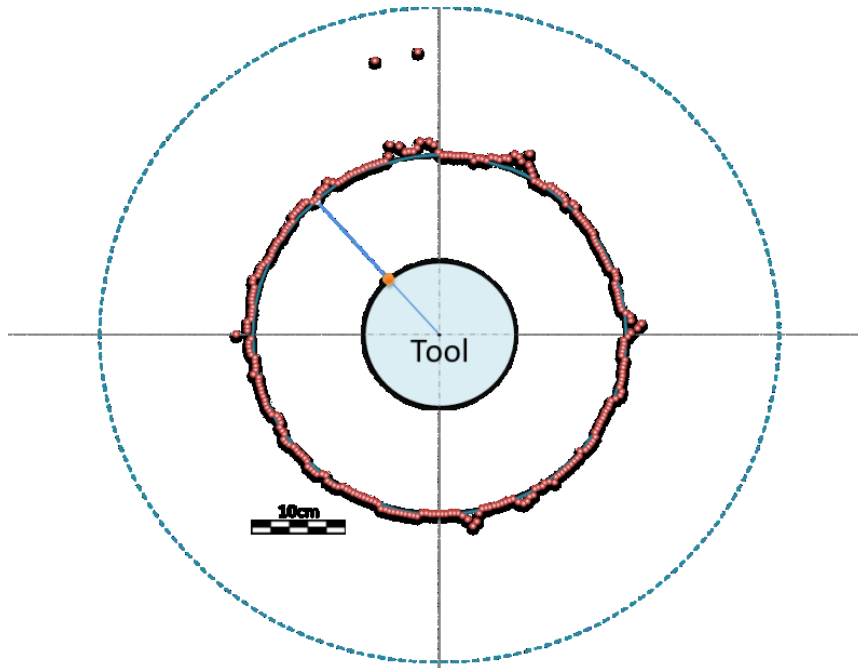
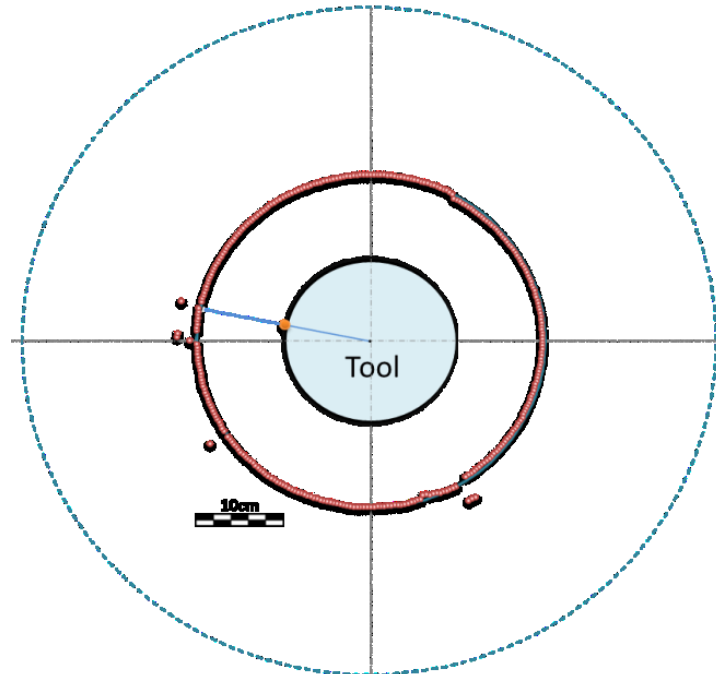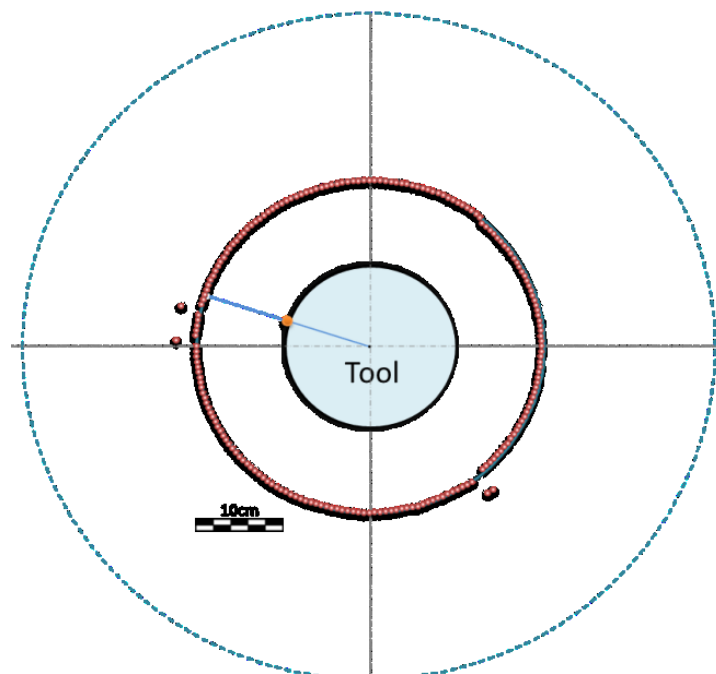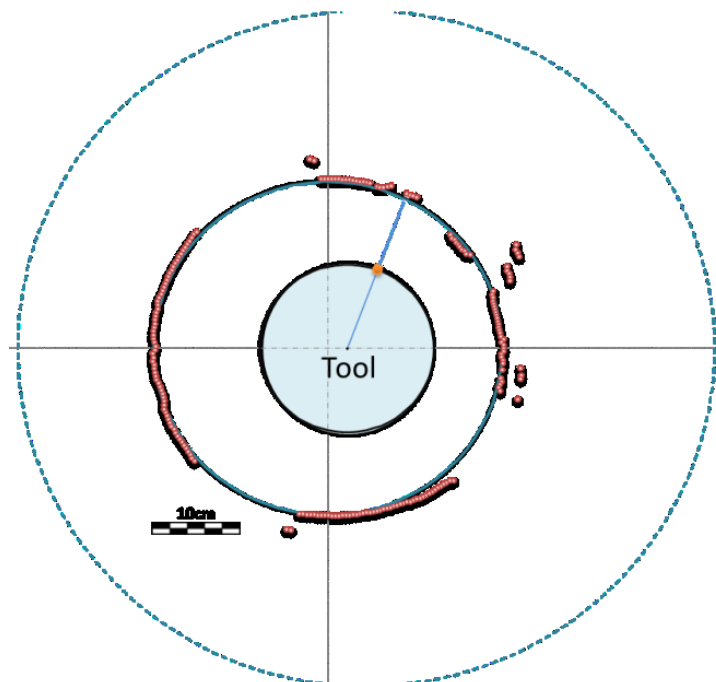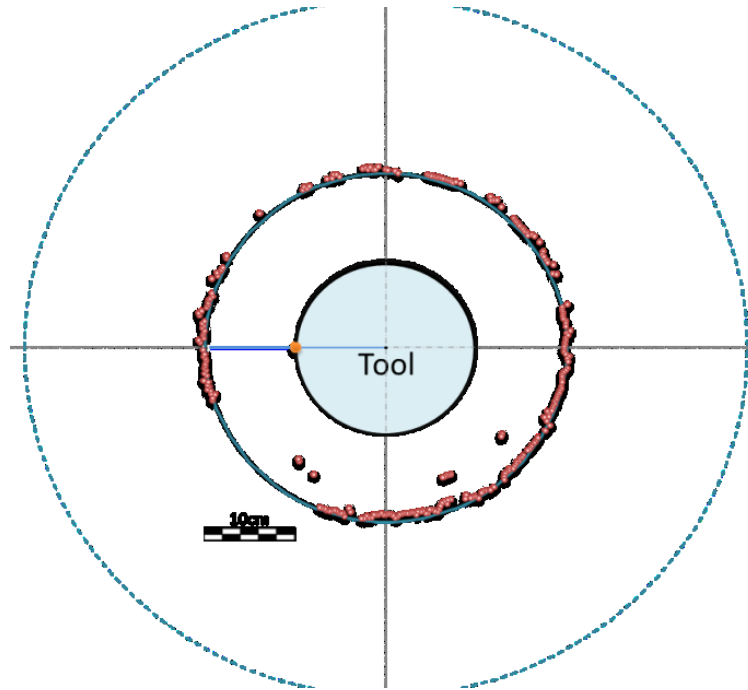**Figure 7-1. Sensor rotates in air with 15 RPM in 40 cm diameter wellbore (centralized position)**
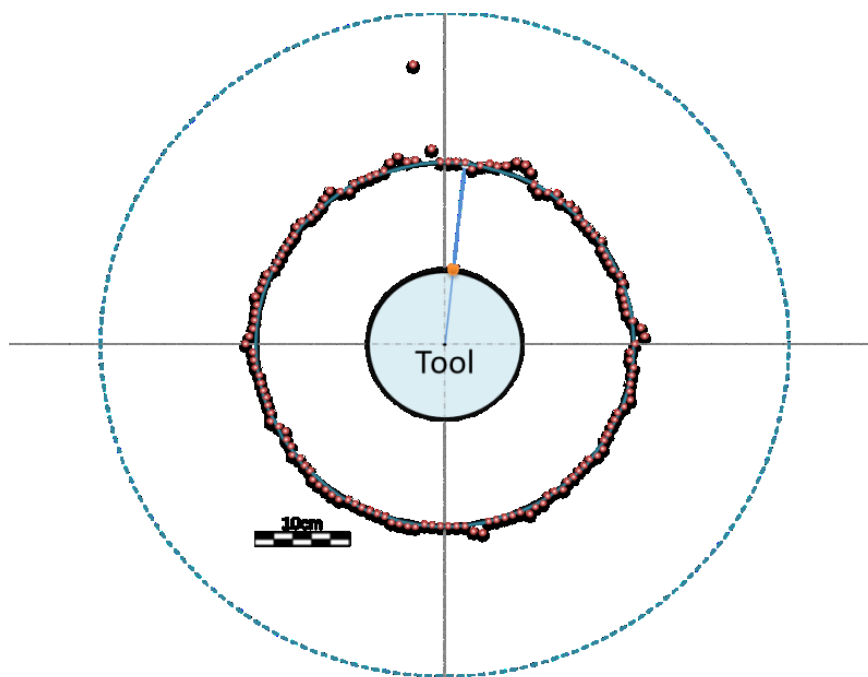
Figure 7-2. Sensor rotates in air with 30 RPM in 40 cm diameter wellbore (centralized position)
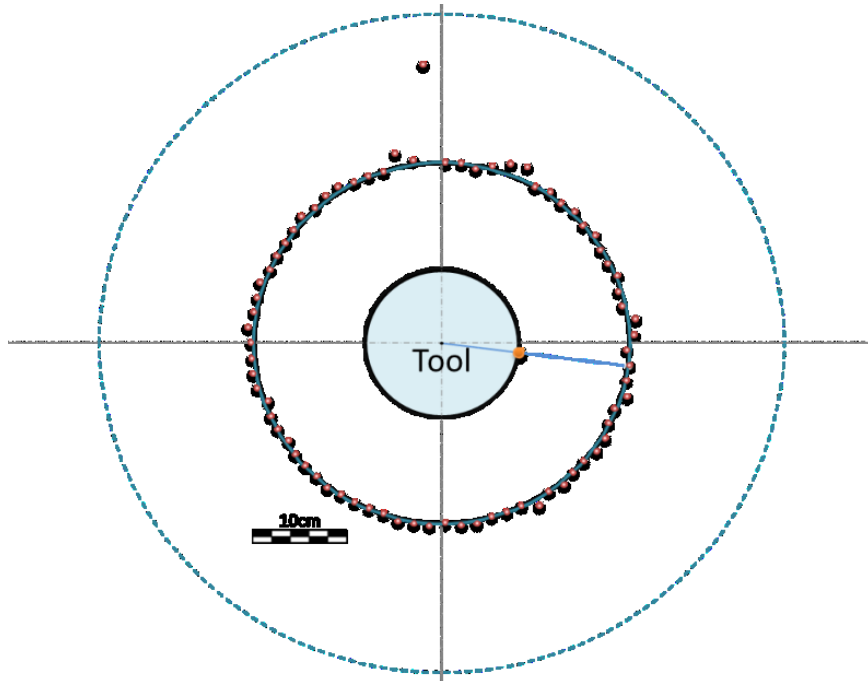
Figure 7-3. Sensor rotates in air with 60 RPM in 40 cm diameter wellbore (centralized position)
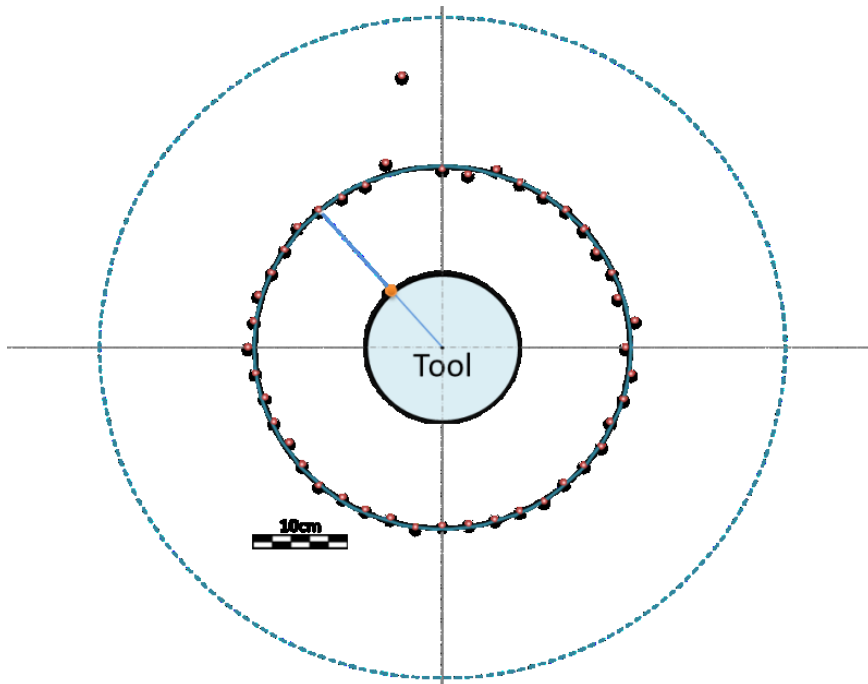
Figure 7-4. Sensor rotates in air with 100 RPM in 40 cm diameter wellbore (centralized position)
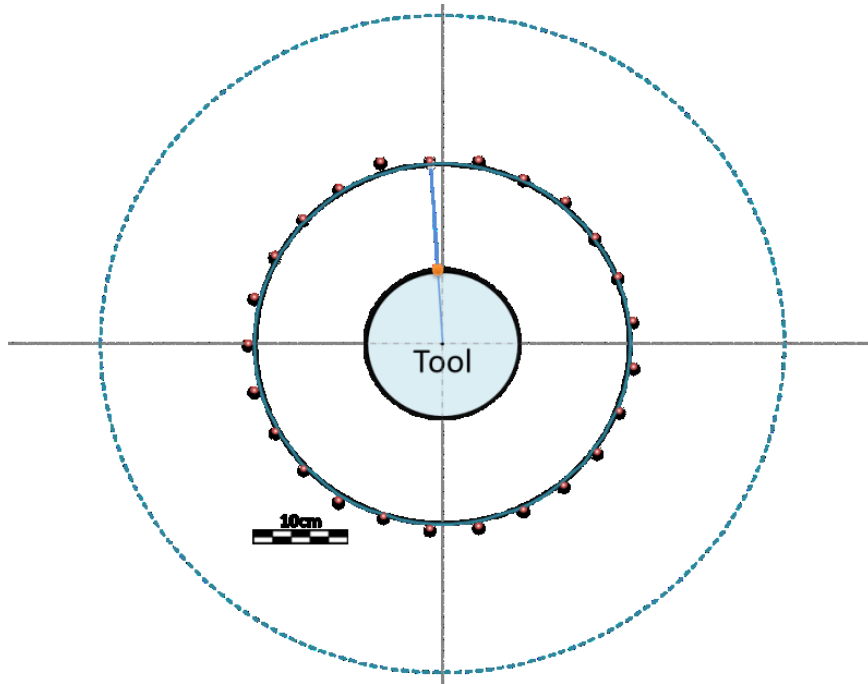
Figure 7-5. Sensor rotates in air with 180 RPM in 40 cm diameter wellbore (centralized position)

7.1.2 Decentralized position of the tool in the wellbore (Air)
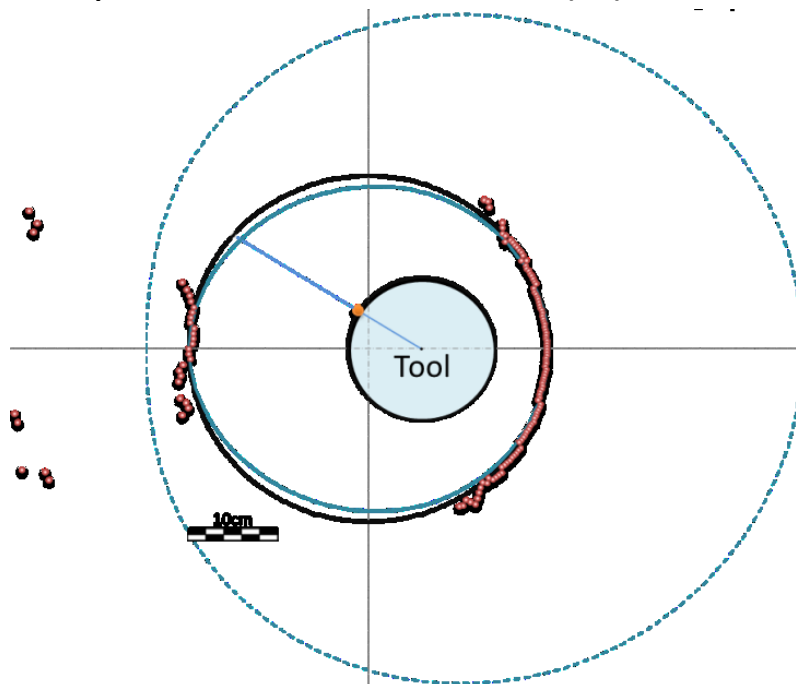
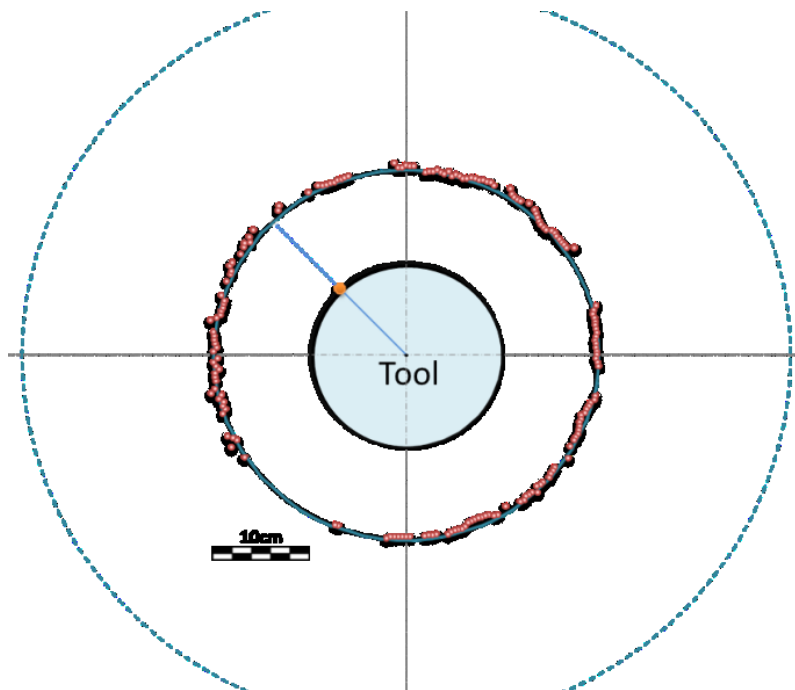**Figure 7-6. Sensor rotates in air with 15 RPM in 40 cm diameter wellbore (decentralized position)**
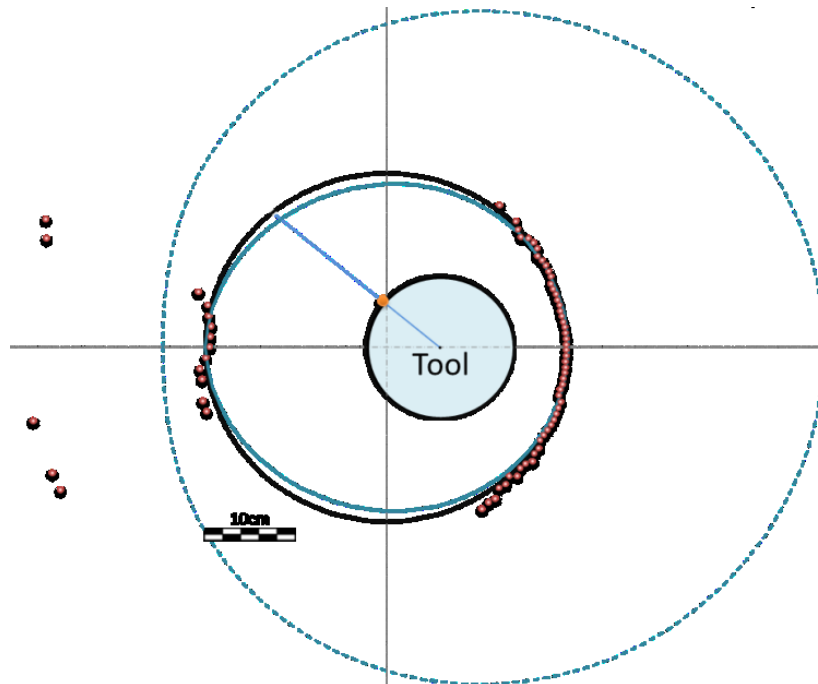
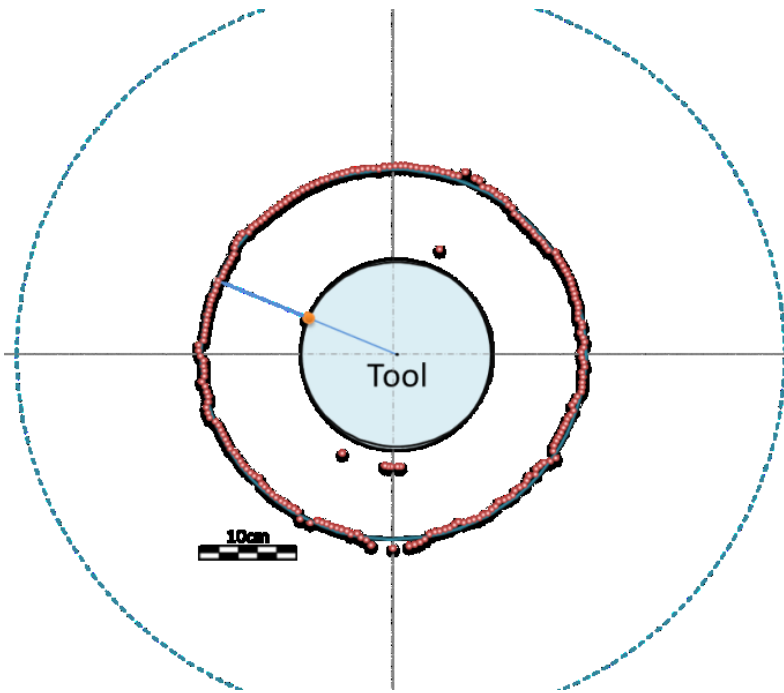**Figure 7-7. Sensor rotates in air with 30 RPM in 40 cm diameter wellbore (decentralized position)**
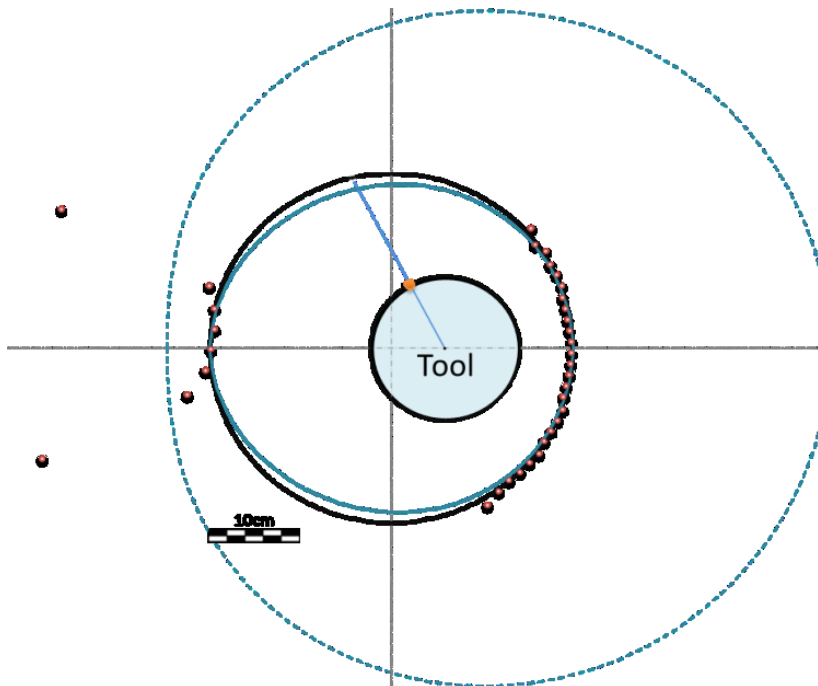
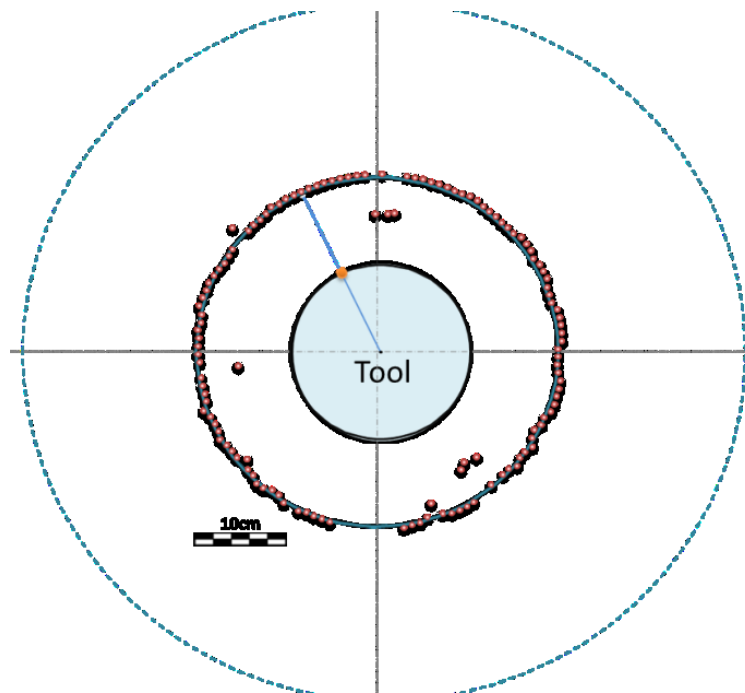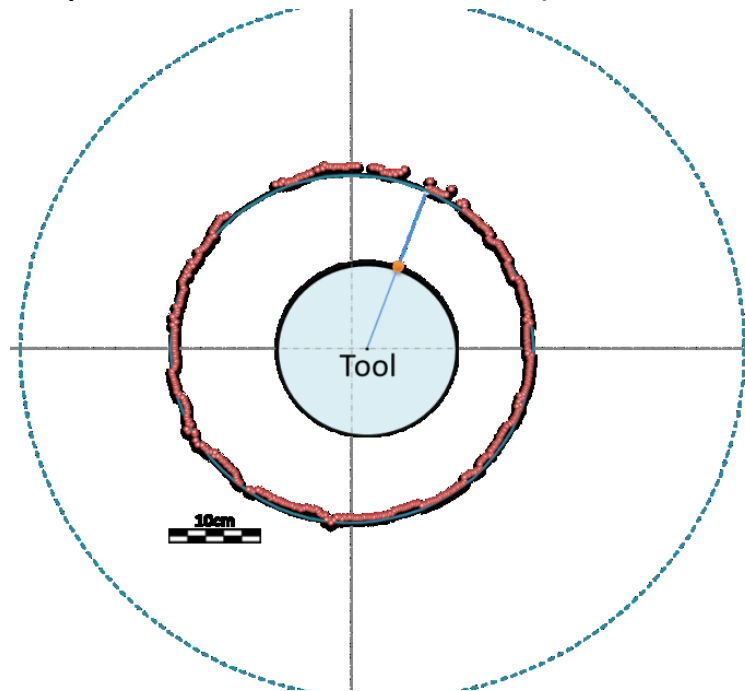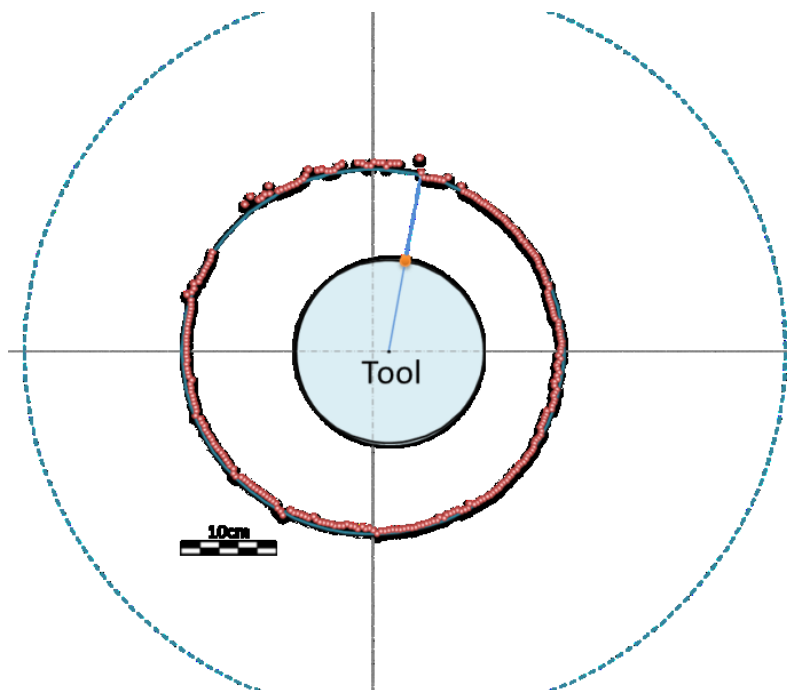**Figure 7-8. Sensor rotates in air with 60 RPM in 40 cm diameter wellbore (decentralized position)**
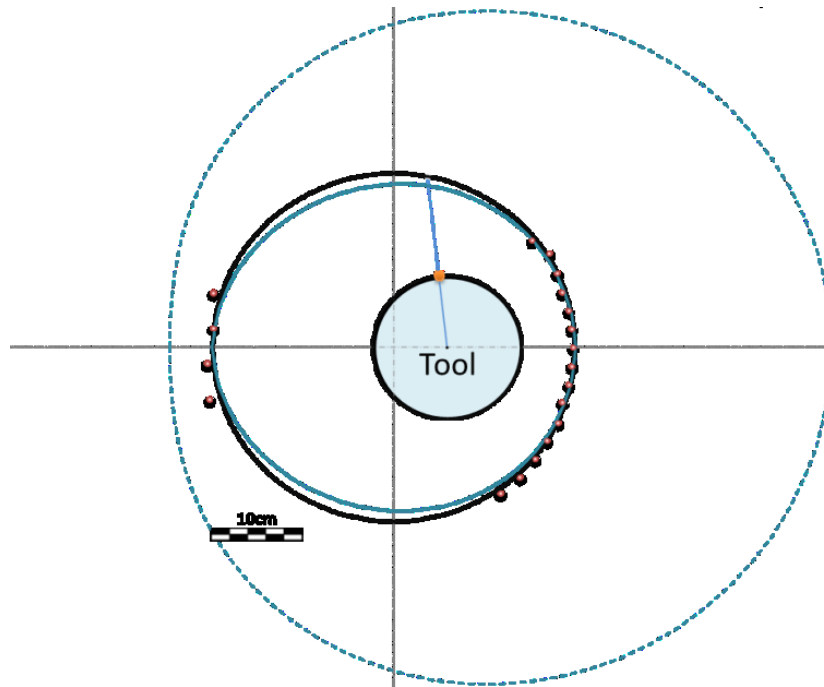
Figure 7-9. Sensor rotates in air with 100 RPM in 40 cm diameter wellbore (decentralized position)
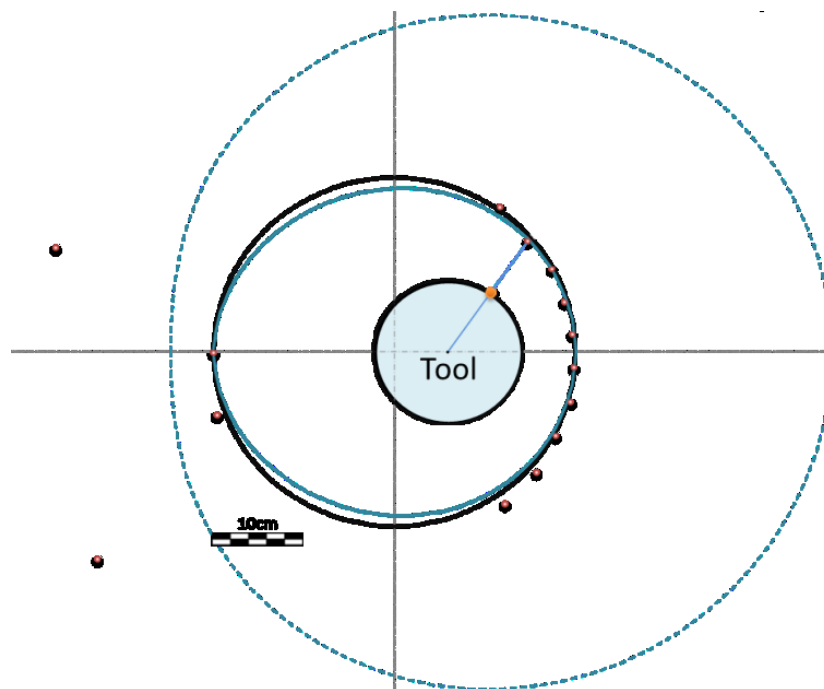
Figure 7-10. Sensor rotates in air with 180 RPM in 40 cm diameter wellbore (decentralized position)

7.1.3 Simulation of squeezed formation (Air)
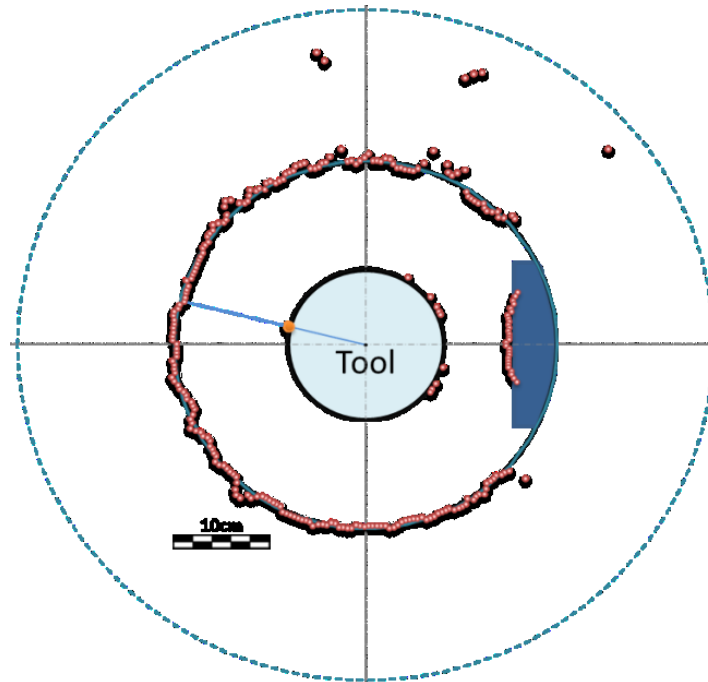
Figure 7-11. Sensor rotates in air with 15 RPM in 40 cm diameter wellbore (simulating squeezed formation)
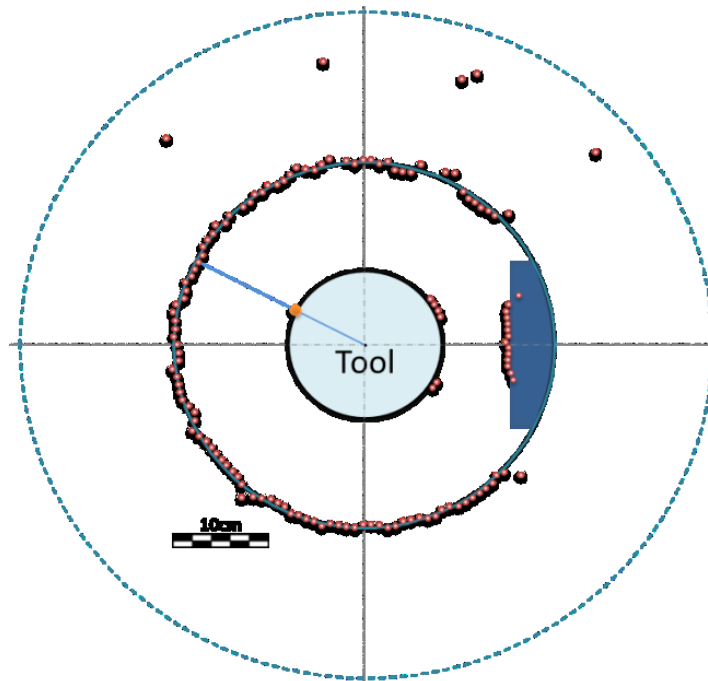
Figure 7-12. Sensor rotates in air with 30 RPM in 40 cm diameter wellbore (simulating squeezed formation)
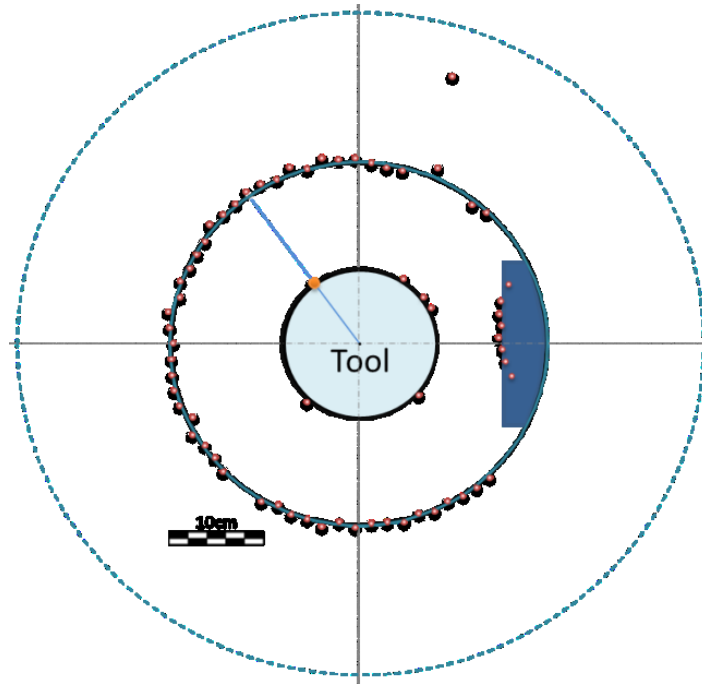
Figure 7-13. Sensor rotates in air with 60 RPM in 40 cm diameter wellbore (simulating squeezed formation)
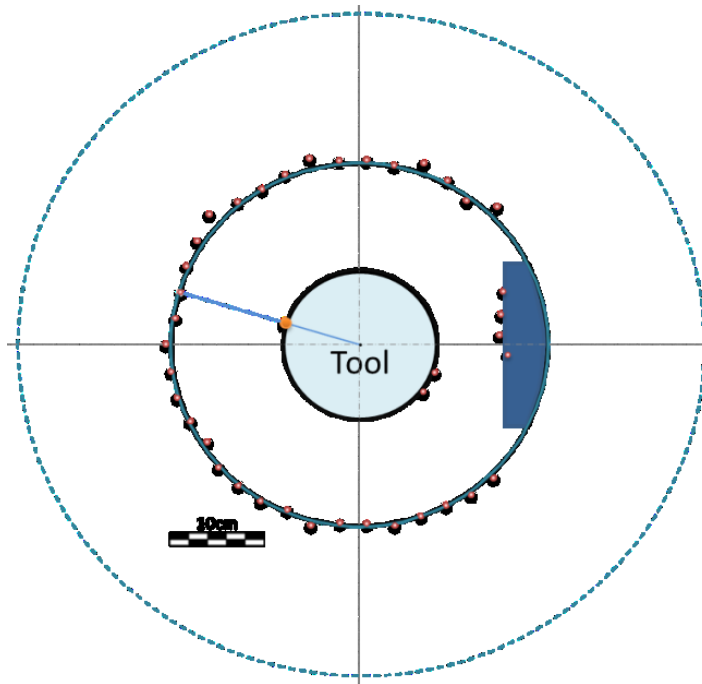
Figure 7-14. Sensor rotates in air with 100 RPM in 40 cm diameter wellbore (simulate squeezed formation)
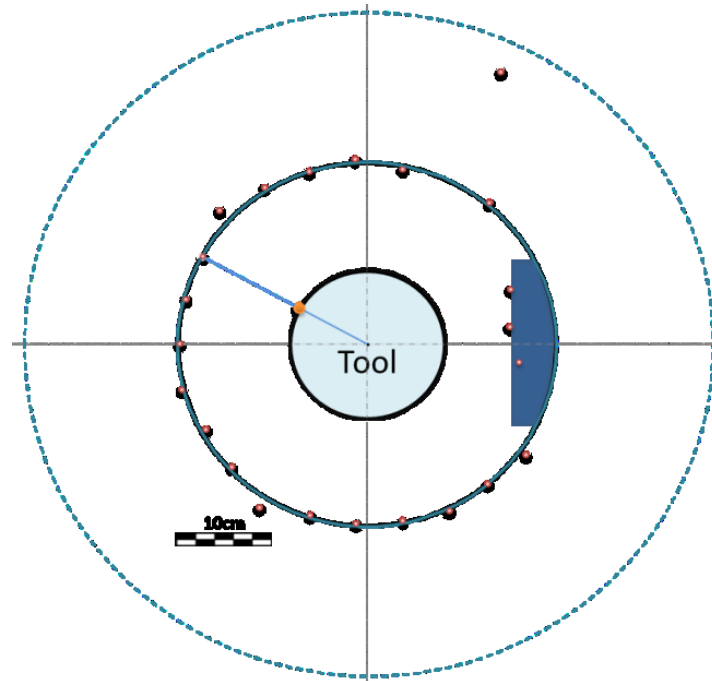
Figure 7-15. Sensor rotates in air with 180 RPM in 40 cm diameter wellbore (simulate squeezed formation)

7.2 Testing in Water

Figure 7-16 to Figure 7-27 show the results of ultrasonic tests and measurement in water. Test results are categorized based on the tool geometry and position on the wellbore.

7.2.1 Centralized position of the tool in the wellbore (Water)

Figure 7-16. Sensor rotates in water with 30 RPM in 40 cm diameter wellbore (centralized position)

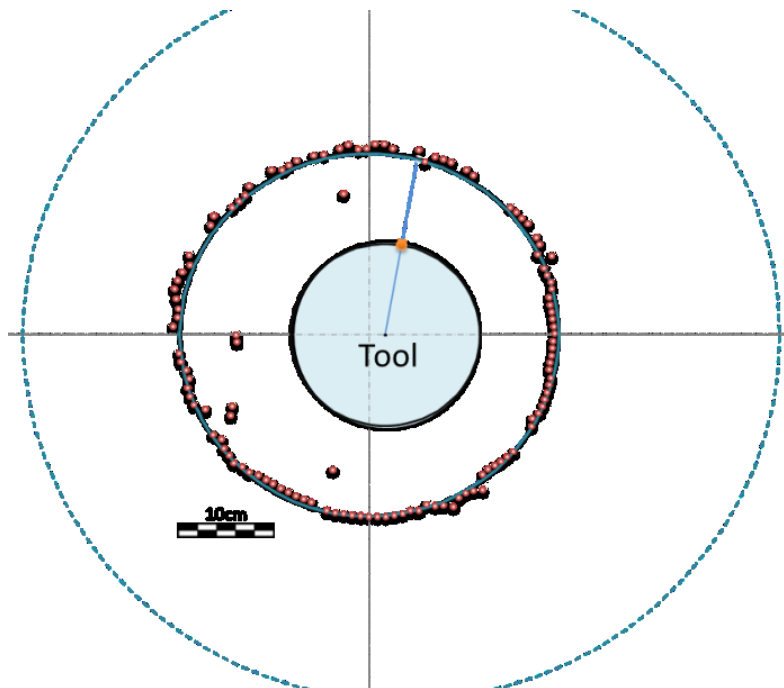**Figure 7-17. Sensor rotates in water with 45 RPM in 40 cm diameter wellbore (centralized position)**
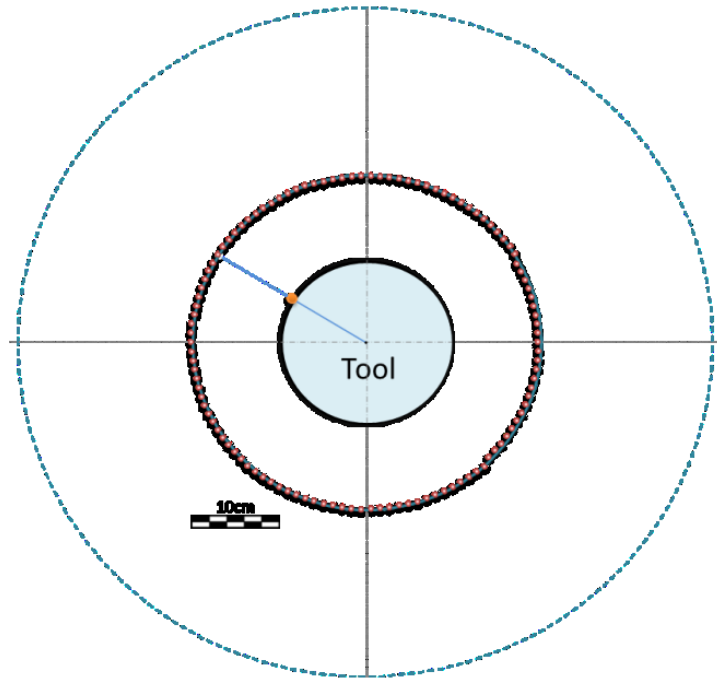
Figure 7-18. Sensor rotates in water with 60 RPM in 40 cm diameter wellbore (centralized position)
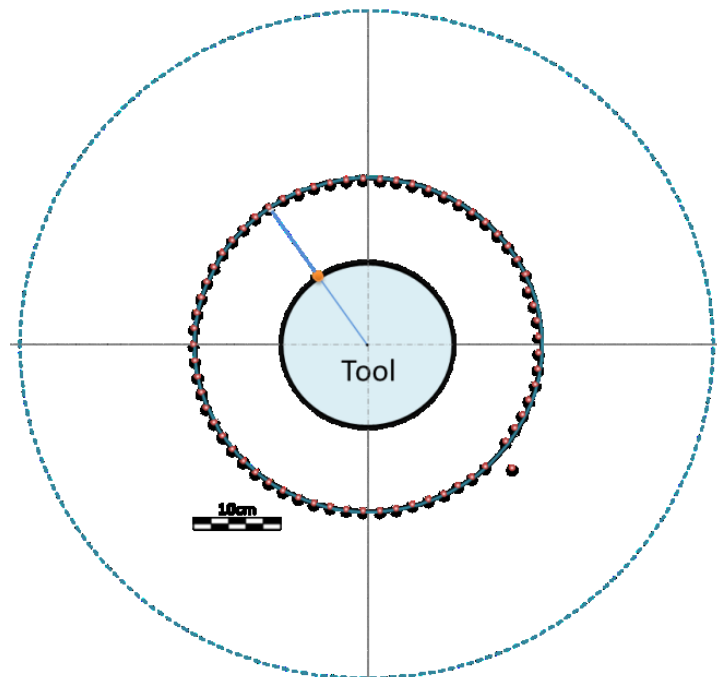
Figure 7-19. Sensor rotates in water with 100 RPM in 40 cm diameter wellbore (centralized position)

7.2.2 Decentralized position of the tool in the wellbore (Water)
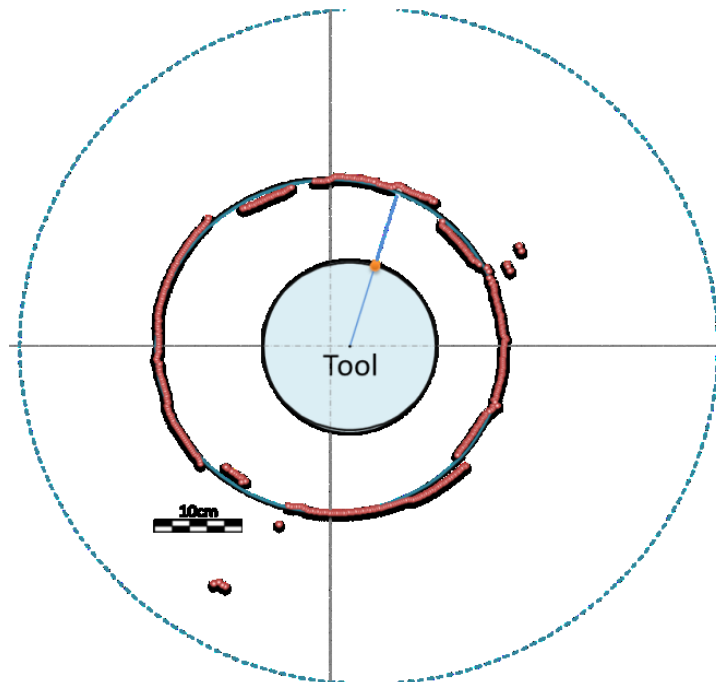
Figure 7-20. Sensor rotates in water with 30 RPM in 40 cm diameter wellbore (decentralized position)

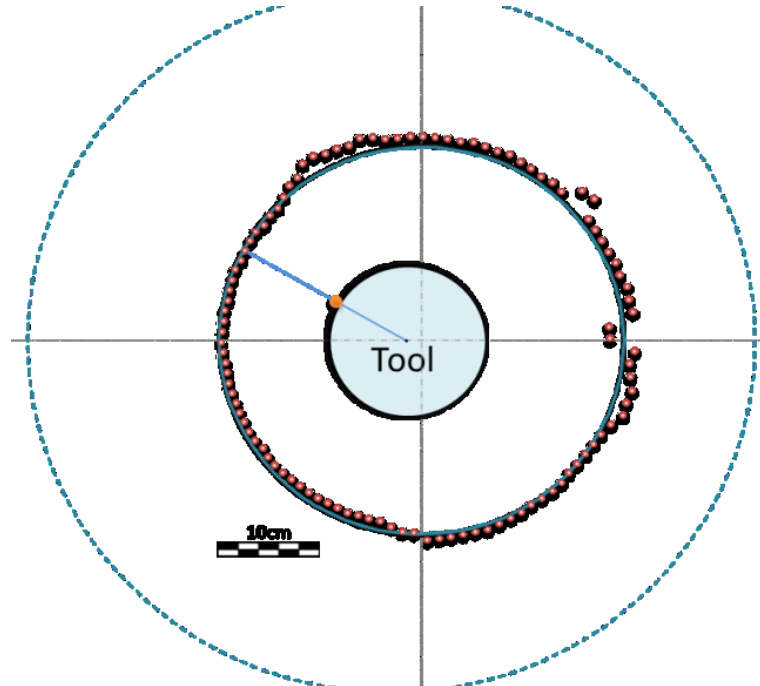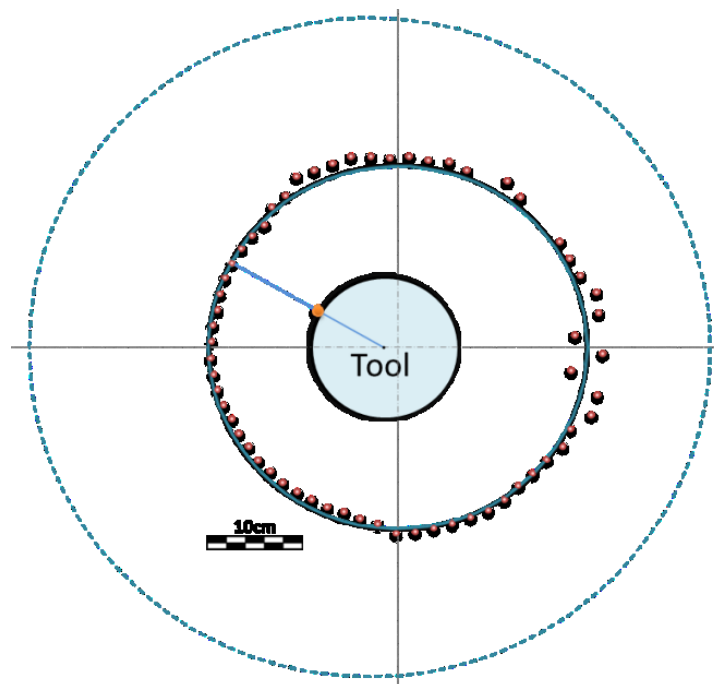**Figure 7-21. Sensor rotates in water with 45 RPM in 40 cm diameter wellbore (decentralized position)**
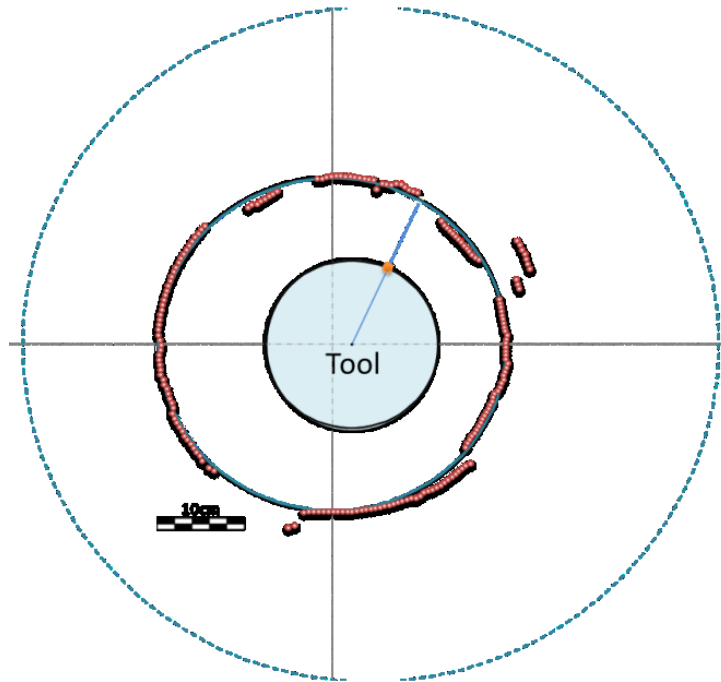
Figure 7-22. Sensor rotates in water with 60 RPM in 40 cm diameter wellbore (decentralized position)
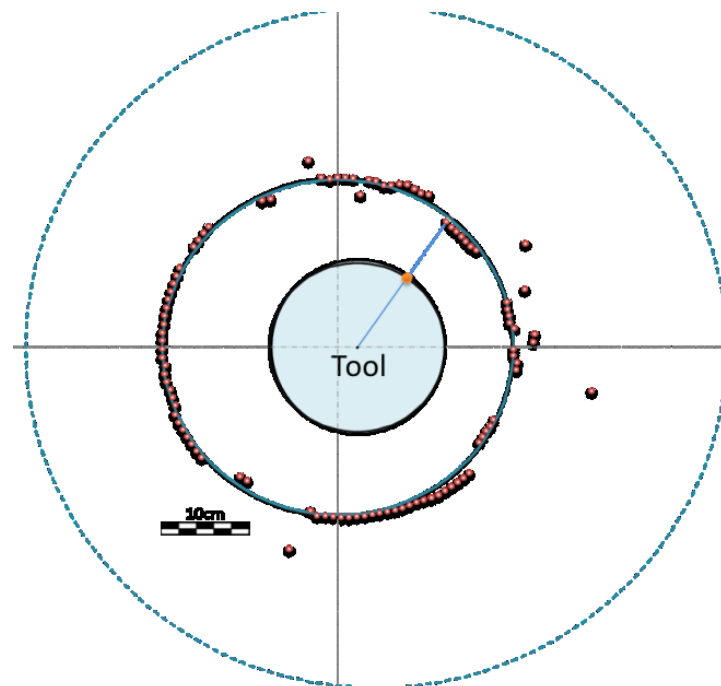
Figure 7-23. Sensor rotates in water with 100 RPM in 40 cm diameter wellbore (decentralized position)

7.2.3 Simulation of squeezed formation (Water)
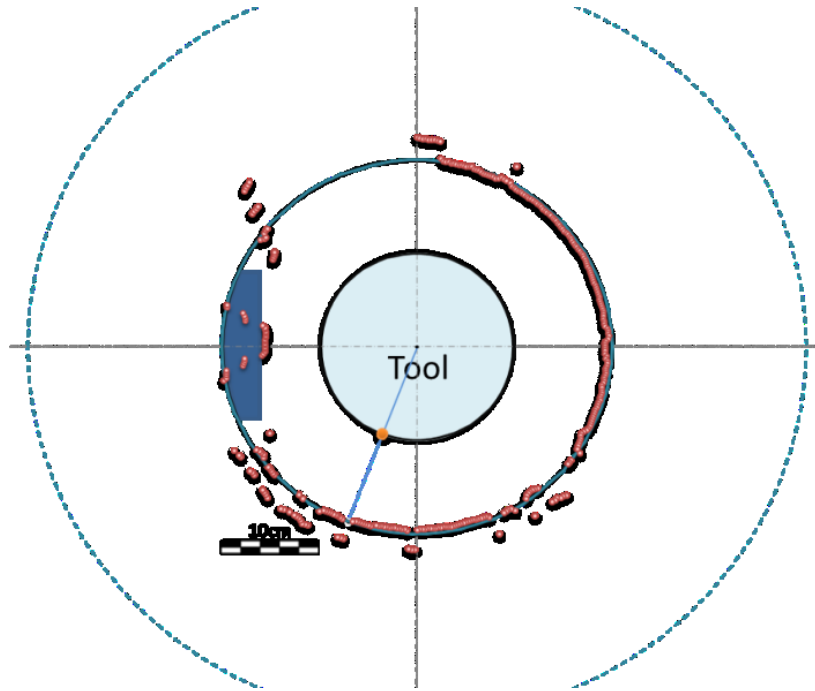
Figure 7-24. Sensor rotates in water with 30 RPM in 40 cm diameter wellbore (simulating squeezed formation)
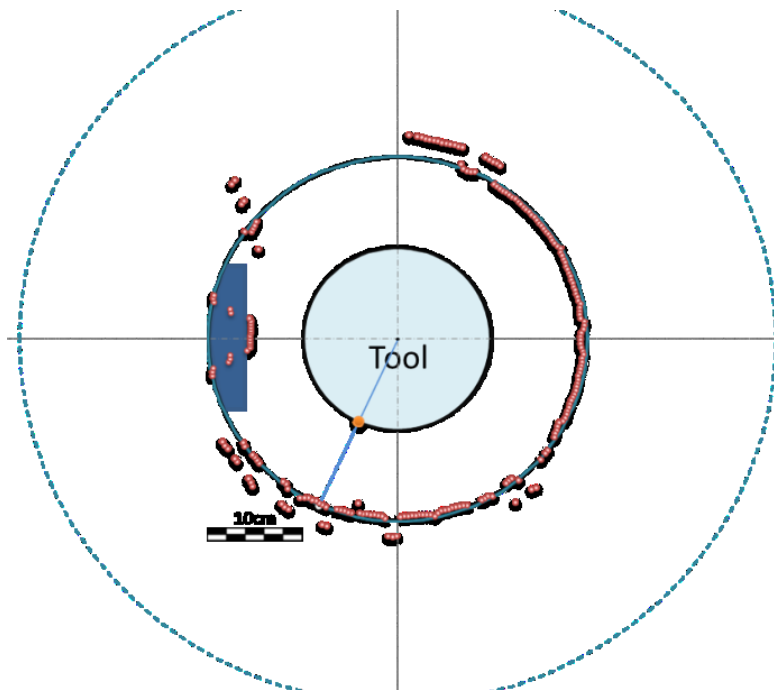
Figure 7-25. Sensor rotates in water with 45 RPM in 40 cm diameter wellbore (simulating squeezed formation)
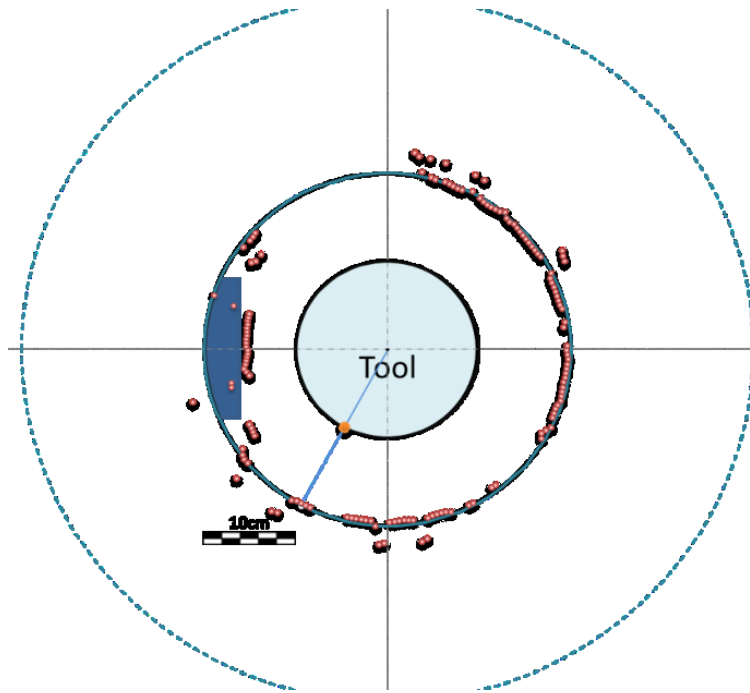
Figure 7-26. Sensor rotates in water with 60 RPM in 40 cm diameter wellbore (simulating squeezed formation)
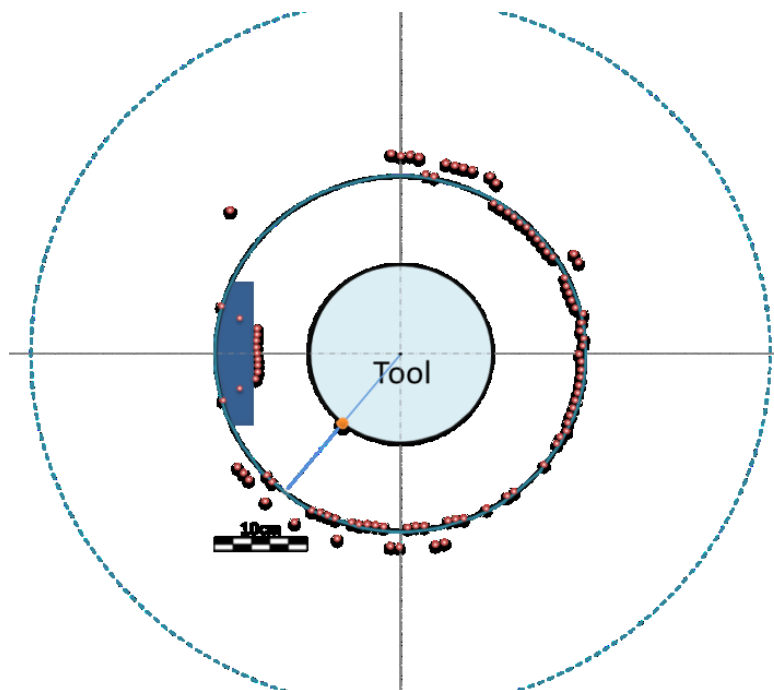
Figure 7-27. Sensor rotates in water with 100 RPM in 40 cm diameter wellbore (simulating squeezed formation)

7.3 Testing in Bentonite Mud

Figure 7-28 to Figure 7-38 show the results of ultrasonic tests and measurement in bentonite mud. Test results are categorized based on the tool geometry and position on the wellbore.

### 7.3.1 Centralized position of the tool in the wellbore (Bentonite Mud)

Figure 7-28. Sensor rotates in bentonite mud with 30 RPM in 40 cm diameter wellbore (centralized position)

Figure 7-29. Sensor rotates in bentonite mud with 45 RPM in 40 cm diameter wellbore (centralized position)

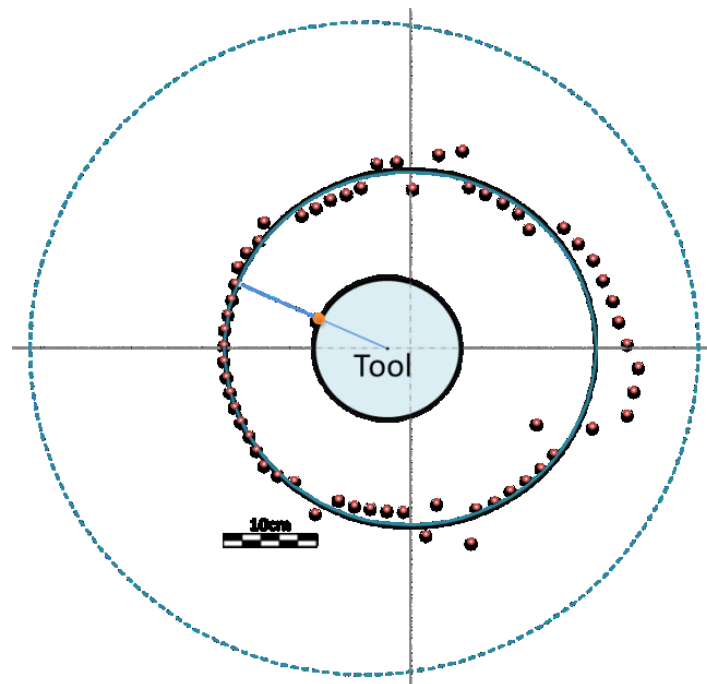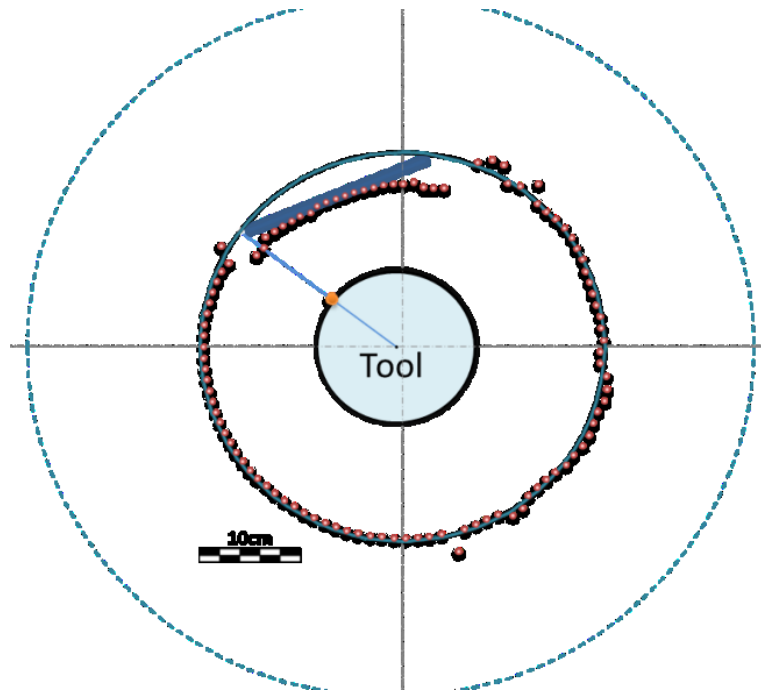**Figure 7-30. Sensor rotates in bentonite mud with 60 RPM in 40 cm diameter wellbore (centralized position)**

Figure 7-31. Sensor rotates in bentonite mud with 100 RPM in 40 cm diameter wellbore (centralized position)

7.3.2 Decentralized position of the tool in the wellbore (Bentonite Mud)

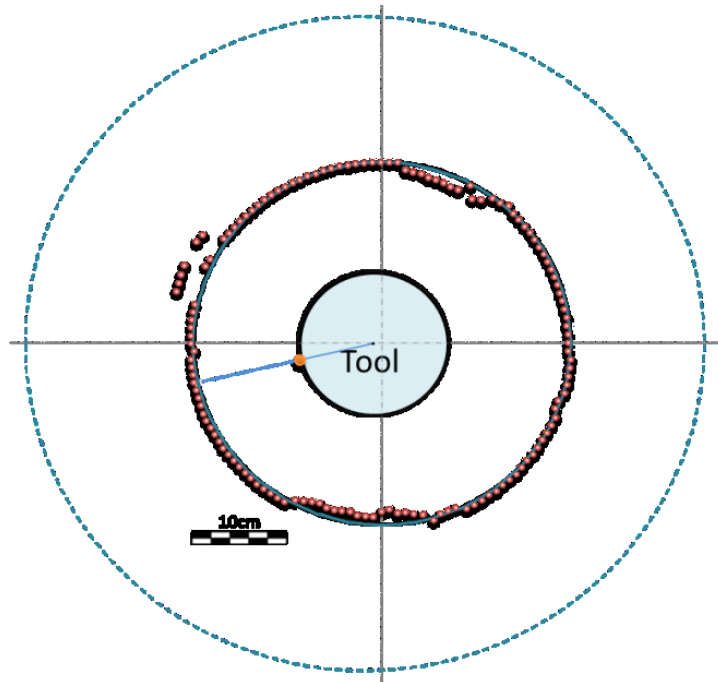**Figure 7-32. Sensor rotates in bentonite mud with 30 RPM in 40 cm diameter wellbore (decentralized position)**

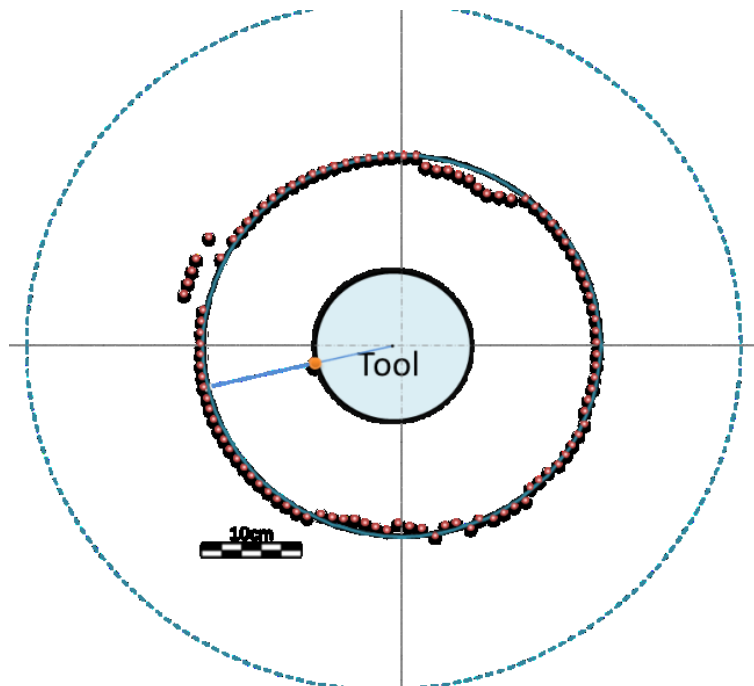**Figure 7-33. Sensor rotates in bentonite mud with 45 RPM in 40 cm diameter wellbore (decentralized position)**
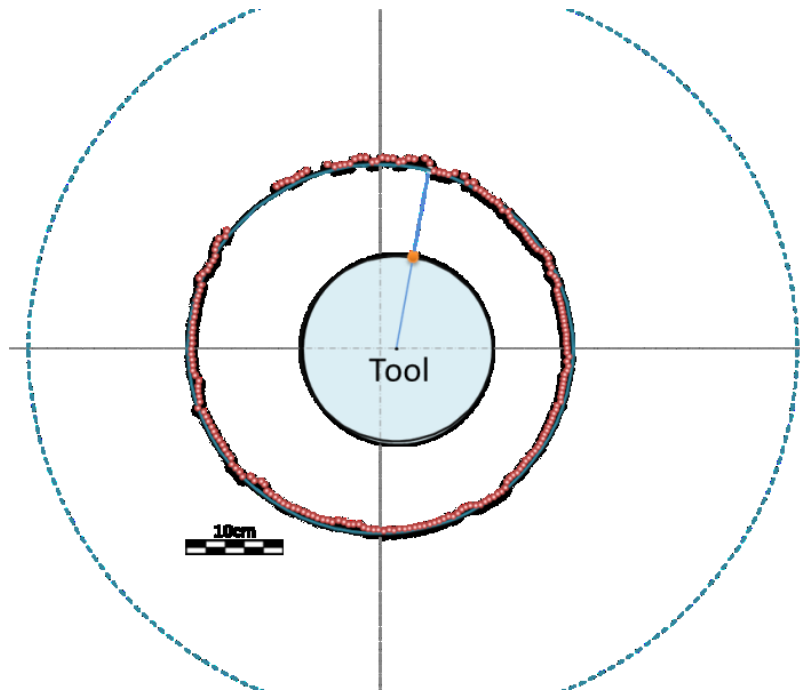
Figure 7-34. Sensor rotates in bentonite mud with 60 RPM in 40 cm diameter wellbore (decentralized position)


Figure 7-35. Sensor rotates in bentonite mud with 100 RPM in 40 cm diameter wellbore (decentralized position)

7.3.3 Simulation of squeezed formation (Bentonite Mud)
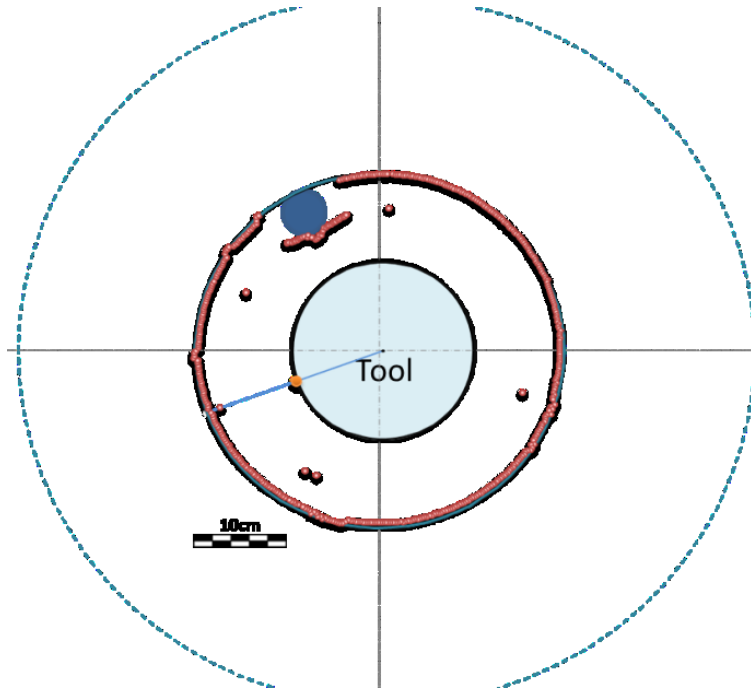
Figure 7-36. Sensor rotates in bentonite mud with 30 RPM in 40 cm diameter wellbore (squeezed formation)
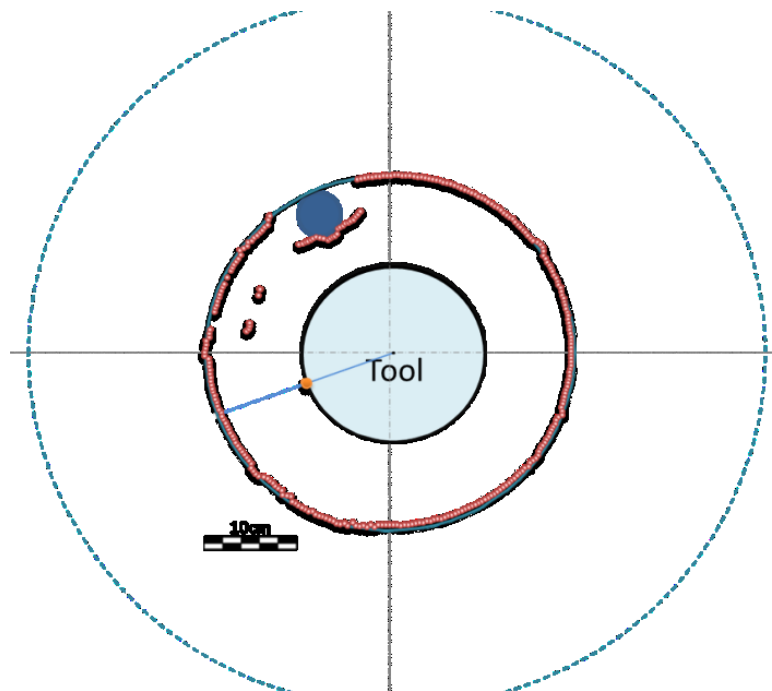
Figure 7-37. Sensor rotates in bentonite mud with 45 RPM in 40 cm diameter wellbore (squeezed formation)
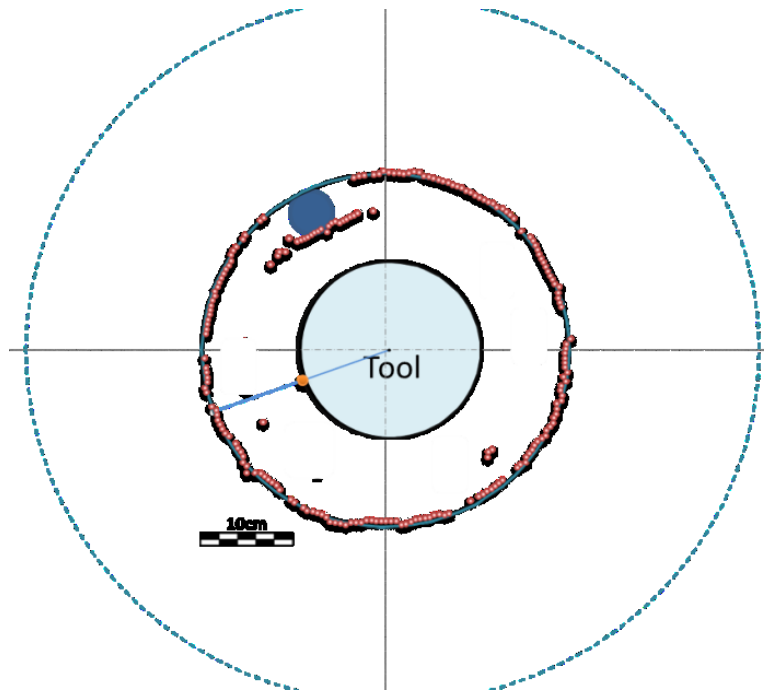
Figure 7-38. Sensor rotates in bentonite mud with 60 RPM in 40 cm diameter wellbore (squeezed formation)

7.4 Effect of Mud Weight

Figure 7-39 to Figure 7-62 Show the results of the tests in drilling fluid with different mud weights like 8.65, 9 and 10 ppg. Drilling fluid is the salt water with different salt concentration. Test results are categorized based on the tool geometry and position on the wellbore.

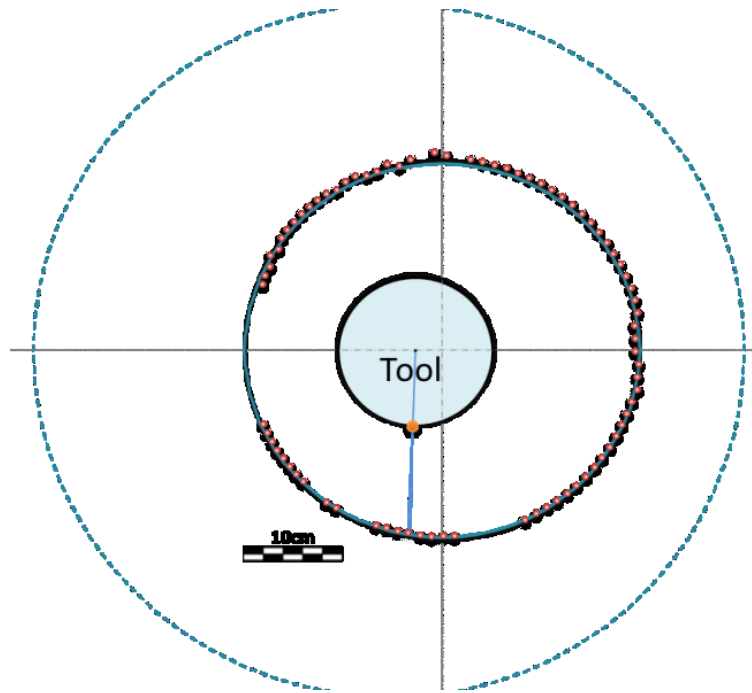### 7.4.1 Salt water with 8.65 ppg density

Figure 7-39. Sensor rotates in salt water, 8.65ppg, with 60 RPM in 40 cm diameter wellbore (centralized position)

Figure 7-40. Sensor rotates in salt water, 8.65ppg, with 100 RPM in 40 cm diameter wellbore (centralized position)
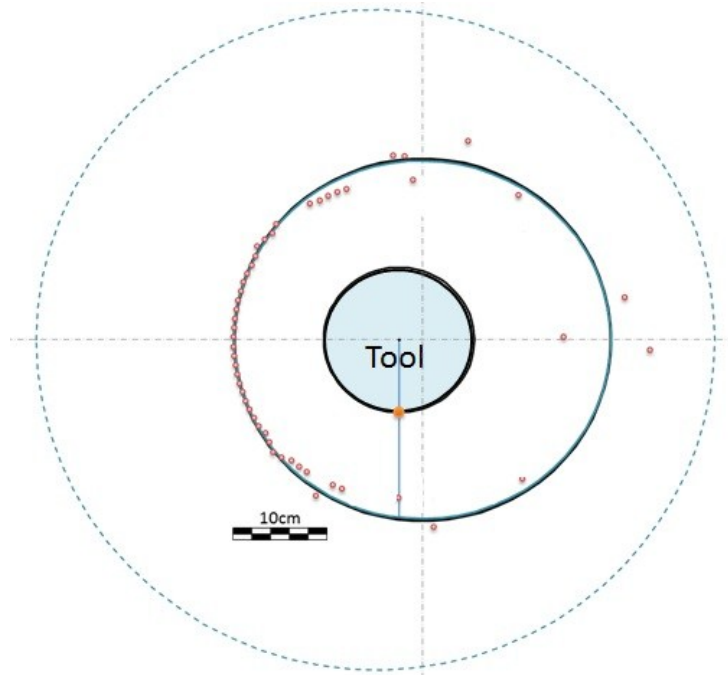
Figure 7-41. Sensor rotates in salt water, 8.65ppg, with 60 RPM in 40 cm diameter wellbore (decentralized position)
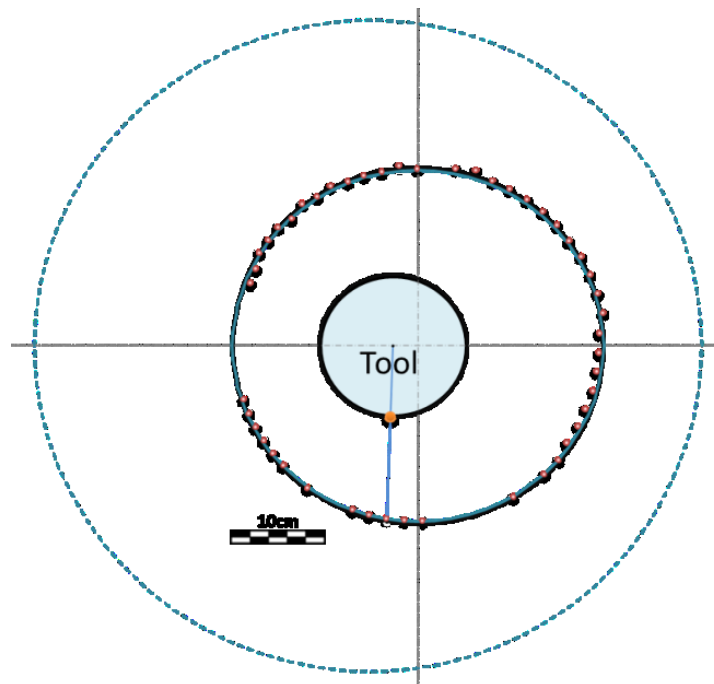

Figure 7-42. Sensor rotates in salt water, 8.65ppg, with 100 RPM in 40 cm diameter wellbore (decentralized position)
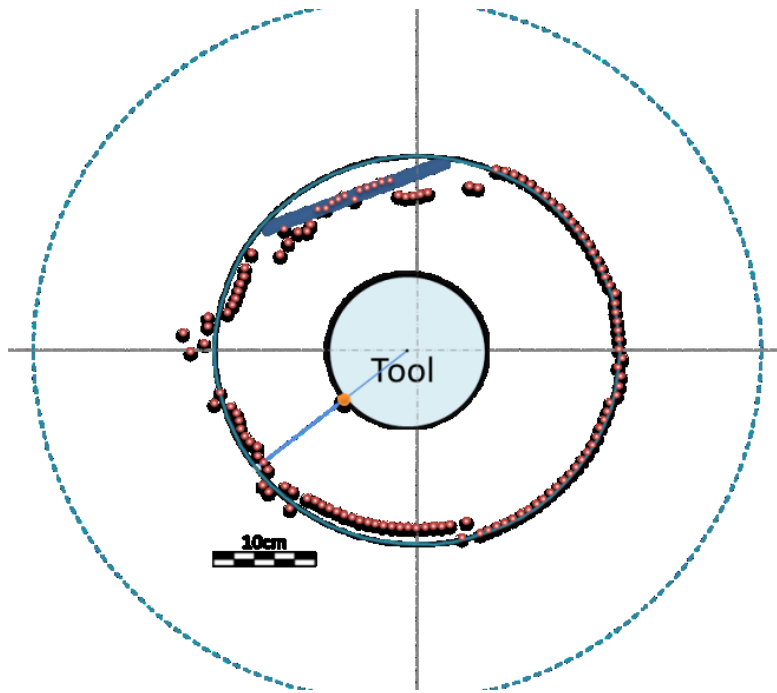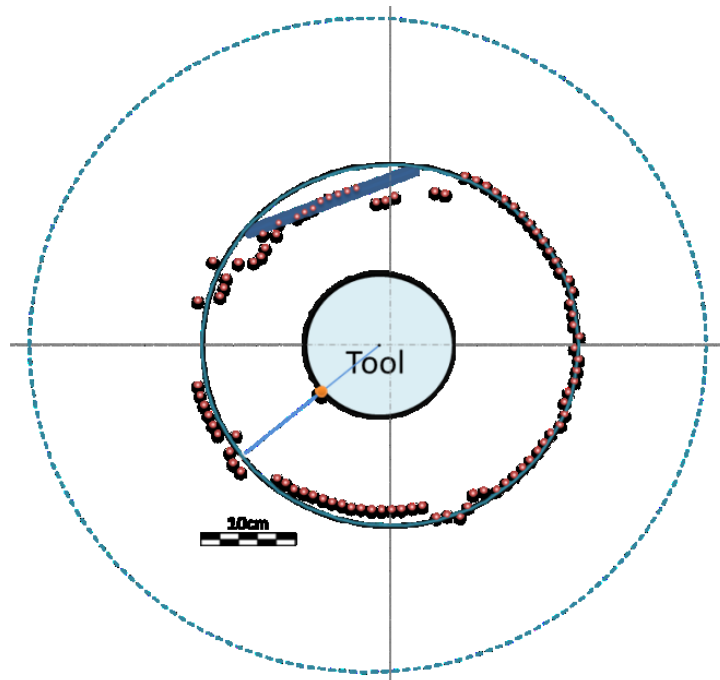
Figure 7-43. Sensor rotates in salt water, 8.65ppg, with 60 RPM in 40 cm diameter wellbore (squeezed formation)
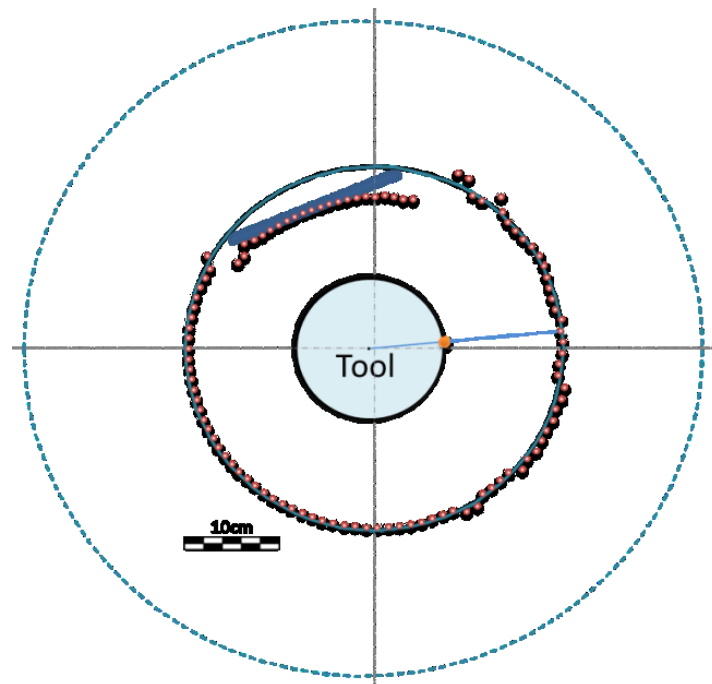
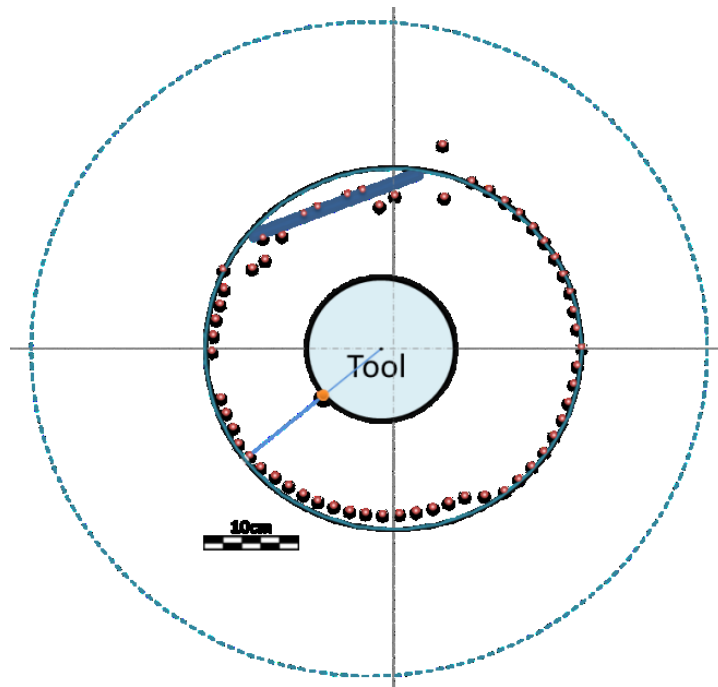**Figure 7-44. Sensor rotates in salt water, 8.65ppg, with 100 RPM in 40 cm diameter wellbore (squeezed formation)**

7.4.2 Salt water with 9 ppg density

Figure 7-45. Sensor rotates in salt water, 9 ppg, with 45 RPM in 40 cm diameter wellbore (centralized position)

Figure 7-46. Sensor rotates in salt water, 9 ppg, with 60 RPM in 40 cm diameter wellbore (centralized position)
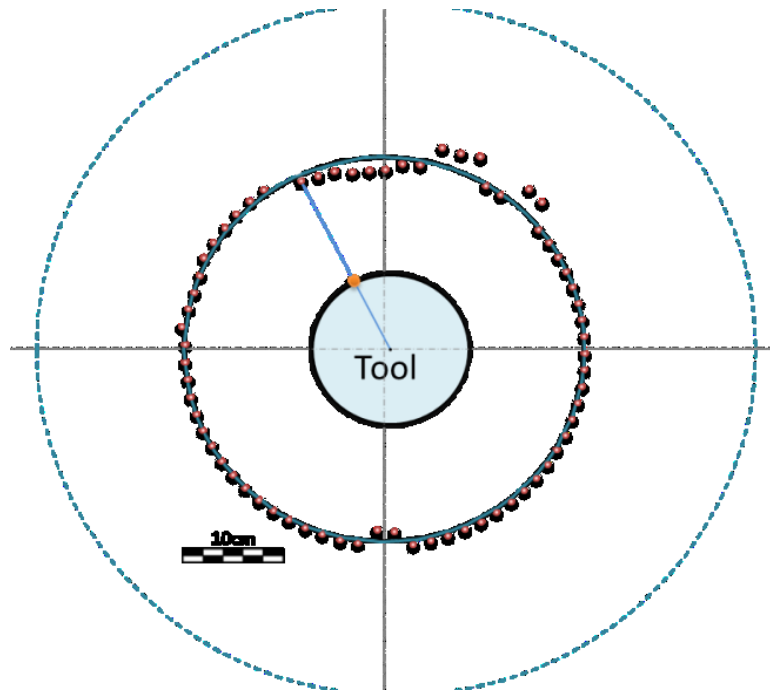
Figure 7-47. Sensor rotates in salt water, 9 ppg, with 100 RPM in 40 cm diameter wellbore (centralized position)
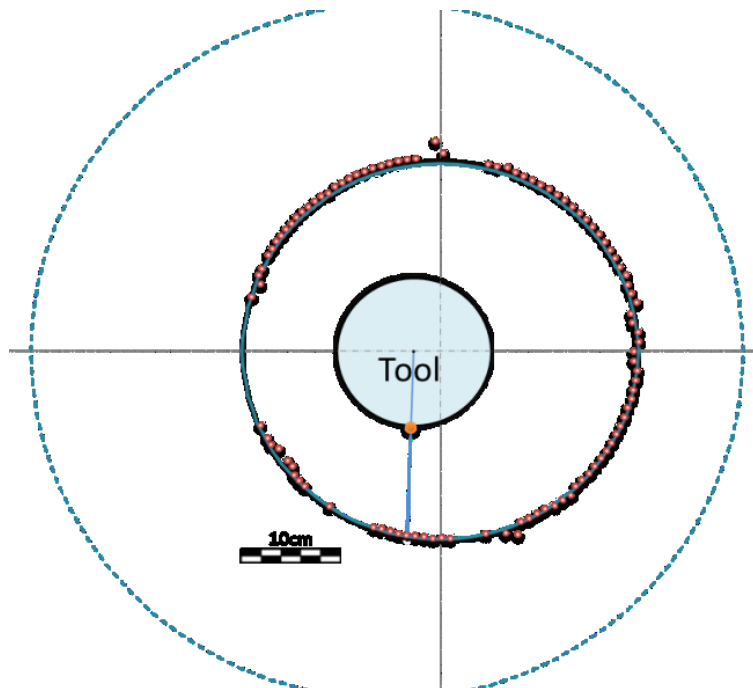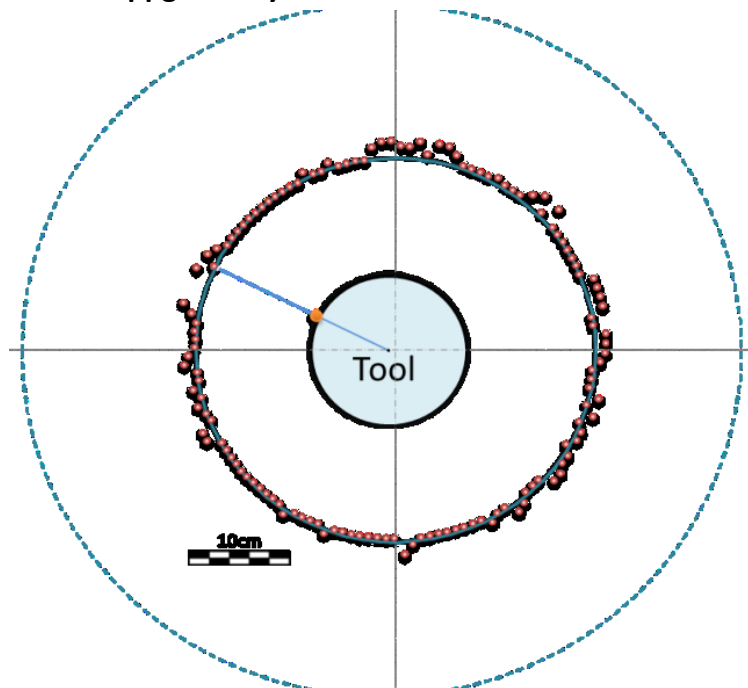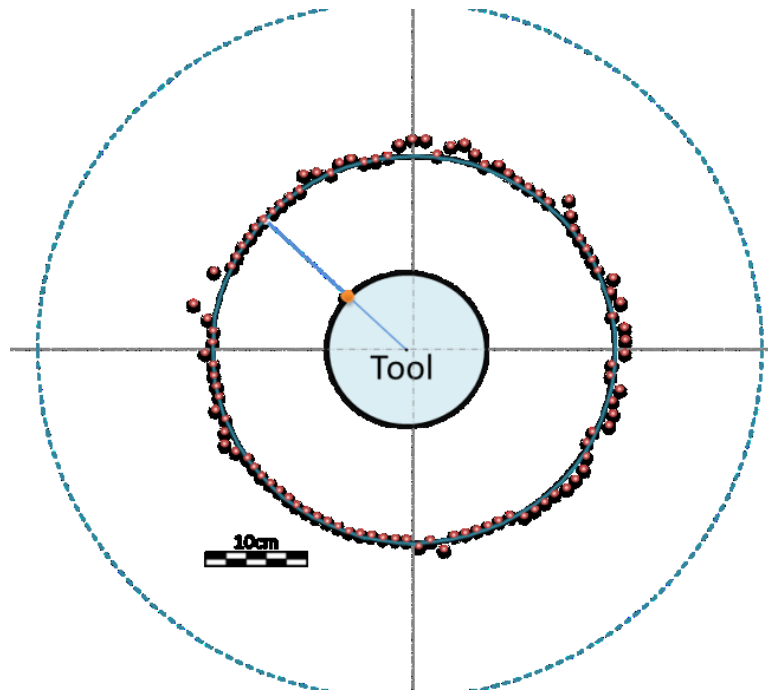

Figure 7-48. Sensor rotates in salt water, 9 ppg, with 45 RPM in 40 cm diameter wellbore (decentralized position)

Figure 7-49. Sensor rotates in salt water, 9 ppg, with 60 RPM in 40 cm diameter wellbore (decentralized position)
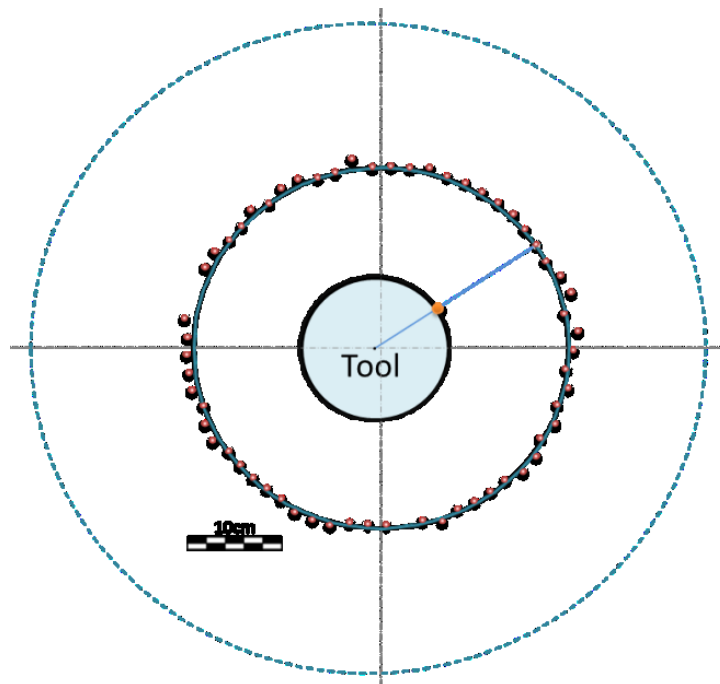

Figure 7-50. Sensor rotates in salt water, 9 ppg, with 100 RPM in 40 cm diameter wellbore (decentralized position)

Figure 7-51. Sensor rotates in salt water, 9 ppg, with 45 RPM in 40 cm diameter wellbore (squeezed formation)

Figure 7-52. Sensor rotates in salt water, 9 ppg, with 60 RPM in 40 cm diameter wellbore (squeezed formation)

Figure 7-53. Sensor rotates in salt water, 9 ppg, with 100 RPM in 40 cm diameter wellbore (squeezed formation)

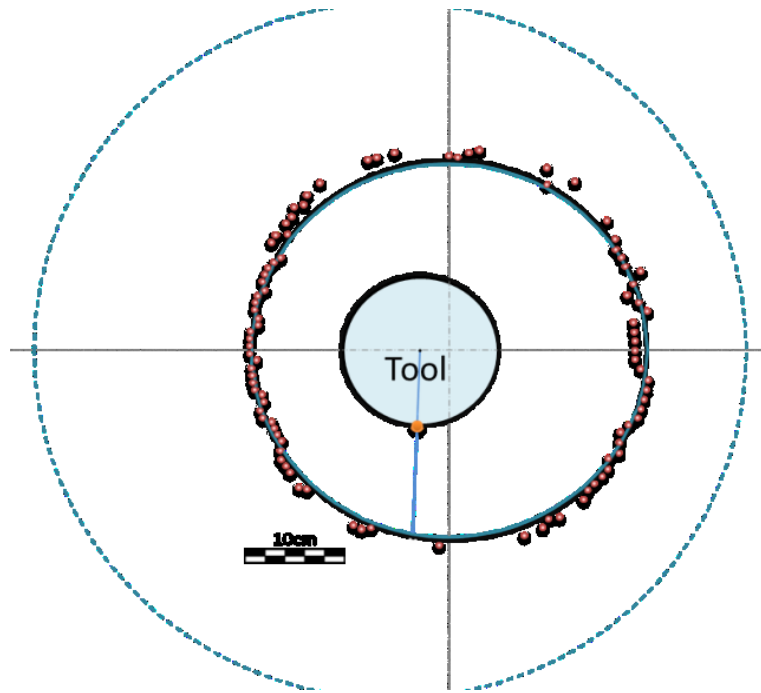### 7.4.3 Salt water with 10 ppg density

Figure 7-54. Sensor rotates in salt water, 10 ppg, with 45 RPM in 40 cm diameter wellbore (centralized position)
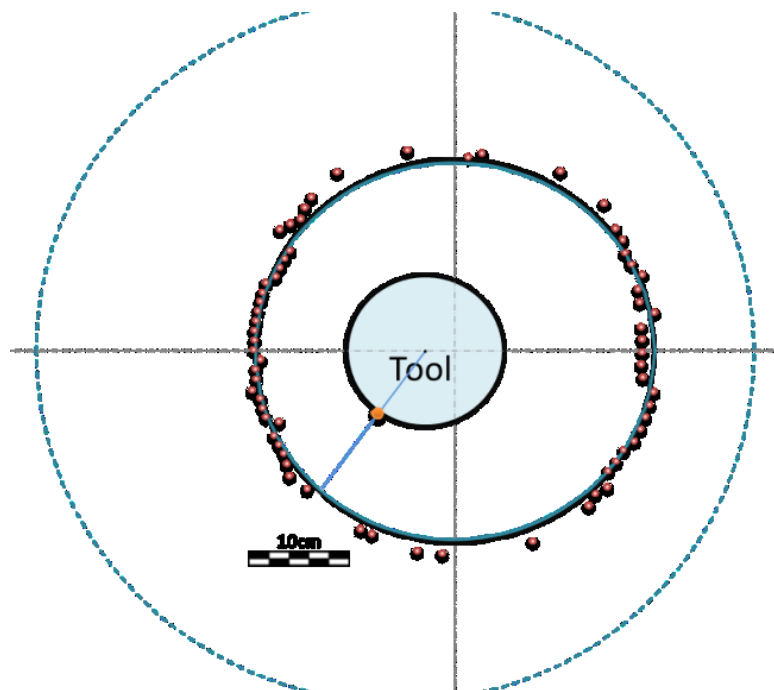
Figure 7-55. Sensor rotates in salt water, 10 ppg, with 60 RPM in 40 cm diameter wellbore (centralized position)
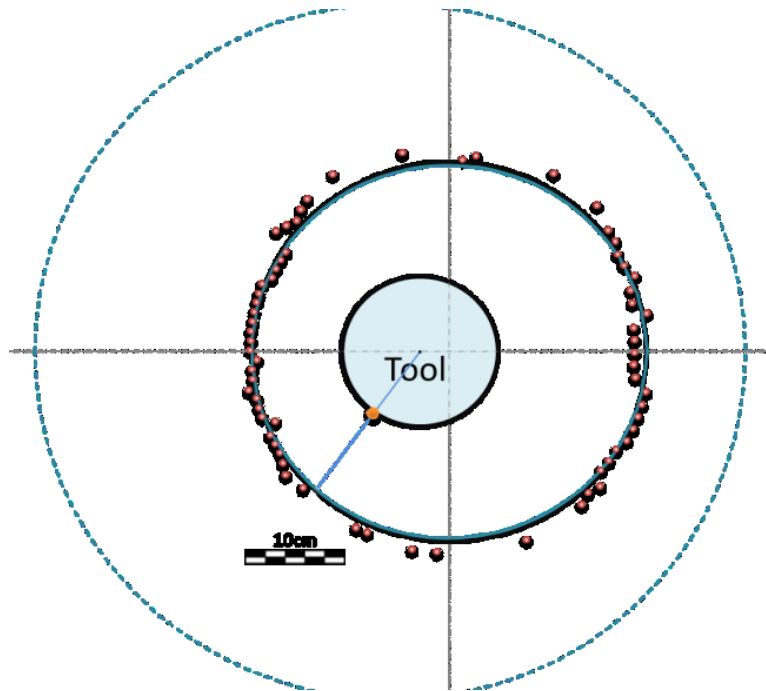

Figure 7-56. Sensor rotates in salt water, 10 ppg, with 100 RPM in 40 cm diameter wellbore (centralized position)

Figure 7-57. Sensor rotates in salt water, 10 ppg, with 45 RPM in 40 cm diameter wellbore (decentralized position)

Figure 7-58. Sensor rotates in salt water, 10 ppg, with 60 RPM in 40 cm diameter wellbore (decentralized position)

Figure 7-59. Sensor rotates in salt water, 10 ppg, with 100 RPM in 40 cm diameter wellbore (decentralized position)
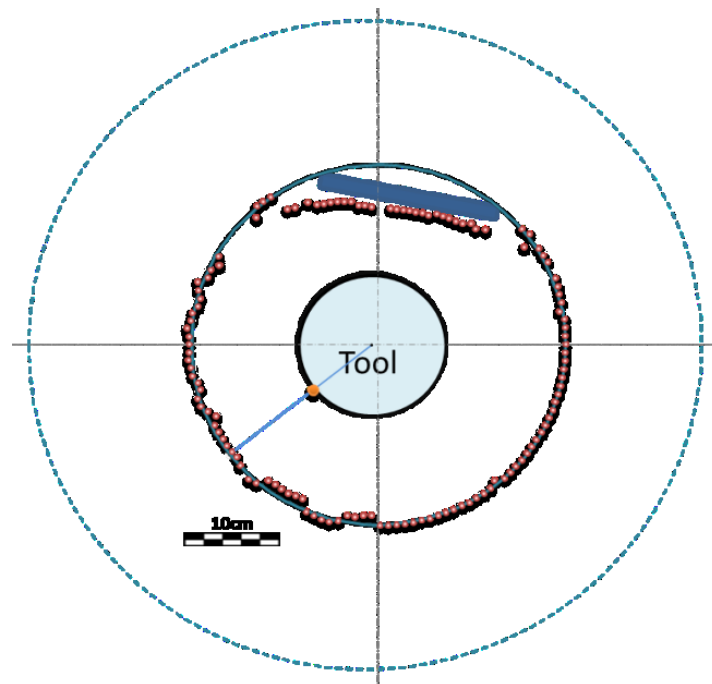

Figure 7-60. Sensor rotates in salt water, 10 ppg, with 45 RPM in 40 cm diameter wellbore (squeezed formation)
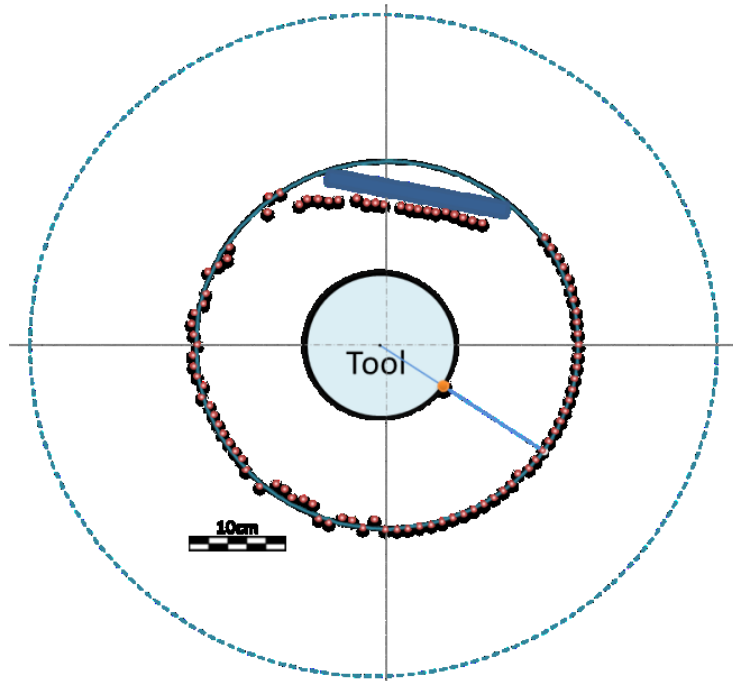
Figure 7-61. Sensor rotates in salt water, 10 ppg, with 60 RPM in 40 cm diameter wellbore (squeezed formation)
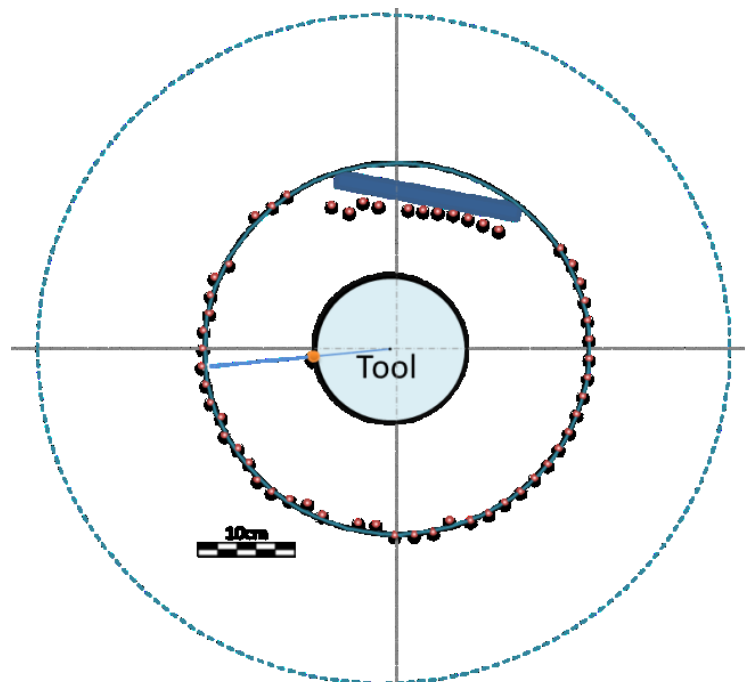

Figure 7-62. Sensor rotates in salt water, 10 ppg, with 100 RPM in 40 cm diameter wellbore (squeezed formation)